Functional Photopolymer Materials for High-resolution 3D Lithography and Nano-optics

Ying Peng

Thèse
de doctorat
de l'UTT

Ying PENG

Functional Photopolymer Materials for High-resolution 3D Lithography and Nano-optics

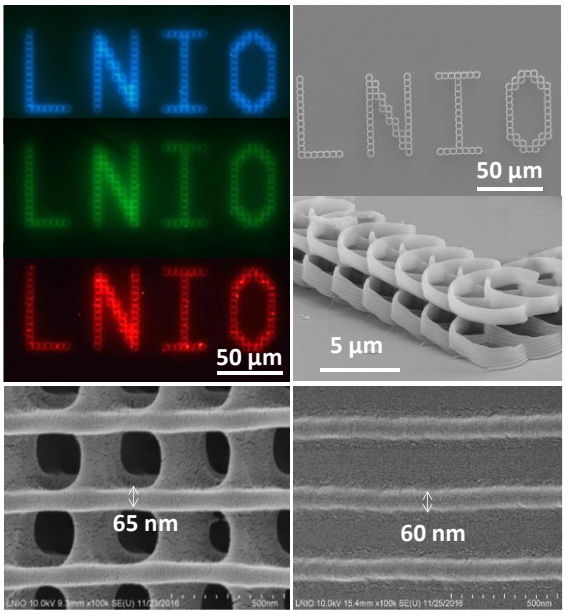

Spécialité :
Matériaux, Mécanique, Optique et Nanotechnologie

2017TROY0039

Année 2017

utt
UNIVERSITÉ DE TECHNOLOGIE
TROYES

THESE

pour l'obtention du grade de

DOCTEUR de l'UNIVERSITE DE TECHNOLOGIE DE TROYES

Spécialité : MATERIAUX, MECANIQUE, OPTIQUE ET NANOTECHNOLOGIE

présentée et soutenue par

Ying PENG

le 20 décembre 2017

Functional Photopolymer Materials for High-resolution 3D Lithography and Nano-optics

JURY

M. P. BALDECK	DIRECTEUR DE RECHERCHE CNRS	Président (Rapporteur)
M. R. BACHELOT	PROFESSEUR DES UNIVERSITES	Directeur de thèse
M. S. JRADI	PROFESSEUR ASSISTANT UTT	Directeur de thèse
M. L. MAGER	CHARGE DE RECHERCHE CNRS - HDR	Rapporteur
M. G. WIEDERRECHT	SENIOR SCIENTIST	Examinateur

Tables of contents

Acknowledgements

It is really a challenge to complete my PhD degree. This PhD thesis is done in the Laboratory of Nanotechnology and Instrumental Optics (LNIO) at University of Technology of Troyes (UTT) with financial funding by China Scholarship Council (CSC), which is the prerequisite for my coming to France for this thesis.

I would like first to express my sincere gratefulness to Dr. Safi Jradi and Prof. Renaud Bachelot for providing me the opportunity to work on this topic and accepting me as a member of the LNIO. Thanks to their guidance and continuous to this research, I can finally finish this work. Thanks to their encouragements and necessary advices, I can work out the project right in the way. Thanks to their optimistic and humorous qualities, I can be always in a very pleasant environment for research. I appreciate the time working with these two brilliant supervisors.

Special thanks to my committee: Prof. Patrice Baldeck, Dr. Loïc Mager and Dr. Gary Wiederrecht for their kind suggestions, valuable and critical comments on the basics on two-photon polymerization. Their comments and guidance have contributed to improvement on the quality of this PhD thesis. I do greatly appreciate them.

I would like to thank our collaborators Prof. Xiao Wei Sun, Hilmi Volkan Demir and Xuan Quyen Dinh who have provided the QDs-containing polymer for this dissertation. Thanks for their help in the preparation of these polymer with high quality and availability, which allow us to achieve reliable fabrication and measurements.

Thanks to the Dr. Christophe Couteau, Dr. Sylvain Blazie and Prof. Jérôme Plain who participated in most of our discussions and for giving helpful suggestions. I would like to give my thanks to the group members Aurélie Broussier, Dandan Ge, Hongshi Chen, Xiaolun Xu, Ali Issa and Stefano Pierini for participation in the project, sharing the ideas, comments and discussions.

Thanks also to the colleagues Jérémie Béal, Régis Deturche, Serguei Kostcheev, and Anne-Laure Baudrion-Béal for the trainings of the equipment in LNIO. Thanks should also be given to Yi Huang, Yinping Zhang, Feng Tang, Zeinab Chehadi, Anisha Gokarna, Agnesizka Gwiazda, Feifei Zhang, Junze Zhou, Shijian Wang, Binbin Wang, Loïc Le Cunff as well as other colleagues from LNIO for sharing with me a very pleasant and memorable

time in this great lab. It was really wonderful to be one of the members in LNIO and having them as my colleagues.

This work is also dedicated to my dear parents and my sister. I would like to show my due respect to my whole family for their persistent love and affection. Finally, I would like to thank CSC for funding my PhD study in France and the various research grants and projects at LNIO and region Champagne-Ardenne grant NANO'MAT platform to give me a wider vision for future research career.

Chapter1. *Introduction to direct laser writing based on two-photon polymerization of functional photopolymers and related applications*

1.1 Two-Photon polymerization

Recent years, rapid progress in micro/nano fluidic devices, biochips, photonics, and nano/micro-electromechanical systems (N/MESMS) is witnessed based on the development of the techniques and technologies for 3D microstructures such as nanotechnology, biotechnology and information technology as well as the advances of the materials. With the growth of demand for decreasing size of devices in electronics, optics (holographic recording and information storage, computer-generated and embossed holograms, manufacture of optical elements, e.g., diffraction grating, mirrors, lenses, waveguides, array illuminators, and display devices), photonics, electro-chemistry, biology and electro-mechanics, it is of great importance to fabricate structures with nanometer-scale [1,2]. In this sense, two-photon polymerization (TPP) is considered as a promising technique providing a real 3D nanofabrication with a spatial resolution of about 100 nm [3–18]. More remarkable, one advantage of this technique is to realize 3D complex objects arbitrarily.

In TPP, the fundamental process is to transform a liquid (or sol-gel) monomer into a solid polymer under optical exposure. Particularly, during the process, when the laser beam is closely focused on the volume of the photo polymerizable resin, the photo initiator (PI) is excited due to the two photon absorption (TPA), resulting in generated radicals and the initiated polymerization reaction [19]. The TPP procedure can be described with equations (1-1)–(1-3):

$$\text{Initiation:}\quad PI \rightarrow PI^{*} \rightarrow R^{\cdot} \qquad (1\text{-}1)$$

$$\text{Propagation:}\quad R^{\cdot} + M \rightarrow RM^{\cdot} \cdots \rightarrow RM_n^{\cdot} \qquad (1\text{-}2)$$

$$\text{Termination:}\quad RM_n^{\cdot} + RM_m^{\cdot} \rightarrow RM_{m+n}R \qquad (1\text{-}3),$$

where PI is the photo initiator, $R^{\cdot}$ is a radical, M is the monomer (n, m indicate the number of the monomer in the backbone of the polymer), PI* is the excited state of the photo initiator PI after absorbing the photon energy, respectively [20].

1.1.1 Two-photon absorption (TPA) basics

In 1931, the theory of simultaneous excitation TPA was predicted [21], and verified contributing to the advent of laser in 1961 [22]. TPP was experimentally reported for the first time in 1965 as the first example of multiphoton excitation-induced photochemical reactions [23].

TPA is a multiphoton excitation approach to initiate the photochemical reaction. There are two mechanisms of TPA: sequential excitation TPA and simultaneous excitation TPA illustrated in Figure 1.1 [20]. In both cases, molecules are exposed to high intensity radiation and two identical photons are absorbed. As a result, the ground state E_0 gets excited to the intermediate state then finally into a high energy level E_1. The main difference between the two mechanisms is that, in sequential excitation the intermediate state is a real state instead whereas it is a virtual state in simultaneous excitation. On the basis of the uncertainty principle of Heisenberg, the life time of the intermediate state can be given by $h/\Delta E$, where ΔE is the difference of energy between the material´s virtual state and the closest real state, and h is the Planck constant. Normally, the lifetime of real state is in the range of 10^{-4} to 10^{-9} s, while virtual state lifetime is about 10^{-15} s. That is the reason why femtosecond laser is widely used for two-photon polymerization fabrications [24]. In the case of TPP, only the simultaneous excitation TPA is involved [20, 25-26].

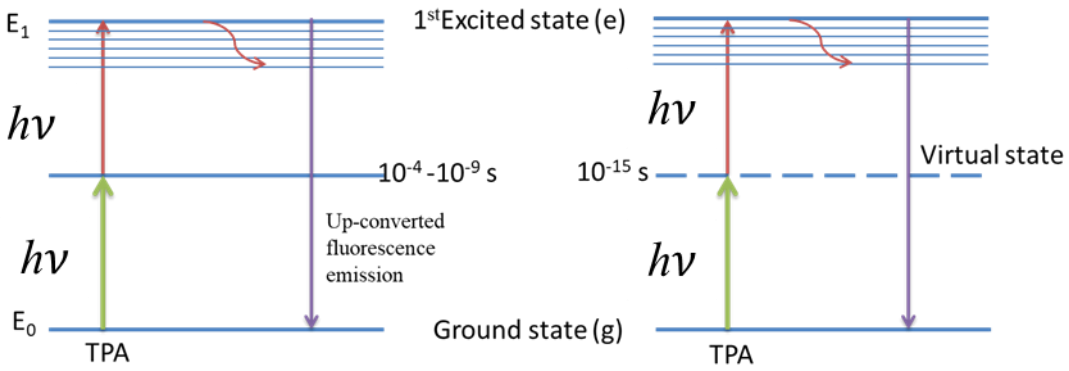

Figure 1.1: Two mechanisms of TPA: (a) sequential excitation and (b) simultaneous excitation.

In terms of quantum mechanics analysis, TPA presents selection rules distinct from one photon absorption (OPA) ones. As shown in Figure 1.2.b, in TPA a photopolymer absorbs two near-infrared photons simultaneously though a single quantum event whose

energy corresponds to the UV region of the spectrum [27, 28]. When a laser beam is closely focused with a high numerical aperture (NA) objective lens into a volume of photo curable resin, photon- density-profiles are formed with a constant total number of photons in the focused spot exploiting the linear response of materials to the light intensity based on OPA (see Figure 1.2.a). On the contrary, *via* TPA, the material response is proportional to the square of the photon density, and the integrated material response is greatly enhanced at the focal point.

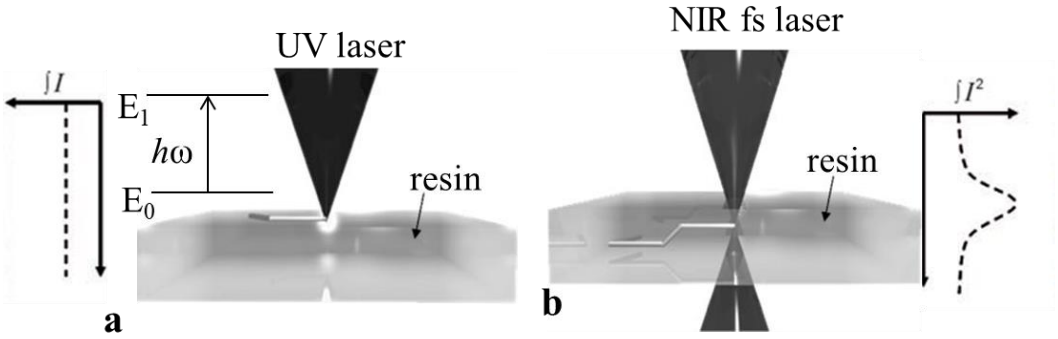

Figure 1.2: Illustrations of photosensitive resins processing by (a) OPA with UV light and (b) TPA with NIR laser [29].

There is a theoretical explanation [30] about the material response to the intensity of laser. The probability of a molecule to absorb one photon is proportional to the intensity of the excitation beam:

$$n^{(1)} = \sigma(v) N_g \frac{I}{hv} \qquad (1\text{-}4),$$

where $n^{(1)}$ is the number of molecules excited by OPA per unit time and unit volume in the material, σ is the cross section of the absorption process at frequency ν, N_g is the volume density of molecules in the ground state g, I is the intensity of the excitation source, and *hv* is the photon energy. By contrary, the probability of a molecule to absorb two photons simultaneously is proportional to the square of the intensity of the excitation beam:

$$n^{(2)} = \frac{1}{2}\delta(v) N_g (\frac{I}{hv})^2 \qquad (1\text{-}5),$$

where $n^{(2)}$ is now the number of molecules excited by TPA in the unit volume per unit time and δ(ν) is the TPA cross section for a photon of energy *hv*. The pre-factor of ½ reflects the fact that two photons are needed to excite one molecule.

Quadratic intensity dependence of TPA allows for spatial confinement of solidification to a resolution beyond the diffraction limit of light. Besides, due to this low probability of absorption, TPA occurs at the focus plane only and can thus be initiated anywhere in the volume of resin as the laser focus can move three-dimensionally through the resin. On the contrary, in OPA process, UV light is absorbed at the surface of resin and only planar structures can be fabricated.

1.2 Direct laser writing by two photon polymerization (TPP-DLW)

As mentioned above, the rate of TPA is proportional to the square of the light intensity, so that the near-infrared or visible light is strongly absorbed only at the focal point within the photopolymer. As a result, TPA enables TPP-DLW with a confinement of the photo-modification to submicron dimensions, beyond the diffraction limit of light [7, 13-14], even less than 100 nm.

1.2.1 Photosensitive materials and applications for TPP-DLW

TPP-DLW is a well-established approach for producing various 3D nanostructures. The basic components include photo initiators and polymer that can be either monomers or oligomers and that is the main skeleton of the final structures. In practice, more components are used, such as multiple photo initiators, photo sensitizers and some functional molecules or inorganic doping agents [31-34]. There are several reviews about the progress of the PI for TPA [35, 36]. In this section, the photopolymer used in TPP-DLW is concerned.

In the beginning when the TPP-DLW was applied for 3D microfabrication, commercially available photopolymers were used such as urethane acrylates and epoxies [5, 8]. Among different monomers available, acrylates have been the most widely used for microfabrication [37-46]. This is because of a wide range of acrylates with tailored properties: chain length, viscosity, polarity, number of reaction functions and refractive index. In addition, acrylates exhibit a higher reactivity and good mechanical properties (Reduced Young's modulus >500MPa) allowing fabricating complex 3D structures compared to those of epoxides. Until now, most research on TPP-based micro fabrication has demonstrated the interest of using the acrylates for photo polymerization. For instance, photo resins based on a monomer of PETA (pentaerythritol triacrylate) mixed with photo initiator have been used to

fabricate microlenses [41-45], light concentrator [46] with submicron-scale resolution *via* direct laser writing. There are also several studies which have been carried through with tailored acrylates for special applications, for example, biocompatible materials for delivery devices [47], active materials doped with nanoparticles for actuated structures [48], and hydrogels for optical devices [49,50].

1.2.1.1 Applications in MEMS/NEMS and microfluidic

There are extensive polymeric nano/microstructures used in Micro/Nano Electro-Mechanical SYSTEM (MEMS/NEMS), electronic and optical devices, and so on. As an example, micropillars were fabricated as specimens for compression test by TPP technique using the resin SCR500 (is a mixture of urethane acrylate monomer, oligomer and a photoinitiator(2-benzyl-2-dimethylamino-1-(4-morphoinophenyl)butanal-1-hydroxychlorohe xylphenylketone)[49]. NOA63 resin (Norland Products, Mercapto-ester Trially Isocyanurate, optical polymer glue) was used to produce the microrotors by TPP-DLW. The few microns sized rotor was held and rotated by the laser tweezers and the system was driven by the rotating propeller [51].

Moreover, TPP-DLW has also been used for fabrication of microfluidics [52, 53] and lab-on-chip (LOC) systems [54-57], owing to its unique advantages: 3D arbitrary geometry capability. SU-8 (Bisphenol A Novolac epoxy, a negative near-UV photoresist) solid photopolymer was found to be critical to building the thin shells and the suspending component. In general, SU-8 is essential and broadly used in the functionalization of LOC system (see Figure 1.3). Nowadays, it is possible to integrate single units into chips by DLW. For examples, micro valves and micro channel can be implemented as overpass or junction [57].

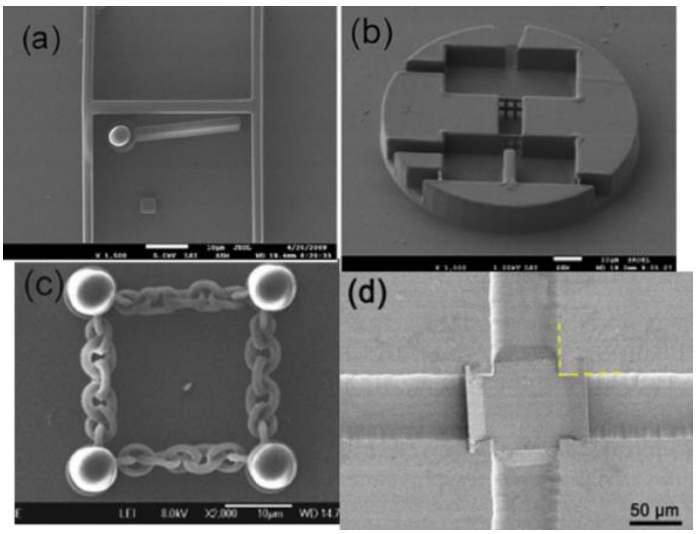

Figure 1.3: SEM images of devices fabricated by TPP-DLW with SU-8 resist (a) microfluidic channel and a 25 mm length movable micro-valve, (b) Two infiltration networks with six 2 mm sized bores, (c) a chain structure consisting of 5 and 20 rings and (d) an overpass fabricated at the junction of a crossed microchannel which is used for 3D chips [55, 57].

There are also some other resists used for LOC fabrication by DLW. For instance, Amato L. et al [57] integrated a 3D filter with micron-sized pores in a microfluidic chip. In this work, the filter is fabricated using TPP-DLW with a SZ2080 resist. SZ2080, which is a 20:80 mixture of zirconium–silicon with methacrylate, is a hybrid organic–inorganic sol–gel material that has high optical quality, good post processing, chemical and electrochemical inertness, and good mechanical stability [6, 58]. Additionally, its low shrinkage properties (during the polymerization, the polymer shrinks owing to the higher mass density of solid phase than that of the liquid phase) make it suitable for applications sensitive to structural deformations. Thus, SZ2080 has been frequently used in TPP-DLW fabrications in recent years [58].

Besides, polydimethylsiloxane (PDMS), which is another polymer widely used in the fabrication of micro fluidic circuits [59], was used to produce flexible micro units *via* two-photon-initiated hydrosilylation and radical-initiated crosslinking [60]. The fabrication of PDMS-based 3D structures by TPP-DLW can be of benefit to modify generic microfluidic channels, to possess higher functionality and complex 3D networks [61].

1.2.1.2 Applications in plasmonics and photonics

Metals or metallic oxide nanoparticles (NPs), nanostructures or thin films have given rise to growing interests for electrical connections in devices as well as for their plasmonic

applications. 3D structures of polymer-metal/metallic oxide nanoparticle composite materials are promising to play an important role in the field of functional devices. Some works have been reported on the fabrication of 3D structures by TPP-DLW. For instance, sub-micrometric plasmonic structures with gold nanoparticles in SU-8 polymer matrix were fabricated by TPP-DLW [62]. Guo Q. C. et al. demonstrated the applicability of TPP-DLW to achieve 3D structures with Ormocers-Ormocore b59 resists containing TiO_2 NPs [63]. There is a report on Surface-Enhanced Raman Spectroscopy (SERS) substrate using 3D structures containing Au-NPs manufactured by TPP-DLW [64] where hexadecyltrimethyl ammonium bromide (CTAB) was used as binder and mixed with gold salt ($HAuCl_4$) as precursor and (2, 4, 6-trimethylbenzoyl)-phosphine oxide (TPO) as photo initiator. As the solution was irradiated by the pulsed laser, randomly shaped Au NPs are formed and self-assembled as linear structures(shown in Figure1.4), which will be the building blocks of the 3D patterns. The manufactured structures present plasmonic activity, as well as excellent properties as SERS substrates for quantitative position-resolved measurements; else, they are successfully applied for detection of the fungicide thiabendazole [64]. The same approach of fabrication was reported using one photon absorption process at the extremity of single and multicore optical fibers [65, 66].

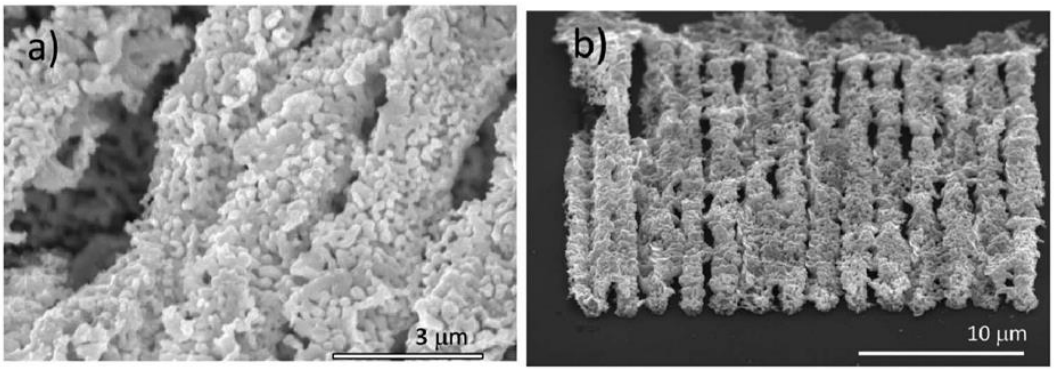

Figure 1.4: SEM images of the Au NP-based structures: (a) linear arrangement of the AuNPs in the structures; (b) single-layer structure consisting of 30mm-lines [64].

With the uniqueness of obtaining real 3D structures, TPP-DLW is a promising alternative to produce Photonic Crystals (PCs) [67-73] and photonic 3D metamaterials [67-77], such as gold helices as circular broadband polarizers [67], SU-8 polymeric photonic crystals with polarization stop bands [68] and 3D chiral photonic super lattices [69].

Over recent decades, intensive research efforts have been put forward to the design and fabrication of photonic crystals (PCs) in order to provide a novel platform for the realization

of integrated photonics and theoretical modelling of propagation of light through periodic structures [70]. For instance, 3D woodpiles of two different polymers (Ormocers and SU-8) were fabricated by DLW. The resulting structures possess a photonic band gap in the near infrared spectral range. The central frequency of the band gap could be tuned by varying the crystal's period [71]. As illustrated in Figure 1.5, G. von Freymann and coworkers [71] fabricated 3D woodpile PCs with defects by DLW in SU-8 together with supplementary silicon double-inversion. This novel method based on the use of DLW with subsequent double-inversion to design resonator is of great importance as dielectric defects cannot be reliably fabricated by chemical vapor deposition.

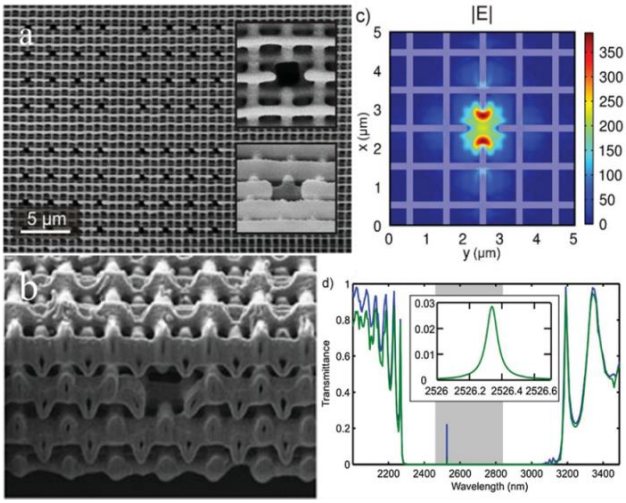

Figure 1.5: (a) SEM image of a woodpile photonic crystal containing several defects in its top-most layers with magnified views (b) FIB cross-section of a Si photonic crystal with defect (c) Numerical calculation of the mode profile (d) Perpendicular incidence transmittance spectra into the forward direction (entire-half space) of a structure containing one resonator, green (blue) solid curve. The inset is a close-up of the transmittance into the forward direction. The grey area displays the width of the complete photonic Bandgap [71].

Metamaterials are artificial metallic material that exhibit controlled both magnetic and dielectric functions at optical frequencies. DLW is considered to be one promising methods for direct manufacturing of 3D metamaterials with sub-100 nm resolution. It can also be compatible with metal deposition method like electroless plating, which is a wet-chemical metallization technique that does not require an external current source, and can fill the polymer structures produced through TPP-DLW [72-75]. For instance, 3D structures were fabricated by DLW with Z7012C resin and coated with silver by electroless plating [74, 75]. As another example, TiO_2 nanoparticles (NPs) were employed into the fabrication of PCs

[74], 3D diamond PCs which consisted of SCR 500 resin and TiO_2 was directly fabricated by DLW. A nonlinear optically active sol-gel, methacryloxypropyl trimethoxysilane (MAPTMS) containing azodye chromophore Disperse Red-1was used to fabricate functional 3D PCs *via* TPP-DLW. The PCs have band stops in the near-infrared, with the optical properties which can be controlled by the material's optical nonlinearity and photochemical switching capabilities of the chromophore [73].

Polymer/metal composites structures fabricated by TPP-DLW have been recently attracted the attentions in the field of plasmonics, owing to the plasmonic resonance enhancement effect of the structures obtained [76-78]. For instance, the Methyl Methacrylate (MMA) resin with dispersion of gold nano-rods was employed in the fabrication by TPP-DLW. As a result, the shapes of the structures changed with the increasing intensity used for polymerization, and the polymerization only occurred in the gap between gold nanorods where the field enhancement is very strong. It provides a potential application for TPP-DLW in the emerging field of nanophotonics and nanoplasmonics.

1.2.1.3 Applications in biology

The TPP technique is also of great potential in biological applications, including tissue engineering like scaffold fabrication [79, 80], drug delivery [81, 82], tissue engineering [83, 84]. In real 3D manufacturing by TPP-DLW, the resists employed are supposed to be transparent in location other than the focus plane. It enables the writing in the region exposed by the laser, where TPA occurs allowing for the formation of 3D structures.

With precise control on the 3D geometry of the scaffold and right materials, *via* TPP DLW, it is possible to model and reproduce the cellular microenvironments. Polymer matrixes and sol-gel materials have been widely used due to their biocompatibilities. [79]. Drakakis T. S. et al. [79] demonstrated the capability of the fabrication of 3D biopolymer (ORMOCER-biotin-streptavidin) structures by exploiting DLW, which offers a possibility to produce a high active area in a small size and high detection sensitivity. Biopolymer-functionalized 3D structures can be directly fabricated by TPP-DLW by exploiting the binding capabilities of the biotin–streptavidin system. By combining DLW and biotin-avidin mediated assembly on ORMOCER, 3D patterning of amyloid peptide fibers was prepared for various applications from molecular electronics to tissue engineering [80]. Additionally, several biological materials such as trypsin, collagen precursors, and proteins

like bovine serum albumin have been recently used for TPP-DLW [81, 82]. In J. D. Pitts group's study [47], the resultant protein structures are porous, and show promise for using as drug delivery devices or sustained release devices.

3D structures fabricated by TPP-DLW make possible the investigation of cell-substrate biophysical interaction focused on cell adhesion, shape, migration and function to be carried out by controlling 3D microenvironment. Therefore, fabrication of microenvironments is of interest for monitoring bacteria growth and motion, such as, how they proliferate and contaminate organism. The mostly utilized materials are Ormocomp® and poly(ethyleneglycol) hydrogels with several functionalization for case of the biological applications. For instance, two types of microenvironments were fabricated by TPP-DLW: the first one consists of an array of cylinders where the central cylinder is doped with ciprofloxacin, an antibiotic used in the treatment of bacterial infection. This system has been used to evaluate the inhibition of bacterial growth; the second one consists of micro-fences to trap bacteria [83]. This demonstrates the capability of TPP-DLW to the fabrication of microenvironments, which may constitute a potential platform for drug delivery system.

Moreover, Farsari's Group proposed a new approach for hard tissue regeneration based on mineralization of 3D scaffold made *via* TPP-DLW [84], illustrated in Figure 1.6. In their study, aspartate-containing self-assembling peptides targeted for calcium binding was fabricated, and the suitability of the peptides to proliferation and cell attachment was investigated by coupling on Zirconium propoxide (ZPO). The response of pre-osteoblastic cells on 3D scaffolds and surfaces was also evaluated. The results showed that the mineralized peptide coupled on ZPO strongly supports cell adhesion, enhances a proliferation, and exhibits a significant increase of bio-mineralization. This study presents a 'scaffold on scaffold' approach for hard tissue regeneration. Furthermore, the high resolution of TPP-DLW along with the fast speed of the laser writing leads to multi scale structures that are characterized by centimeter-to-millimeter sized structure possessing sub-structures of micron (or even nanometer) scale. This multi scale enables high sensitivity for detection of biological materials.

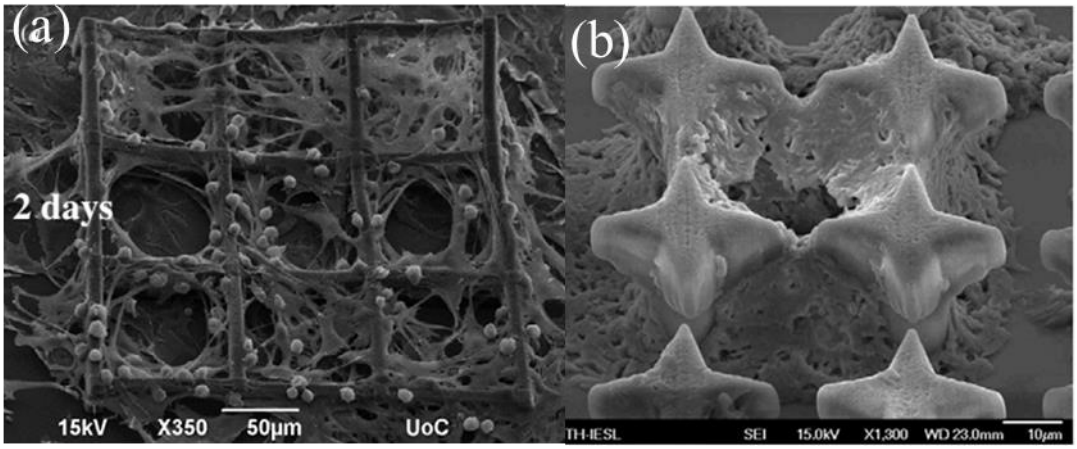

Figure 1.6: SEM images of 3D structures fabricated by TPP-DLW (a) pre-osteoblastic cells cultured on DDSGAITIG (aspartic acid–serine–glycine–alanine–isoleucine–threonine–isoleucine–glycine, a peptide) peptide-functionalized and mineralized woodpile-shaped scaffolds (b) peptide fibril-covered, calcium-mineralized 3D structures [84].

In general, it is of necessary to take the materials into consideration before fabrication. The above-referred applications are based on the use of different photoresins. It is thus crucial to select the right resin for a given aimed application.

1.2.2 Resolution of the structures *via* TPP-DLW

In the past decade, the rapid improvement of spatial resolution of the TPP-DLW fabrication has been witnessed, which shows a potential to compete with various nanofabrication processes such as electron-beam lithography, and focused ion-beam lithography. Thus, it is of prime importance to have a clear conception and measurement of resolution. In most works, resolution corresponds to the lateral and axial size of the voxels (volumetric pixels) defining the ability to differ from the neighboring features on the substrate.

Assuming the intensity distribution of the laser beam is a Gaussian, we can express the intensity distribution at the focal plane (z=0) with the following relation:

$$\mathrm{I}(r_0, 0) = I_0 \exp\left(\frac{-2{r_0}^2}{w_0^2}\right) \qquad (1\text{-}6),$$

where I_0, r_0 and ω_0 are the beam intensity at the central axis in the focus plane, the radial position within the beam, and the radius of the focused beam spot, respectively.

Furthermore, at $z > 0$, the laser intensity can be given as follows, assuming the geometry of the beam shape is given by a hyperbolic function:

$$I(r_z, z) = \frac{2P_t}{\pi\omega(z)^2} exp\left[\frac{-2r_z{}^2}{\omega(z)^2}\right] \qquad (1\text{-}7)$$

$$\omega(z) = \frac{\lambda}{\pi \tan\left[\sin^{-1}\left(\frac{NA}{n}\right)\right]}\sqrt{1+\left(\frac{\lambda z}{\pi\omega_0{}^2}\right)^2} \qquad (1\text{-}8),$$

where P_t, r_z, $\omega(z)$, λ, n, and NA are laser power, the coordinate along the radial axis of the beam at plane z, the radius of the focused beam along the optical axis (at position z), the wavelength of the laser beam, the refractive index of the medium (immersion oil), and the value of the numerical aperture of the converging beam, respectively.

The threshold of polymerization is defined as the minimum dose below which no polymerization occurs. In this sense, it can decrease the polymerized voxel size by control of the laser-pulse energy (see Figure 1.7). It is assumed that the resin cannot be polymerized, unless density of photo-induced radicals, ρ=ρ(r, z, t) exceeds the minimum one (threshold concentration) ρ_{th}. The density of radicals, ρ(r, z, t) can be calculated by [85-87]:

$$\frac{\partial \rho}{\partial t} = (\rho_0 - \rho)\delta I^2 \qquad (1\text{-}9)$$

where z is the distance to the focal plane in cylindrical coordinates, r is the distance to the optical axis in cylindrical coordinates, t is the total processing irradiation time, ρ_0 is the original initiator density. Hence, the diameter and height of the voxels can be expressed as follows:

$$d(P_t, t, NA) = \frac{\lambda}{\pi \tan\left[\sin^{-1}\left(\frac{NA}{n}\right)\right]}\sqrt{\ln\left(\frac{4\pi^2 P_t{}^2 t\left[\tan\left(\sin^{-1}\left(\frac{NA}{n}\right)\right)\right]^4}{E_{th}\lambda^4}\right)} \qquad (1\text{-}10)$$

$$l(P_t, t, NA) = \frac{2\lambda}{\pi\left[\tan\left(\sin^{-1}\left(\frac{NA}{n}\right)\right)\right]^2}\left(\sqrt{\frac{4\pi^2 P_t{}^2 t\left[\tan\left(\sin^{-1}\left(\frac{NA}{n}\right)\right)\right]^4}{E_{th}\lambda^4}} - 1\right)^{1/2} \qquad (1\text{-}11),$$

where d, l, and E_{th} are the voxel diameter, voxel length, and threshold energy for polymerization, respectively. Theoretically, according to these predictions, the variation of the voxel diameter and length depends on the laser dose, which means that the spatial resolution lies on the laser power and exposure time. Additionally, NA of the objective lens is also a dominant factor on the length of the voxel.

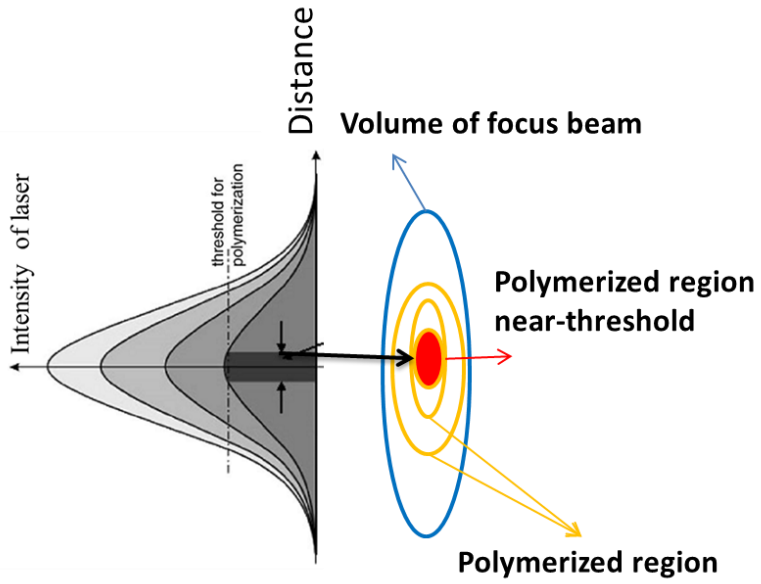

Figure 1.7: Distribution of light in the laser focus [86]

Mentioned in the above sections, in brief, the major advantages of TPP-DLW are: (i) direct fabrication without any photomask, (ii) sub-100 nm resolution, (iii) truly 3D microfabrication with arbitrary geometry, and (iv) various materials can be utilized. Therefore, there are considerable efforts on the development on this process and its applications [88]. However, there still are two main drawbacks for its widespread exploiting in both scientific area and industries. The critical bottleneck is with regard to the resolution, as up to now, the resolution is still 1 or 2 order of magnitude lower than that of other techniques such as e-beam lithography.

For the improvement of resolution, there are different solutions. Part of them may be chemical. Apart from exploiting high efficient photo initiator and advanced photosensitive resins [88, 89], using the radical quenching effect by introducing radical quenchers or inhibitors is demonstrated to decrease the voxel size [90, 91].

Xing et al. [88] demonstrated that a lateral spatial resolution of 80 nm can be achieved by using a highly sensitive initiator (9, 10-bispentyloxy-2, 7-bis [2-(4-dimethylaminophenyl) vinyl] anthracene) (BPDPA) combined with extremely low laser power and fast scan speed. There is a simple model based on two-photon excitation process and radical polymerization process. In this model, the radius R of the polymer chain occupied can be expressed as follows:

$$R^2 = \frac{a}{6} P_n b^2 \qquad (1\text{-}12),$$

where P_n is the polymerization degree, a is a constant related to the number of atoms in the monomer and b is the length of the C–C bond. The degree of polymerization can be given by:

$$P_n = \frac{k_p[M]}{k_t\sqrt{(2k_d f/k_t)[EPI]}+k_{ox}[O_2]} \qquad (1\text{-}13)$$

Here, [M], [O_2] and [EPI] are the concentration of monomer, oxygen and excited initiators, respectively, f is the efficiency of the dissociation of photo initiator, k_p, k_t, k_d and k_{ox} are the reaction rate constants of propagation, termination, dissociation of initiators, and oxygen termination, respectively. With higher efficiency of initiation, the excited initiators could be more, in terms of the following relation:

$$[EPI] = \emptyset \frac{\sigma_2}{2(h\nu)^2}[PI] \int I^2\, dt \times N_{pulse} \qquad (1\text{-}14),$$

where ϕ is the quantum efficiency for photo initiation, $[EPI]$ is the concentration of the excited initiators, $[PI]$ is the concentration of the initiator, $h\nu$ is the photon energy, and N_{pulse} is the number of laser pulse.

In this report [88], due to the high efficiency of photo initiating, the polymerization threshold decreases, leading to smaller feature size. Theoretical calculations showed the same indication that using a more sensitive initiator in the fabrication, the lateral resolution can be improved dramatically. However, for the high efficiency of photo initiating, there still needs plentiful researches involved.

With the presence of quencher, the diffused radical around the focused area is eliminated *via* termination of the chain reaction during polymerization. The group of Lu et al. [91] synthesized a novel PI with a quenching moiety to take part in an intramolecular radical deactivation in order to get a finer structure *via* a much efficient controlling of the radical diffusion. This novel PI is BNMBC, which was designed by introducing a p-methoxybenzyl moiety to the photoinitiator BNBC (3, 6-bis [2-(4-nitrophenyl)-ethynyl]-9-(4-methoxy-benzyl)-carbazole) as a radical quenching moiety.

The volumes of polymer fibers fabricated using BNMBC were decreased to 20%–30% of those formed using BNBC. However, the smallest gaps between two separate adjacent lines and no any high-resolution 3D structures have been demonstrated. Besides, in order to use BNBC, a supplemental process should be required to synthesis the photoinitiator, which is supposed to be time consuming and careful controlling.

Recently, there is another route to better control of the polymerization region proposed [92]. In their opinion, since an immobile quencher, an amine-based monomer (2-(dimethylamino) ethyl methacrylate, DMAEMA), can only result in the increase threshold, a diffusing quencher is proposed to add in the photosensitive system. In this work, this amine interacts with the monomer or become part of the final polymer backbone without conceding the mechanical properties of the obtained structure (Figure1.8). The woodpile structures with 400 nm period were achieved by this method with a single beam. To the contrary, the minimum period achievable for this PC structure was about 900 nm without using this amine-containing monomer [93]. However, the authors have found that the best resolution is achieved contribute to the quenching of radicals, only at slow scanning speed (20μm/s) where the diffusion of quencher (DMAEMA) can efficiently recovers the between line scans. As a result, the writing of high-resolution 3D structures on a large scale is seriously compromised using this approach.

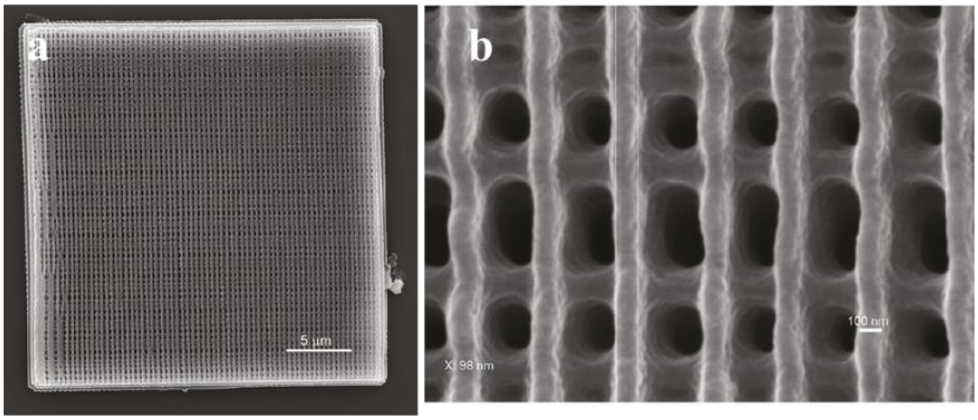

Figure 1.8: 3D amine-containing woodpile structures with 400 nm period: (a) the whole structure, (b) structure detail [92].

The resolution issue can be addressed by optical techniques to significantly reduce the voxel volume and improve the voxel shape. These approaches are controlling the excitation

volume to moderately improve the voxel *via* the optimization of the focal length of the tube lens applied [94], exploiting annular amplitude filters [95], and radially polarization of the using laser [96].

Another promising technique, which has been developed on the base of overcoming by the stimulated emission depletion (STED) microscopy, is called STED-like lithography [97]. In STED, two lasers are used, one is a short laser pulse to excite the photoinitiator molecules into the excited state; the second laser is usually at longer wavelength to deplete these chromophores back to the ground state by stimulated emission. The detailed scheme in a photoinitiator for STED is shown in Figure 1.9. The excitation laser intrigues photoinitiator to a vibrationally excited level E_1^* *via* TPA. Part of the molecules may decay back to E_0 non-radiatively. While most molecules may relax to E_1 and from E_1 they can undergo inter-system crossing (ISC) to the triplet stateT_1 or they may fluoresce. From T_1, the photochemical reaction can be occurred. In STED, a depletion laser is introduced to bring the molecules from E_1 to E_0 via stimulated emission (SE).

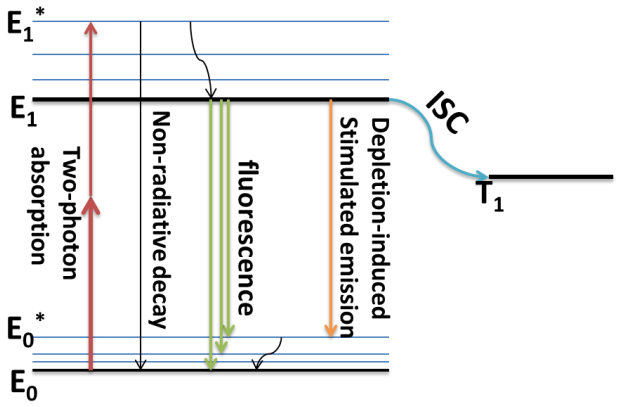

Figure 1.9: Energy level scheme with transitions in a photoinitiator molecule for STED [108]

Recently, it has demonstrated possible to attain resolution of sub-10 nanometers with STED microscopy [98]. Since 2009, STED idea started to be applied together with TPP-DLW [99]. In the frame of the STED-like lithography, there are 3 main mechanisms, (i) Two-color photo initiation/inhibition lithography (2PII), which is based on the photochemical deactivation of photo initiator [100-102], (ii) RAPID (Resolution Augmentation through Photo-Induced Deactivation) lithography which is based on photo physical deactivation process [103-105], and (iii) STED lithography [104-112].

In one case of 2PII fabrication, the photo initiator, camphorquinone (CQ)/ethyl-4 (dimethylamino) benzoate (EDAB) is excited at 473 nm and the photo inhibitor, tetraethylthiuram disulfide (TED) is activated with 364 nm radiation. The formation of cross-linked insoluble polymer network is preventing, resulting in a decreasing polymerization rate. Using a donut mode shape of deactivation beam leads to a lateral voxel of 65 nm [102]. Cao et al [100] claimed that 40 nm dots can be achieved by using a highly photosensitive resin, ethoxylated bis-phenol-A dimethacrylate based photo resin (BPE-100) in the method of 2PII. Although it is attractive to use inexpensive continuous laser, it is not a simple way to get a true 3D fabrication. Besides, the photo initiator and photo inhibitor system should be specifically chosen during 3D fabrication as the consumption of this system along the pathway of laser is space dependent on the concentration of photo-active species. Moreover, the reported approaches are based on single photon absorption, which will have a limit as focusing deeper into the photoresist volume because of the attenuation of the two lasers through the absorbing resin. On the contrary, 2PII based on TPA process could avoid this problem; however, no experiments have been ever reported so far.

In the issue of RAPID lithography, malachite green carbinol base (MGCB) was used as photo initiator. MGCB was specifically chosen due to the high extinction coefficient [103]. In the study of Fourka's group [104], an excitation beam (800 nm) with femtosecond pulse and a deactivation beam (760 nm-840 nm) with continuous mode were used using MGCB as the photo initiator. As long as the photo initiator was excited, two relatively stable radicals generated. These radicals initiate the polymerization on a time scale which is longer than that repetition time of the fs laser used. By controlling the repetition time, the radicals can not diffuse apart and absorb a photon from the deactivation beam leading to the depletion of radicals before they react. By spatial shaping of the phase of deactivation beam, 40 nm feature size could be achieved. Three broad classes of dyes are demonstrated capable to be used as photo initiator by RAPID lithography [103]. However, the resulting polymer linewidth increases as the scan speed decreases using malachite green carbinol hydrochloride (MGC-HCl) as photo initiator, which is opposite to that in the issue of using MGCB. Therefore, combining such photoinitiators and MGCB, it is possible to yield a photoresist with no scan-speed-dependent linewidth. The depletion time-constant is between 15 ms and 350 ms in the RAPID lithography, writing speed is assumed to be comprised ranging from 30 μm/s to 150 μm/s [103, 105]. In principle, the resolution of RAPID is limited by material

properties, especially the minimum size of the polymer voxel. Proper deselection of photo resist and photo initiator and precise optical configuration to make more efficient deactivation process will be promising to get a better resolution. Up to now, the RAPID lithography enables sub-100 nm resolution but is still time-consuming and complicated in the laser beam controlling. In additionally, the slow speed can be an obstacle for its use in industry.

Briefly, for efficient STED, molecules should have large oscillator strength to favor the depletion, and exhibit strong fluorescence quantum yield. Moreover, the lifetime of the excited state is long, about few ns. On the contrary, common photoinititor (PI) exhibits low oscillator strength and presents ISC during polymerization. Additionally, the excited state lifetime is usually around 100 ps. With large pulse energy, depletion computes with TPA leading to undesired polymerization. So, in the STED-like lithography, PI is of high requirements as well as the laser condition (wavelength, scan speed, pulse delay). Compared to the resolution of STED nanoscope reaching to sub-10 nm, STED-like lithography resolution is still an order of magnitude weaker. This is not surprising according to its high requirement on the PI used and laser beams. However, owing to its current and unique fabrication potential regarding to its high scan speed as 5 $m \cdot s^{-1}$[107], growing interests will be expected in the future. Until now, there are several applications in photonics. For instance, 3D polarization-independent carpet cloak for visible light have been fabricated by the Wagener's group [106] and also 3D photonic crystals [108] which for the first time, the lateral resolution is exceeding the lateral Abbe criterion. In particular, 3D photonic crystals fabricated by STED-DLW using pentaerythritol tetraacrylate (PETA) as monomer and 0.25 wt.% DETC as photo initiator show brighter colors than those made by regular DLW (Figure 1.10). These colors correspond to the Bragg-reflection of periodic structure. For a given period, the structures are much more colorful compared to those made by regular DLW, which means that the structures have larger sizes in STED-DLW. Obviously, STED-DLW allows for significantly smaller periods while maintaining functionality and stability. Additionally, STED-like lithography has been investigated for data storage application [109], and for fabricating nano-anchors used in biology [110].

Although the resolution of structures is improved by STED-DLW, two laser beams are necessary, many parameters have to be controlled (frequency, pulse duration time, wavelength, laser power, etc.) and extra modification is supposed to be done with the

deactivation beam shape with the purpose of obtaining a finer structure. Additionally, as mentioned former, the photoinitiator is specifically chosen.

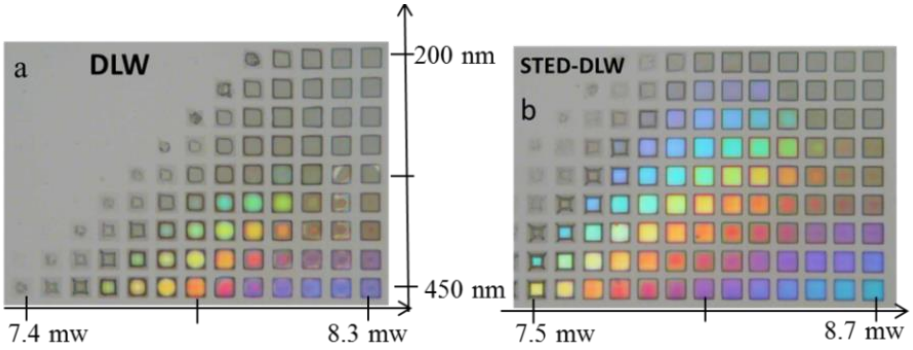

Figure 1.10: Color reflection-mode optical graphs of woodpiles which have 24 layers with size 20×20 μm^2 (a) fabricated *via* regular DLW; (b) fabricated by STED-DLW. [108]

Last but not the least, other methods have recently been put forward into the improvement of the resolution. For example, *via* combination of chemical and optical approaches, 40 nm feature size can be achieved [111]. In this work, from the chemical point of view, by adding cross-linker DPMA (pentacrylate derivative) to the sol-gel Zr-hybrid material to tune the chemical process of TPP, a feature size of 82.5 nm can be achieved compared with 150 nm in the case without addition of DMPA exposure with a 50 fs pulse laser (1 MHz). Additionally, without addition of cross linker, the feature size can also be improved to 90 nm *via* the use of 8 fs laser (80 MHz) instead of the use of 50 fs laser. Moreover, combining together the use of 8 fs laser and addition of DMPA, the feature size of 45 nm can be reached, as shown in Figure 1.11. Nevertheless, no further enhancement of the resolution in 2PP with this used materials and laser system is expected owing to the determined energy threshold which is close to the TPP fabrication.

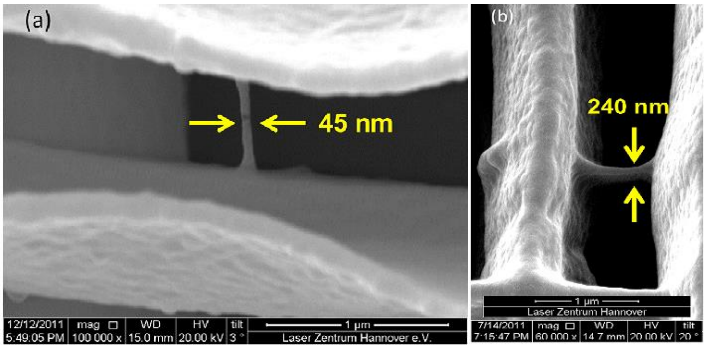

Figure 1.11: SEM images of the free hanging line structure : (a) Magnification:100000 x, (b) the same structure observed under an angle of 20°. Magnification: 60000 x [111].

To conclude, the developments of TPP-DLW and improvement of resolution have attracted growing interest in the recent decade. The diffraction limit has been broken *via* STED-like lithography or quenching assisted TPP-DLW. However, specific laser systems are required of precise controls and adjustments (deactivating laser intensity, pulse duration time, shape mode, initiating laser intensity, etc.) are needed. Additionally, the photosensitive systems should be specifically chosen (special photo initiator, special photo resist, photo inhibitor, etc.). The writing speed is generally pretty slow. New techniques and new photosensitive systems are still required to obtain intrinsic resolution improvement with low cost simple process, common commercial materials and less time-consuming procedure.

In this thesis, a common quencher (MEHQ) has been utilized with PETA resin for the fabrication *via* TPP-DLW. The process is supposed to be simple to repeat and carry out with fast speed and improved resolution in both 2D and 3D structures.

1.3 Hybrid 3D luminescent structures via TPP-DLW in photopolymers containing QDs

Photopolymerizable resins have been broadly used in the fabrications of 3D structures. Considering the functional devices for further applications in optics, electronics, MEMS/NEMS, photonics and biology, the materials used for 3D manufacturing are required to be functionalized. Hybrid 3D luminescent structures with high emission efficiency and resolution are of great interest for photonics.

Luminescent semiconductor quantum dots (QDs) have drawn tremendous attention due to their unique optical properties in the recent decade not only for the diagnostic and sensory but also for photonic/plasmonic applications [112, 113]. Since the first synthetic water-soluble QDs achieved in 1998 [114], numerous researches have been put forward to the QD synthesis, which will not be mentioned and described in this thesis. Excellent reviews or reports can be found [e. g. 115,116]. In this thesis, a brief introduction on the optical properties of QDs and hybrid QDs-polymer 3D patterning *via* TPP-DLW, as well as the coupling of QDs with surface plasmon resonance will be presented. The basis of this thesis is working on the fabrication of hybrid 3D plasmonic structures containing QDs *via* TPP-DLW.

1.3.1 Optical properties of QDs

Nowadays, mostly used QDs are mainly composed of CdSe (cadmium selenide), as well as synthesized by using II-VI groups such as CdTe, CdS, ZnS, III-V groups like InAs, InP, GaAs, or IV-VI materials. Normally, these QDs exhibit emission in the range from ultraviolet (UV) to near infrared (NIR) [114-116]. Due to the small size of QDs, with a diameter of 1-10 nm, they exhibit exciting optical properties compared to the bulky semiconductors [114,117]. As shown in Figure 1.12, QDs possess valence band and conducting band as classical semiconductors, and the energy of the band gap is related to the size. The resulting emission wavelength thus depends on the size too. When a photon is absorbed by a QD, an electron-hole pair is formed as the electron is promoted from the valance band to the conducting band by energy absorption. In the same time, the missing electron in the valence band leaves a hole with opposite charge, resulting in an exciton. Then, by the related Coulomb force, this hole will promote electron. By this way, light with a wavelength related to bandgap energy is emitted though exciton relaxation [114,117].

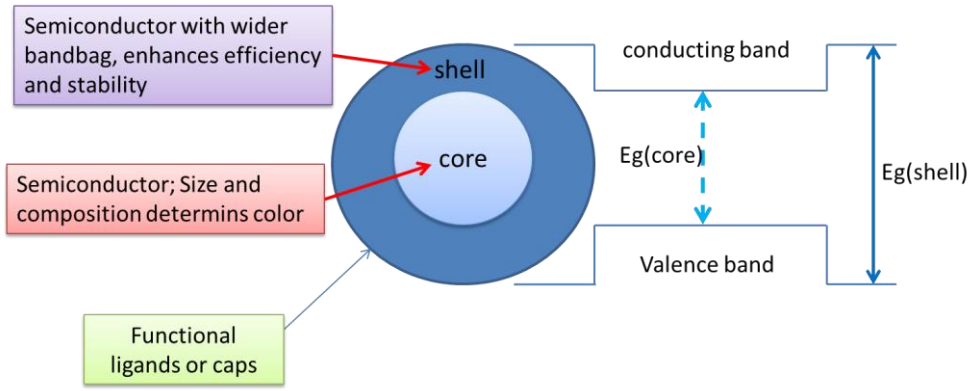

Figure 1.12: Schematic representation of QDs and their band structure [Eg: energy gap].

Due to the quantum confinement effects, QDs have unique optical and electronic properties, as compared to organic molecules and bulky semiconductors:

- They exhibit high fluorescence quantum yields and high stability against degradation and photobleaching compared to conventional fluorophores [117-119], which enables QDs for highly sensitive detection;
- They possess size-controlled and shape-controlled absorption and luminescence features, contributed to the quantum confinement of the electrons in the particles: small QDs have bigger bandgaps, the luminescence energies are blue-shifted to higher

energies [120,121]. Besides, nonsymmetrical particles such as rods exhibit longitudinal excitons controlled by the aspect ratio of the nano-objects. Luminescent properties covering broad spectral region can be available by controlling the size and shape of QD;

- The fluorescence spectra of QDs are usually characterized by narrow emission bands compared to conventional organic fluorescent dyes, as a result, the fluorescence signal of QDs can be significantly separated from the light of excitation source, which is of benefit to coupling with other functional molecular (either QDs or organic fluorophores) [122,123];
- Due to the core-shell structure of QDs, seen in Figure 1.11, and the advancing synthetic methodologies, tailored functionalities can be added to the QDs, allowing the electronic or plasmonic coupling [124,125].

Owing to these unique properties and the developments on the synthesis as well as the surface functionalization strategies, QDs have given rise to a wide range of applications in imaging, electroluminescent devices, lasers, photonic crystals photodetectors, photovoltaics, organic light emitting diodes, etc. [126, 127]. It is of great importance to guarantee the photoluminescence (PL) stability of QDs in solid state when incorporated in light emitting materials and devices. However, there are still some challenges to fabricate efficient light emitting devices involving QDs: (i) QDs PL quantum yields can be reduced *via* a solvent transfer step during the fabrication procedures, for example, altering the initial ligands of QDs surfaces leads to decreased quantum yields [128]. (ii) PL QYs can be significantly decreased by continuous excitation in solid state taking account of the moisture, oxygen, heat and especially light unlike solution phase where there typically exist excess of surface ligands passivating the QD surface. [129]. (iii) QD aggregation can lead to red-shifted optical spectra [130, 131]. There are several strategies to solve this PL quantum yield decrease via a solvent transfer: exchanging the surface ligands [129], addition of a second layer, encapsulating QDs into amphiphilic molecules, such as polymers [132] that can improve the solubility of QDs in the matrix, as well as through in-situ nanocrystal growth, electo-static interactions and cross-linked processes [128]. However, these methods could not yield nearly monodispersed QDs at the delicately required size for their optical properties and photoluminescence

quantum yield. There are still increasing researches devoted to the synthesis the water-soluble QDs with high photostablity which is not in this thesis.

With regard of advantage of TPP-DLW, hybrid 3D luminescent structures can be available to fabricate with the QDs-containing photosensitive resins. Furthermore, in view of the QDs application for optical sensing, quantum communication, energy conversion and storage, the interaction between the emitter and the local optical environment is of paramount importance to be explored, which can also offer the prospect of exploiting nano-fabrication techniques to design quantum optical systems. In this thesis, there will present several researches involved the coupling between QDs and surface plasmons.

1.3.2 Hybrid QDs-polymer composites and fabrication in TPP-DLW

With the aim of getting hybrid luminescent 3D structures fabricated by TPP-DLW, it is requisite to prepare QDs-polymer resin. To the best of our knowledge, the reports of 3D luminescent QDs-polymer structures have not been of widespread coverage [70]. The possible reason for this is that uniform dispersion of QDs in photosensitive resins is hindered by separation and cluster aggregation with regard of the solubility of QDs in the matrix-resin. In turn, the inhomogeneity of dispersion makes the photo resin non-transparent, which is detrimental to the fabrication of 3D structures *via* TPP-DLW.

One of the routes to prepare QDs-polymer composite is chemical modification of photosensitive moiety or special treatment on the reactivity of QDs surface to the polymer matrix. Suitable ligand of QDs can ensure their good adhesion with the polymer matrix and avoid their aggregation; as a result, homogenous dispersion of QDs can be obtained. Alternatively, the photo resin can also be functionalized with suitable organic groups enabling the effective interaction with QDs. For instance, an epoxy photosensitive resist with presynthesized trioctyl phosphine oxide/trioctylphosphine (TOPO/TOP)-capped CdSe/ZnS QDs solved in combination of selected solvent was used in UV lithography to fabricate 3D structures [133]. The solvent used for dispersion plays a significant role on the photoluminescence of QDs [134]. Thus, in the modification of QDs or organic groups, it is possible to get the photo resist lack of the ability to structuring.

Given that the emission properties of QDs is dependent on the size, in order to realize 3D structure of QDs-polymer and to facilitate their application in photonic devices, it is of importance to explore a feasible, reliable and suitable approach to fabricate 3D structures of

QDs-polymer composites with controllable size of embedded QDs. There are several methods to get the hybrid QDs-polymer 3D structures, such as doping metal solutions into resin and in-situ synthesis during DLW. For example, Titanium (IV) (Ti^{4+}) ions were doped in SCR 500 photo resin [68]. During the polymerization by DLW, TiO_2 nanoparticles were generated in the 3D photonic crystals that consisted of polymer-composite. The photonic bandgap of this diamond photonic crystal was confirmed. In the base of this, it should be likely to obtain 3D micro-scale or nano-scale structures with unique properties using various functional materials, such as nanoparticles and QDs.

It was reported that CdS-polymer nanocomposites were in-situ synthesized during polymerization [135]. The emission property of this composite can be efficiently controlled by adjusting the molar ratio of acrylic acid to cadmium acrylate in the designed resins. The same group also illustrated the capability of 2D and 3D structures of CdS-polymer composites combining the use of laser interference, as illustrated in Figure 1.13 [136]. However, this laser interference beam technique requires extreme controlling on four laser beams while in TPP-DLW, only one laser beam needs to be optimized.

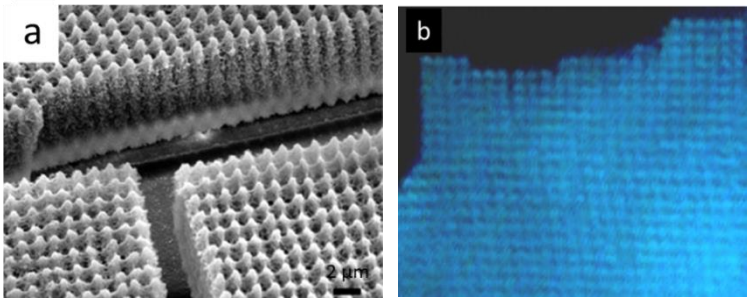

Figure 1.13: Microstructures of CdS–polymer nanocomposites fabricated by the laser four-beam interference technique (a) SEM image and (b) fluorescent image [136].

For fabrication *via* TPP-DLW, materials should be transparent at the wavelength of the laser used. Therefore, the well dispersion of QDs in the photo resins plays a key role in keeping the resin transparent. Apart from the above-mentioned method, there is another routine to functionalization of QDs-polymer resin [137]. As reported, core-shell CdSe/ZnS QDs composed of a photopolymerizable methacrylate outer corona constituting methacrylate and an inner siloxane layer was synthesized, shown in Figure 1.14. It was also demonstrated that this functional QDs can be uniformly dispersed into a photopolymerizable resin to fabricate QDs embedded 3D microstructures. On the basis of this report, acrylate and urethane acrylate resin integrated with acrylate-terminated QDs were able to fabricate

microstructures with uniform quantum dot dispersion by TPP-DLW, which shows the potential of these functionalized nanomaterials for application in full color display devices.

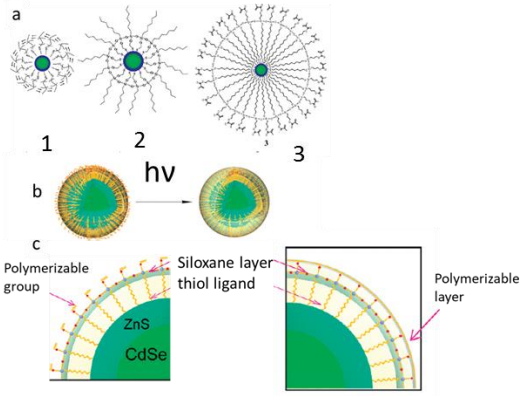

Figure 1.14: (a) 3 types of QDs synthesized: 1 the alkyl-terminated, 2 siloxane inner layer containing alkyl-terminated, 3 QD with siloxane inner layer and the photopolymerizable methacrylate corona (b, c) Working of the photopolymerizable corona. The methacrylate groups in the outer periphery of 3 are photopolymerized in (b) [137].

In brief, up to now, much effort has been put forward on achieving homogenous photosensitive and patternable QDs embedded photo resins with the aim of fabricating 3D luminescent nanostructures. However, in these recent years, no report has been focused on the resolution issue of QDs-polymer structures *via* TPP-DLW, which can be important to control the fluorescent properties or functionalities with clear awareness on the influence of parameters on the resolution.

1.3.3 QDs coupling with plasmon

A surface plasmon polariton (SPP) is an intrinsically surface electromagnetic wave associated to a 2D electronic excitation on the surface of metal. The electromagnetic field is confined to the near vicinity of the dielectric–metal interface and decays exponentially with distance from the surface [138]. Owing to this confinement effect, the electromagnetic field at the interface is strongly enhanced, leading to an extraordinary sensitivity of SPPs to surface conditions (surface roughness, adsorbates on a surface…) and making possible surface-enhanced optical phenomena like second harmonic generation (SHG), fluorescence, and Raman scattering [139,140]. This sensitivity allowed for development of many kinds of SPP-based devices including sensors and detectors [141,142]. The 2D nature of SPPs provides the flexibility in integrating SPPs-based circuits for optical communication and optical computing [143,144].

As mentioned in the previous section, QDs are a kind of materials that exhibit tunable optical properties and possess high photoluminescence quantum yields, making them promising in developing plasmonic devices [145]. In addition, QDs have already shown as quantum emitters and remarked as an attractive candidate for single photon sources which is essential key in the optical quantum information processing [146-149]. With the aim for quantum optics application, the crucial point is the coupling of QDs with nanostructured environment (nanowires, waveguides, micro cavities, films…).

There are several reports working on cavity-enhanced light-matter interactions, which are based on the strong coupling between QDs with various shaped cavities [150-153]. This pushes the optoelectronics down to single particle level. In the near future, local quantum information of electronic states can be transferred over large distances, which is fascinating: it would be possible to entangle different electronic states at different locations in integrated photonic circuits. For instance [151], by drop-casting CdSe QDs on a gold (Au) subwavelength hole array, the strong coupling can be achieved with SPP modes and excitons of QDs (see Figure 1.15). Rabi splitting energy up to 220 meV can be obtained leading to a phonon bottleneck effect. High Rabi splitting energy means a higher light-matter interaction. However, further efforts are necessary in the fabrication technology by controlling the QDs position and the fabrication of cavities without post-fabrication tuning by deposition or monolayer oxidation. These can be possibly available *via* TPP-DLW although since now no reports have ever mentioned.

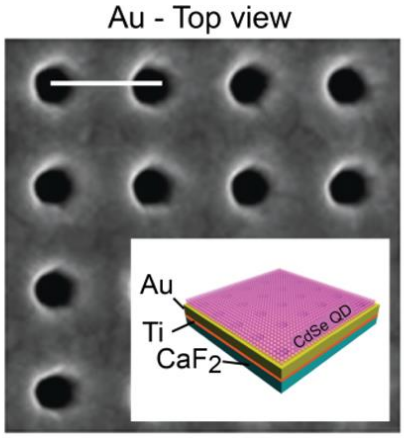

Figure 1.15: SEM image of Au hole hybrid nanostructure. The white bar is 350-420 nm. The inset shows the overall device: From top to down is CdSe QDs layer, 200 nm thick Au layer, 5 nm Ti layer and a thick layer of CaF_2 [151].

The simplest plasmonic structure is a thin metallic film supporting propagating surface plasmons [152]. Gómez D.E. group [153] has demonstrated that strong SP coupling between CdSe QDs and an Ag film can be obtained, and 112 meV of Rabi splitting energy can be achieved at room temperature. This coherent interaction provides an opportunity to develop nonlinear plasmonic devices and study the regime of the coupling in this QDs-film system. In their following study [154], this CdSe QDs-Ag film system was used to study the dynamics of coupling *via* the investigation on the steady-state and transient reflectivity measurements in the Kretschmann geometry. It was found that the wave vectors and compositions of hybrid exciton/SPP states are dependent on the angle of incident probe beam, see Figure 1.16. Moreover, the dynamics in transient reflectivity measurement are sensitive to the composition of hybrid states. The obtained results might be important for applications like amplification of SPPs by optical pumping of a surrounding gain medium.

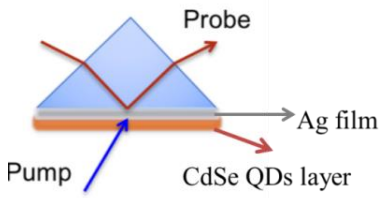

Figure 1.16: Diagram of the experiment for strong coupling [153].

Plasmonic optical antennas are broadly used to control the luminescence of (single) photon sources in order to enhance emission rate, enhance light emission intensity and control the direction [155]. This kind of coupling corresponds to a weak coupling.

On the other hand, the coupling of single emitters to optical waveguides is critical to on-chip photonic applications, thus, much attention are devoted to the coupling between emitters and crystal waveguides[156], plasmonic waveguides [150, 147] and nanowires [159, 160].

Coupling quantum emitters to nano-scale photonic waveguides enables to concentrate and channel light, which is promising for realization of single-photon transistors and single-photon sources. For instance, by dispersing CdSe/CdS QDs onto Ag 2D gratings, SPPs were excited to propagate along the surface, which makes the luminescence of QDs enhanced, polarized and well-directed [156]. Recently, a device, which consists of two orthogonal waveguides, shown in Figure 1.17, with a single InAs/GaAs QD locating 90 nm from the center of the intersection along the diagonal, was demonstrated to be capable to optical

control of emission direction by the polarization of the optical pump and the directional control can reach to ±35% [147]. However, to achieve high efficiency coupling, it still requires appropriate waveguide configuration and deterministic coupling mode between the QDs and waveguide, which can make sure that the coupling system exhibits moderate losses as well as strong mode confinement.

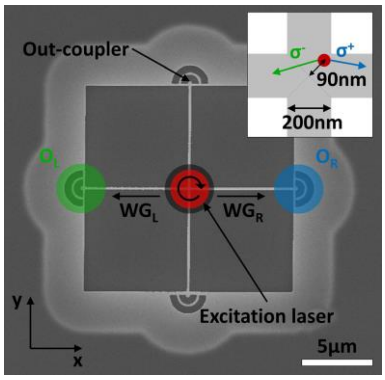

Figure 1.17: SEM image of the crossed-waveguide device and FDTD simulation of coupling between QDs and waveguides [147].

Coupling QDs into plasmonic nanowires (NWs) has potential applications in bioanalysis, optics and quantum plasmonic devices. In QDs-NW system studies, there are 3 different processes. Shown in Figure 1.18, process I, when the laser was focused on one end of Ag NW, surface plasmon was launched and propagate on the NW. Process II illustrated that the excitation of QDs leads to the propagating surface plasmons in the NW [158, 159]. In process III, the launching of SPs at the discontinuity of NW leads to generation of the excitons owing to the interaction of SPs with QDs, and the excitons would decay in form of photons [158]. However, the ability to remotely excite SPs needs elaborate designing of functional plasmonic structures.

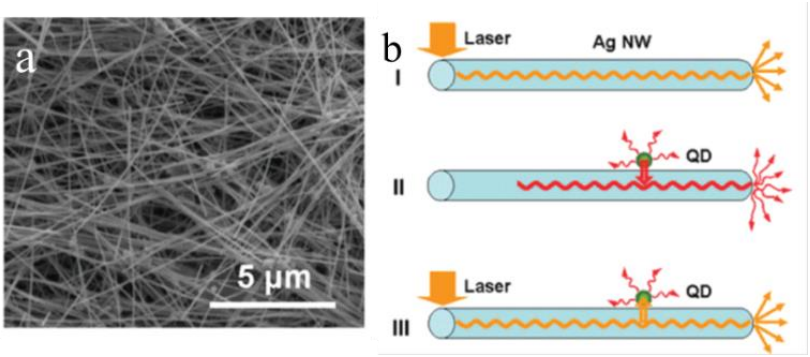

Figure 1.18: (a) SEM image of the Ag NWs. (b) Schematic illustration of the processes of the Ag-QDs system [158].

In brief, in most researches, chemical growth of QDs deposited on the NWs, or by two-step EBL depositing QDs onto waveguides, or spin coating QDs on the metallic films were used in order to achieve the coupling of QDs with SPs [147-159]. In this sense, the localization of QDs is either by random, or with complicated procedures. Regarding the advantage of TPP-DLW, it may enable us to achieve the localization of QDs in the detersive position with given geometry and size, which is promising in the application on the integration of quantum emitters in photonic, electronic or bio-sensing devices.

1.4 Summary & motivations of the thesis

In this chapter, we have enumerated several solutions of improving the resolution *via* TPP-DLW including photochemical and optical routes. By optical techniques, although the voxel volume can be reduced, however the alignment of the laser system is in extremely precise demand and the limitation of the resolution still depends on the diffraction limit of the optical devices. Additional constrains including 2 lasers, specific spatial shaping mask and and photo initiator are required. Common inhibitor, MEHQ which is going to be utilized in this work, along with the use of TPP-DLW, 3D structures with improved resolution is supposed to obtain fast and easy-in-procedure.

Hybrid 3D luminescent structures are essential to the optical devices. Regarding the unique properties of QDs, QDs-polymer 3D structures have been showing the great potential in various fields such as in biology, optics, plasmonic, etc. Emission properties of QDs-polymer hybrid structures and synthesis of QDs-polymer photo resins have been reported. As far as QDs containing photopolymers, laser parameters, involved physical and chemical phenomenon, and resulting spatial resolution have never been studied in details. Therefore, in the following chapters, the fabrication of high resolution and hybrid QDs-polymer 2D/3D structures will be deeply discussed. In both cases, the influence of inhibitor and QDs on the resolution as well as writing parameters will be studied. The improved resolution of the prepared structures containing QDs was realized *via* TPP-DLW.

Last but not least, the enhanced effects of surface plasmon polaritons with the presence of QDs make the hybrid 2D/3D QDs structures promising in the future application in emitters' optoelectronic devices. Among variety of researches on the hybrid nanoemitters-metal

plasmonic structures, the most frequent method is by chemical growth or simple deposition of QDs, which the localization of QDs is by random. In chapter 4, the coupling of QDs with nanowires and waveguides will be presented. In particular, we will discuss the use of direct laser writing method for the control of QDs localization relatively to the geometry of photonic and plasmonic structure they are coupled to.

Chapter2. Experimental details

2.1 Introduction

In this thesis, combination of TPP-DLW and addition of inhibitor, here is MEHQ, is the main method to fabricate 3D structures with improved resolution. Characterizations of resolution on the samples (either containing MEHQ or without addition of MEHQ) allow us to highlight the improvement of resolution resulting from the use of MEHQ in the procedure of fabrication.

Hybrid 3D luminescent structures can be obtained in this work using PETA grated QDs. The luminescent properties and resolution of the obtained structures will be characterized.

This chapter presents the details in all experimental processing involved, beginning with the materials used, followed by the set-ups, fabrication and characterizations.

2.2 Materials for polymerization

PETA(pentaerythritol triacrylate), well known for multifunctional acrylates widely used[41-46, 123], is a viscous liquid, in which small quantity of initiator is usually soluble, that enables DLW in bulk material without additional, time consuming processing such as post-exposure bake and specific development time. The properties of PETA, as well as those of other used species, are presented in Table 2.1. IRGACURE 819 is a versatile photo initiator for radical polymerization of unsaturated resins upon UV light exposure. Given to this, the polymerizable resin used in this work is PETA (Sigma-Aldrich), with 1 wt. % photo initiator IRGAURE819 (Ciba Co.). A radical inhibitor, 4-methoxyphenol (MEHQ, Sigma-Aldrich), is added in some formulations to improve the spatial resolution of writing. All the molecular formulas of the chemical components are shown in Figure 2.1.

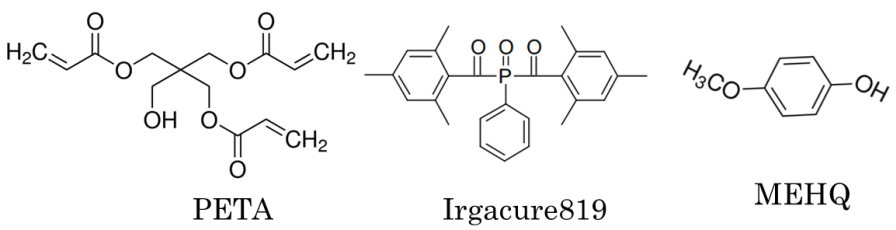

Figure 2.1: Chemical molecular formulas

Table 2.1: Properties of PETA, Irgacure 819 and MEHQ

	PETA	IRGACURE819	MEHQ
Molecular formula	C14H18O7	C26H27PO3	C7H8O2
Molecular weight	298.28852 g/mol	418.46 g/mol	124.14 g/mol
Form	Gel	Yellow powder	Neat
Viscosity	790 (mPa.s at 25°C)	-	-
Melting Point	-	127-133 °C	54-56 °C
Refractive index	1.485	-	-

The PETA grafted QDs used in this work were provided by Nanyang Technological University, in the context of the France-Singapore international project "ACTIVE-NANOPHOT".

Table 2.2: PETA grafted QDs

PETA grafted QDs	Emission color	Maximum Emission wavelength	Composition	Size
QDs G	Green	501 nm	CdSe/ZnSeS	7 nm
QDs R	Red	620 nm	CdSe/CdS/ZnS	8 nm
QDs B	Blue	460 nm	ZnCdS/ZnS	6 nm

Three formulations, shown in Figure 2.2, were tested. The composition is given in Table 2.2. QDs G were prepared using one-pot synthesis method [123, 161]. QDs R and QDs B were prepared by multiple injection method [161]. The details are described as follows: In a 50 ml 3-neck flask, 0.1 mmol of cadmium oxide (CdO), 4 mmol of zinc acetate ($Zn(Acet)_2$), and 5 mL of oleic acid (OA) were loaded and heated to 150 °C under vacuum leading to the formation of cadmium oleate ($Cd(OA)_2$) and zinc oleate ($Zn(OA)_2$). Following by the addition of 20 ml of 1-octadecene (1-ODE) in the flask, then the reactor was filled with nitrogen (N_2) and heated up to 300 °C. As the temperature elevated to 300 °C, 4 mmol of sulfur (S) and 1.6 mL of trioctylphosphine (TOP) dissolving 0.15 mmol of selenium (Se) were injected into the flask swiftly. The reaction mixture was maintained at 300 °C for 10

minutes in the reactor for the green emitting QDs growth. As for the synthesis of red-emitting QDs, 2 mmol of Zn $(Acet)_2$, 1 mmol of CdO and 5 mL of OA were loaded in a 3-neck flask and heated to 150 °C under vacuum. Then, 25 mL of 1ODE was added in the same flask and the reactor was then filled with nitrogen and heated up to 300 °C. At 300 °C, 0.2 mL of TOP dissolving 0.2 mmol of Se was promptly injected into the flask. After 150 seconds, 0.3 mL of dodecanethiol (DDT) was slowly added into the reaction system. 20 minutes later, 1 mL of TOP dissolving 2 mmol of S was injected into the flask at 300 °C for 10 minutes in order to grow the QDs. The synthesized QDs were cooled down to 25 °C and then extracted by acetone and methanol, finally centrifuged. The as-prepared QDs were finally dispersed in PETA with a concentration of 5 mg/mL under vigorous magnetic stirring.

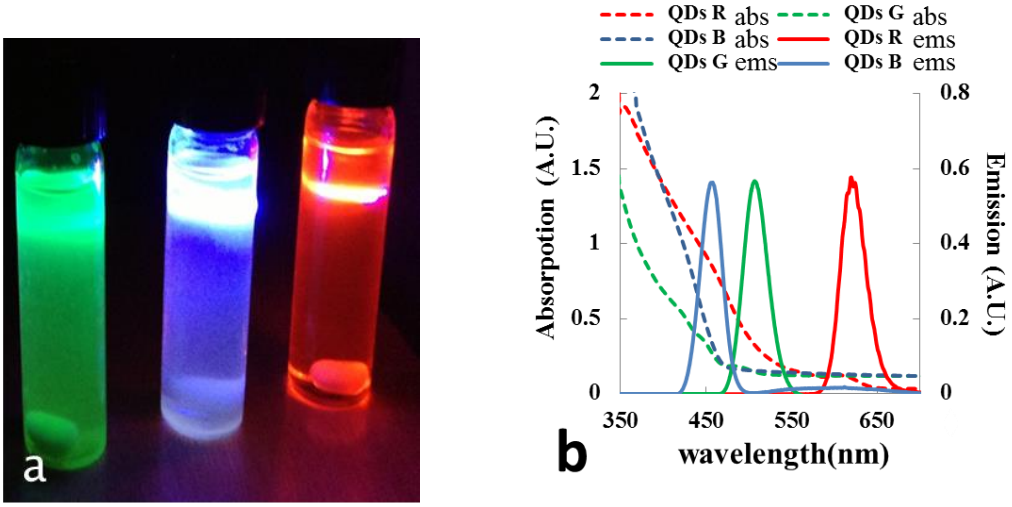

Figure 2.2: (a) Photoluminescence images of QDs-grafted PETA excited by UV lamp (b) absorption and emission spectra of red emitting QDs, green emitting QDs and blue-emitting QDs respectively.

2.3 Setup for photopolymerization

As writing system, we use Photonic Professional GT from Nanoscribe GmbH Company, shown in Figure 2.3. This set-up is embedded along the 3D printing workflow and combined with software package (NanoWrite, DeScribe). It enables the rapid fabrication of high-resolution structures in a high degree of automation. "DeScribe" is the tool here for generating writing jobs in the format of General Writing Language (GWL), which enables the import with mesh-fixing in STL format automatically. GWL scripts can also be edited using Describe to control the laser focus movement and writing process. In addition, it can provide an interactive 3D preview with voxel visualization. NanoWrite is the user-friendly graphical interface for operating the DLW process.

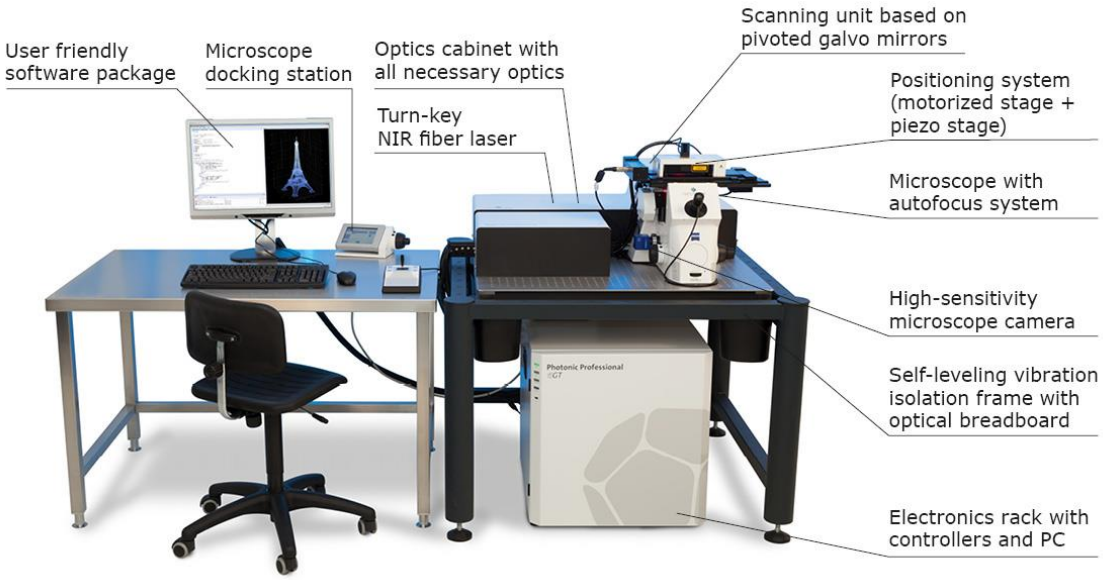

Figure 2.3: Photo of Photonic Professional GT from Nanoscribe GmbH [162].

For the fabrication, a pulsed Ti: sapphire laser at 780 nm was used as an irradiation source. The laser beam is focused by a microscope objective lens (100×, Zeiss oil lens with N.A=1.4) into the volume of the photoresist, which is mounted on a XYZ positioning stages. By moving the laser focus, 3D structures with complex patterns can be written.

2.4 Procedures

2.4.1 Two-photon polymerization fabrication

Substrate cleaning

It is known that rigorous impurities controlling is important in microscale/nanoscale fabrication in order to avoid contamination with dust particles or other chemical elements. The substrate cleaning is critical. Herein, the glass substrates used in this work are 170 μm-thick coverslips. Usually, they have to be cleaned. The cleaning is all done in ultrasound. The substrates are sonicated at 45 degree in Decon 90 solution (2%-5% of concentration in distilled water for 10 minute). Then they are rinsed with distilled water for another 5 min. It is followed by rinsing in acetone and then isopropanol for 5 min in each. Finally, they are dried with N_2 blow.

2D/3D microstructures design and fabrication

As mentioned above, the script should be in ".gwl" file format, herein, we made use of the Describe software to design the microstructure expected with 3D or 2D location parameters. For some complex structures, Blender software can be also used although the ".stl" file should be sliced by Nanosclier software to get the final script. All the scripts should follow the set phrase mode with variable parameters (laser power, scan speed, repeat times, and the coordinates in xyz direction…) which can be used in Nanowrite.

Writing

For the writing the laser used was a pulsed laser at a wavelength of 780 nm with an average output power of 120 mW at 120 MHz. As seen in Figure 2.3, resin was drop-casted on the coverslip glass which was mounted 3D piezo. Then start the writing job scripts by Nanowrite.

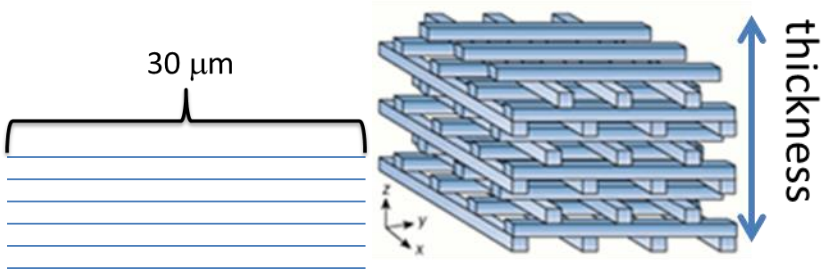

Figure 2.4: Schematic diagrams of 2D lines and 3D woodpiles

In this work, 2D lines with a length of 30 μm in different periods and 3D structures such as woodpiles with a size of 20 × 20 μm were written in three resists. These structures are illustrated in Figure 2.4. The details for the writing and compositions of the photochemical formulation are listed in Table2.3 and Table 2.4. With the aim to figure out the influence of the resolution of the structures obtained, the structures were fabricated in different writing parameters such as scanning speed and laser power with variable period of the structures.

Table 2.3: Type of photoresists and writing parameters used for the 2D lines.

Photoresist	**Laser power (mw)**	**Scanning speed(μm/s)**	**Period(nm)**
PETA+IRG819(1 wt.%)	6-20	100	250-1000
PETA+IRG819(1wt.%)+MEHQ	8-20	100	250-1000
PETA+IRG819(1 wt.%)+QDsR	8-20	100	250-1000

Table 2.4: Type of photoresists and writing parameters used for the 3D woodpiles.

Photoresist	Laser power (mw)	Scanning speed (μm/s)	Period (nm)
PETA+IRG819 (1 wt.%)	8-14	100	250-1000
PETA+IRG819 (1wt.%)+MEHQ	8-14	100	250-1000
PETA+IRG819 (1 wt.%)+QDs R	8-14	100	250-1000

Sample development

In order to remove the unpolymerized resists, the sample is immersed in acetone for 10-15 minute, and rinsed in isopropanol for 5 minute. Lastly dry it with N_2 blow softly. For example, the polymer lines after development can be observed by optical microscope, shown in Figure2.5.

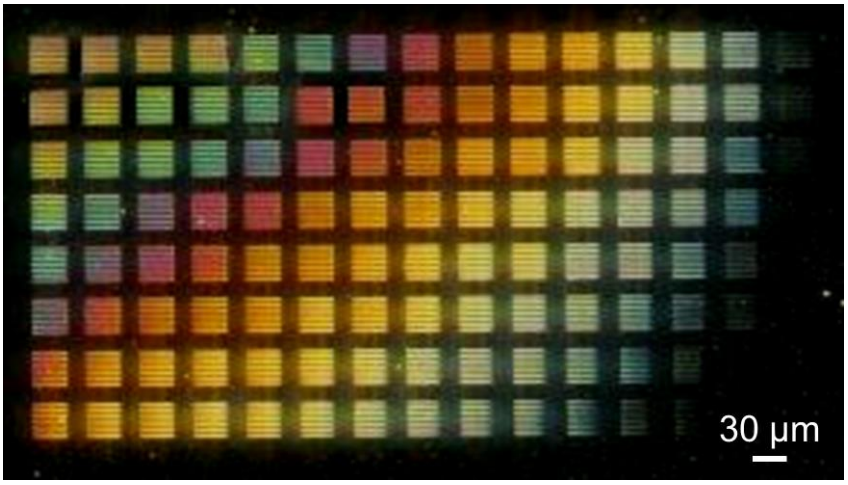

Figure 2.5: Dark field Optical microscope image of the polymer lines fabricated *via* TPP-DLW (after development).

2.4.2 Fabrication of plasmonic coupling gratings and deposition of silver nanowires

Hybrid luminescent structures are of great interest in applications such as photonics and optics. On-chip integration of solid-state photonic and plasmonic systems has attracted increasing interest in emerging technologies. Considering the challenges to integrate QDs on plamonic or photonic devices, novel routes have been in exploration for recent decades. This thesis is devoted to realization of the local integration of QDs into different plamonic and photonic structures. Here, for example, QDs were supposed to locate on Au-gratings and Ag-nanowires.

2.4.2.1. Fabrication of Au-gratings

The gratings were fabricated by electron beam lithography (EBL), which is a technique extensively used to manufacturing the waveguides and gratings. In simple terms, as for this method, the polymethyl methacrylate (PMMA) is used as a mask, on which by electron beam, the designed patterns can be obtained. The procedures specified in this case are listed as follows (shown in Figure 2.6):

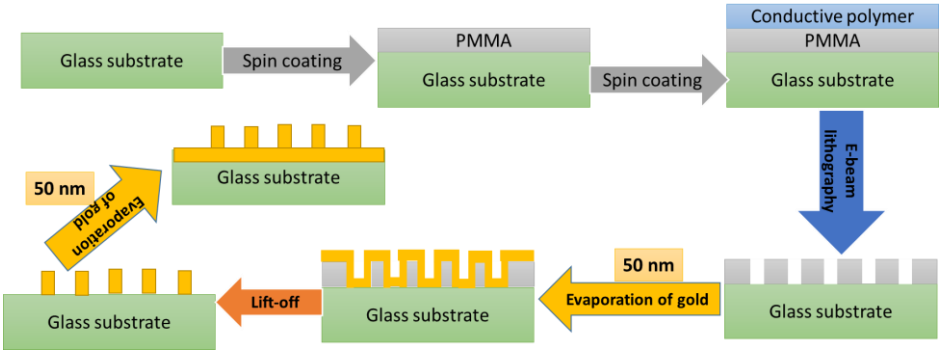

Figure 2.6: Scheme of electron beam lithography procedures on glass substrate for the fabrication of gold gratings

Spin coating of PMMA

The PMMA utilized is solved at a concentration of 30 g/L in methylisobutyl ketone (MIBK). A PMMA layer of around 150 nm thickness is needed for the 90 nm gratings. The spin coating parameters are 4000 rpm/s of speed, 3000 rpm/sec of acceleration speed and time of 30 sec. Given to the conductivity of PMMA, a conductive polymer layer is of necessary to be coated before lithography.

When the spin-coating is done, it is followed by a heating procedure, which is in order to evaporate MIBK and have fewer defects in the layer as well as dissipate the stress in the film. To heat the substrate is putting it on a hot plat at 170 °C for 15 min.

Electron beam lithography

HITACHI S-3500 scanning electron microscope (SEM) is used in this procedure. Patterns of the gratings are designed by the software Design CAD. The irradiation condition is under the control of the nanometer pattern generation system (NPGS). A tension of 30 kV and 10 pA current are used.

Sample development

Firstly, it is required to remove the conductive layer by simply rinsing in deionized water in 1 minute. In order to remove PMMA, the sample is immersed in MIBK:IPA (1:3) solution for 1 minute, and rinsed in IPA for 1 minute. Lastly, the sample is dried with air.

Evaporation of Au layer (two times)

For the gratings designed, a layer of gold with a thickness of 50 nm is needed. The evaporator PLASSYS is used for the evaporations.

Lift-off

The sample should be immersed in acetone for about 12 hours to dissolve the PMMA film. Afterward, it is immersed in IPA.

2.4.2.2. Deposition of silver nanowires

In this thesis, TPP-DLW is used to integrate the QDs on the nanowires. The deposition of Ag NWs on the glass substrate is of necessary.

Silver nanowires (Ag NWs) were commercial supplied from Sigma Aldrich, and the properties are listed in the following table (Table 2.5). As for the deposition, first, 1 ml Ag NWs solution was diluted into isopropanol with a weight ratio 1:400. Then, by spin coating of this diluted solution, the nanowires were deposited on the glass substrate (22x22 mm).

Table 2.5: Properties of AgNWs

Silver Nanowires(AgNWs)	
Form	Liquid(suspension) nanowires
concentration	0.5% (isopropyl alcohol suspension)
diam. × L	115 nm × 20-50 μm
impurities	<5 wt. % non-volatile organics (TGA)

2.5 Characterizations

2.5.1 Morphology

For optical imaging of fabricated structures, Nikon Eclipse LV100 Polarizing Microscope was used. On the other hands, fluorescence images of microstructures were obtained by Olympus IX73 inverted microscope using an excitation laser at 404 nm with maximum energy of 100 mw it is depending on which image you are talking about (Coherent

Inc.) and microscope (S Plan Fluor, Nikon). The UV light is from the setup Superlite UV (Lumatec Inc.) for the observation of photo luminescent images. For precise and quantitative measurements, scanning electron microscope was used. In this work, SU 8030 (Hitachi microscope) was used. Before the observation of SEM, due to the poor electrical conductivity of the structures made in polymer, it is necessary to deposit a thin film of metal such as gold or palladium. Herein, a SC7640 sputter coater was used to simply operate magnetron sputtering on the samples in order to gain better images.

2.5.2 Photoluminescence measurements

Steady state fluorescence measurements on the solutions were performed on a CARY 100 scan UV-visible spectrophotometer. The fluorescence measurements on the fabricated structures were performed with a homemade set-up which consists of a 404 nm laser; a Maya spectrometer and the OLYMPUS IX73 microscope (see Figure 2.7).

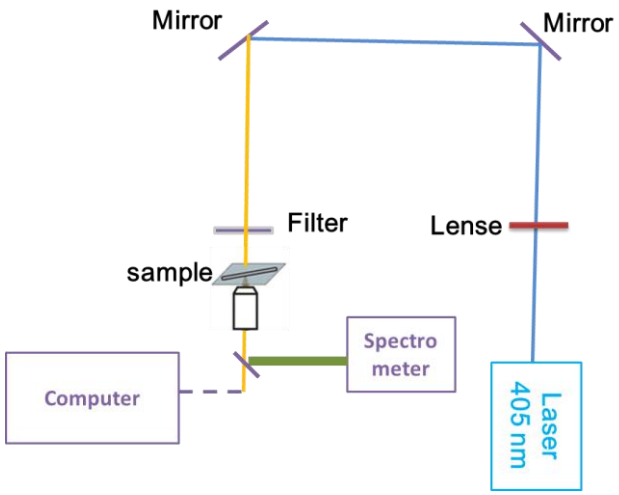

Figure 2.7: Sketch of the set-up for photoluminescence measurement.

2.5.3 Infrared absorption spectra

Infrared spectroscopy is used to determinate the presence of the functional group in the organic molecule. It is particularly notorious that the bonds in the molecules vibrate at a well-determined frequency which not only depends on the bonds of atoms but also on the surroundings of the atoms or bonds. Hence, these bonds resonate at a given frequency based on the energy absorbed by the molecules. Therefore, according to the absorption spectra, it is certain to distinguish the type of bond. In this work, the conversion rate of the monomer is related with the diminution of absorption intensity. Based on the spectra, it enables us to get

the unfolding of the conversion rate by time. From the curve of the monomer conversion rate versus time, it is possible to conclude the polymerization rate $R_p/[M_0]$, shown in Figure 2.8.

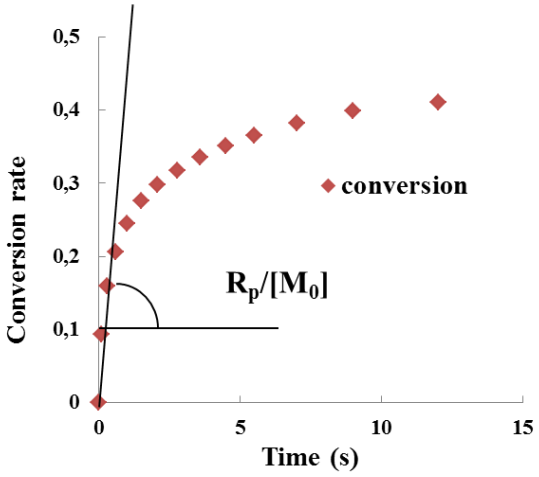

Figure 2.8: Schematic diagram of the method to conclude the polymerization rate Rp.

As shown in this figure, the slope of the conversion rate curve as a function of time, in the very beginning of polymerization, is regarded as the speed of polymerization, (see expression (2-1)-(2-4)).

$$\phi_{c\,(t_x)} = \frac{[M]_{t_0} - [M]_{t_x}}{[M]_{t_0}} = \frac{A_b(1635cm^{-1})_{t_0} - A_b(1635cm^{-1})_{t_x}}{A_b(1635cm^{-1})_{t_0}} \qquad (2\text{-}1)$$

$$R_p = -\frac{d[M]}{dt} = \frac{[M]_{t_1} - [M]_{t_2}}{t_2 - t_1} \qquad (2\text{-}2)$$

$$R_p = \frac{[M]_{t_0} - [M]_{t_2} - ([M]_{t_0} - [M]_{t_1})}{t_2 - t_1} \times \frac{[M]_{t_0}}{[M]_{t_0}} = \left(\frac{[M]_{t_0} - [M]_{t_2}}{[M]_{t_0}} - \frac{[M]_{t_0} - [M]_{t_1}}{[M]_{t_0}}\right)\frac{[M]_{t_0}}{t_2 - t_1} \qquad (2\text{-}3)$$

$$R_p = [M]_{t_0} * \frac{\phi_{c\,(t_2)} - \phi_{c(t_1)}}{t_2 - t_1} \qquad (2\text{-}4),$$

where ϕ_c is the conversion rate of monomer, A_b is the absorption of monomer, t_x is a given time of irradiation of the sample by a 365 nm lamp, $[M]_{t_x}$ is the concentration of monomer at a time x. In this work, the absorption peak at 1635 cm^{-1} is used as the main measurement base, which is corresponded to the elongation of the bond of C=C. Following the equation (2-4), the initial rate of polymerization R_p can be determined from the slope of the linear part of the curve $\phi_c = f(t)$ at the very beginning of the polymerization reaction. Indeed the slope is equal to $\frac{R_p}{[M]_{t_0}}$. In the next chapter, initial concentration of monomer will be simply indicated by [M].

The sample for the conversion rate measurements of monomer is prepared as shown in Figure 2.9. First, a droplet of the photopolymerizable solution is sandwiched between two polypropylene films that are transparent at 1635 cm^{-1}. Then, the sandwich is put between two NaCl tablets. As for comparison, a reference sample is needed. The difference in the reference sample is no solution placed between two films. It is worthwhile to pay attention to the thickness of the droplet at any time. It is of necessity to at least make sure the thickness each time is mostly the same. Once the drop of solution spreads throughout and the thickness of the film is constant, the sample is subjected to 365 nm UV lamp at variable intensity with varying exposure time.

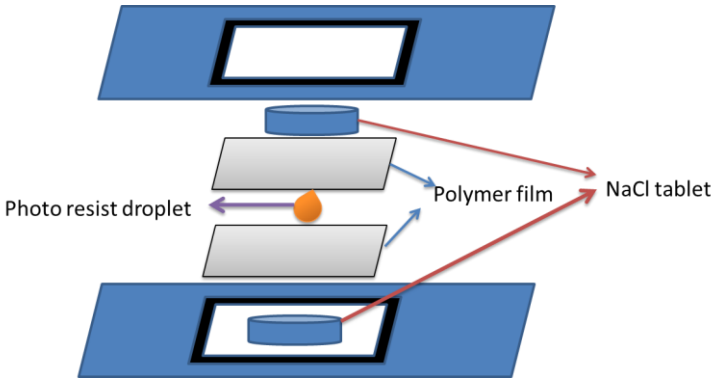

Figure 2.9: Schematic indication of the preparation of the samples to be characterized by IR spectrometer.

2.6 Summary

To summarize, this chapter contains the main experimental techniques and procedures to fabricate and characterize the 2D and 3D structures. In particular, attention is focused on the writing parameters such as laser power, scanning speed, gradients of resists, etc., with the aim to get an optimized resolution. The important thing in this step is to find out how the inhibitor works to improve the resolution during DLW. Besides, some procedures for the fabrication of hybrid 3D luminescent structures containing QDs were presented as well as the preparation of PETA containing QDs.

Chapter 3. Fabrication of 3D nanostructures using high resolution and photo luminescent photopolymer *via* TPP-DLW

As have been pointed out in previous chapters, the fabrication of the polymer nanostructures is used to find out the impact factors of inhibitor and QDs on the spatial resolution of the structures and photopolymeization during TPP-DLW. This chapter exhibits some results of the characterization of the 2D and 3D structures in different resists: containing MEHQ, containing QDs and the reference resist. The investigation about the influence of the parameters on the resolution is subsequently carried out afterwards the exploration on the polymerization kinetics in both cases. This part was done in the frame of the project "Nanomatériaux 3D" funded by the "Conseil Régional de Champagne Ardenne".

In order to understand the influence of inhibitor and QDs on the polymerization kinetics, it is of importance to figure out how the radical photopolymerization happens. Typically, in free radical photo polymerization, the kinetic model involves five processes: initiation, propagation, termination, inhibition and chain transfer. In this work, the photo initiator is Irgacure 819, the generation of radicals is present in Figure 3.1.

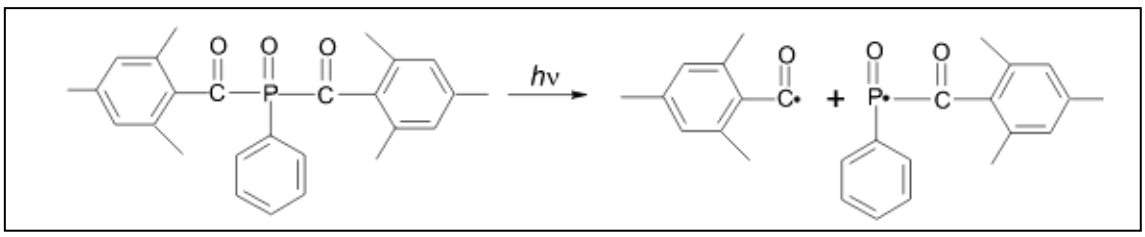

Figure 3.1: Sketch diagram the initiation by Irgacure 819 [163].

As the procedure undergoes, the primary radicals ($R^{\bullet}$) generated from the photo initiator attack the monomer (M) to from ($M^{\bullet}$) which propagates and becomes a macro radical ($RM_m^{\bullet}$) to build up the polymer chains (or network). As soon as the macro radicals meet up and the termination works, the polymerization ends. The corresponding kinetic equations are listed as follows:

- Initiation:

$$PI \xrightarrow{\phi_{diss}} R^{\bullet} \qquad (3\text{-}1)$$

$$R^{\bullet} + M \xrightarrow{K_i} RM^{\bullet} \qquad (3\text{-}2)$$

$$R_i = \phi_i I_{abs} \qquad (3\text{-}3)$$

$$I_{abs} = I_0[1 - e^{(-2.3A)}] \text{ and } \Phi_i = \Phi_{diss} P \qquad (3\text{-}4)$$

$$R_i = \phi_i I_0[1 - e^{(-2.3A)}] \qquad (3\text{-}5),$$

where PI is the photo initiator, ϕ_{diss} is the dissociation quantum yield of PI that relates the number of radicals produced per photon absorbed, R_i is the initiation rate, k_i is the initiation kinetic constant, ϕ_i the initiation quantum yield that corresponds to the number of starting polymer chains per photon absorbed, *P* is the probability for the reaction of the primary radical $R^{\bullet}$ with the monomer M, I_{abs} is the absorbed intensity, I_0 intensity of the incident light, and A is the absorption by the PI [157-166].

- Propagation :

$$RM_m^{\bullet} + M \xrightarrow{K_p} M_{m+1}^{\bullet} \qquad (3\text{-}6),$$

where $RM_m^{\bullet}$ corresponds to the propagated radicals with "m" degree of polymerization and K_p is the propagation kinetic constant.

Within very densely cross-linked parts of the polymer network, radical trapping may be considered as one way of radical deactivation. Thus, two types of termination reactions may be considered [164, 165]:

- Bimolecular Termination, which involves the reaction between two radicals:

$$RM_m^{\bullet} + RM_n^{\bullet} \xrightarrow{K_{tb}} RM_{m+n} \qquad (3\text{-}7)$$

$$R_{tb} = K_{tb}[RM_m^{\bullet}]^2 \qquad (3\text{-}8),$$

According to the approximation of quasi-stationary states:

$$\frac{d[RM_m^{\bullet}]}{dt} = R_i - R_t = 0 \qquad (3\text{-}9)$$

$$R_i = \Phi_i I_{abs} = K_{tb}[RM_m^{\bullet}]^2 \qquad (3\text{-}10)$$

$$[RM_m^{\bullet}] = \left(\frac{\phi_i I_{abs}}{K_{tb}}\right)^{0.5} \qquad (3\text{-}11)$$

$$R_p = \frac{d[M]}{dt} = K_p[RM_m^{\bullet}][M] \qquad (3\text{-}12)$$

$$R_p = \frac{K_p}{(K_{tb})^{0.5}}[M](\Phi_i I_{abs})^{0.5} = \frac{K_p}{(K_{tb})^{0.5}}[M][\Phi_i I_0(1 - e^{(-2.3A)})]^{0.5} \qquad (3\text{-}13),$$

where K_{tb} is the bimolecular termination kinetic constant, R_{tb} is the bimolecular termination rate and [M] is the initial concentration of monomer.

- Monomolecular termination is a process involving only one radical that can be mainly trapped due to a high rigidification of the reactive medium:

$$RM_m^{\bullet} \xrightarrow{K_{tm}} \text{trapped } RM_m^{\bullet} \qquad (3\text{-}14)$$

$$R_{tm} = K_{tm}[RM_m^{\bullet}] \qquad (3\text{-}15),$$

where $[M^{\bullet}]$ corresponds to the concentration of radicals generated from the initiation and propagation steps, K_{tm} is the monomolecular termination kinetic constant and R_{tm} is the monomolecular termination rate. According to the approximation of quasi-stationary states:

$$R_i = R_{tm} = \Phi_i I_{abs} = K_{tm}[RM_m^{\bullet}] \qquad (3\text{-}16)$$

$$[RM_m^{\bullet}] = \frac{\phi_i I_{abs}}{K_{tm}} \qquad (3\text{-}17)$$

$$R_p = \frac{K_p}{K_{tm}}[M]\Phi_i I_0\left(1 - e^{(-2.3A)}\right) \qquad (3\text{-}18)$$

In case the 2 termination processes occurs simultaneously, the equation (3-18) becomes:

$$R_p = K_p[M]\left(\frac{\Phi_i\left(1-e^{(-2.3A)}\right)}{K_{tb}}\right)^{1/\alpha} {I_0}^{1/\alpha} \qquad (3\text{-}19),$$

with $1 \leq \alpha \leq 2$. The termination is monomolecular for $\alpha = 1$ and bimolecular for $\alpha = 2$. It should be noted that this equation is valid for one photon activation mechanism [164, 165]. One can consider that $Kp, [M], K_t, \Phi_i$ and A are constant for a given formulation, the equation 3-19 could be simplified into:

$$R_p = K\,{I_0}^{1/\alpha} \qquad (3\text{-}20),$$

with

$$K = K_p[M]\left(\frac{\Phi_i}{K_t}\right)^{1/\alpha}\left(1 - e^{(-2.3A)}\right)^{1/\alpha} \qquad (3\text{-}21),$$

For 2 photon activation, the equation (3-20) becomes:

$$R_p = K'\,{I_0}^{2/\alpha} \qquad (3\text{-}22),$$

where K' is a constant that depends on K_p, K_t,$[M]$,Φ_i and the two photon absorption of PI.

Mentioned above, the polymerization rate (R_p) depends on several parameters, such as initiation rate, the concentration of the monomer and the kinetic rate constants K_p, K_t, etc. Based on the simplified equations (3-20 and 3-22), it is possible to find out the influence of MEHQ and QDs in the polymerization kinetics at both OPP and TPP, and more particularly

on the termination mechanism, which may explain their influence on the spatial resolution of the as-prepared structures by TPP-DLW.

3.1 Fabrication of 2D and 3D structures with addition of inhibitor (MEHQ) by TPP-DLW

3.1.1. Influence of MEHQ on the threshold energy during TPP

Firstly, it should have a clear sense about the amount of the MEHQ will be used in this photo resist. The investigation of different concentrations of MEHQ on the threshold laser power is then studied. This later is defined as the lowest power that allows the fabrication of polymer lines that can be observed by SEM. Meaning that, below this laser power no any polymer lines can be observed after development. Presented in Figure 3.2.a, it can be seen that as the concentration of MEHQ increases, the threshold energy for polymerization increases as well.

Considering the damage by the laser and heating problem during the exposure, the threshold energy of polymerization is normally supposed to be as low enough to intrigue polymerization. However, it is interesting to note that, even the threshold laser power increased the linewidth of the corresponding polymer lines decreased as the concentration of MEHQ increased, shown in Figure 3.2.b.

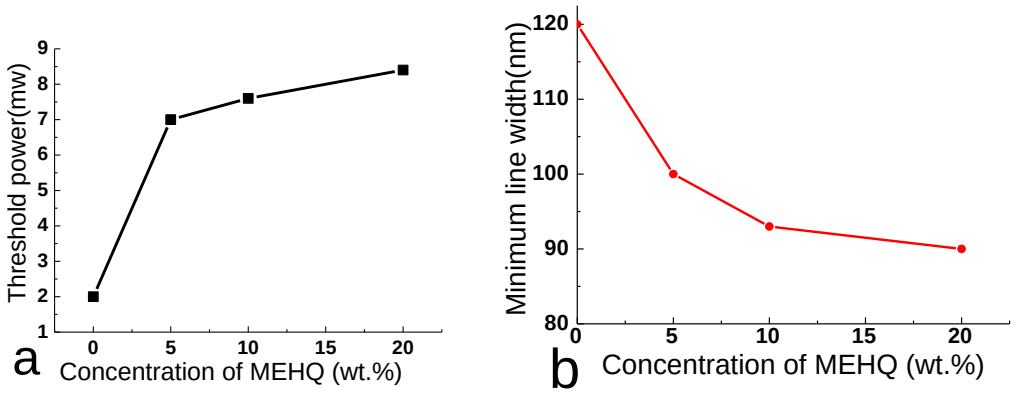

Figure 3.2: Threshold power (a) and smallest linewidth (b) as a function of concentration of MEHQ.

Adding 20% of MEHQ to the formulation has found to affect the stability of both the formulation and resulting 3D polymer structures. The optimal concentration of MEHQ in the base of PETA resist with IRAGURE 819 is opted to 10 wt. %. Based on this constituent, the fabrication of lines in different periods (range from 250 nm to 5000 nm) laser powers (0-20

mw) and scanning speed (25-400 µm/s) were carried out with the aims to improve the resolution of the structures obtained with addition of MEHQ and to find out the influence of MEHQ on the resolution achieved.

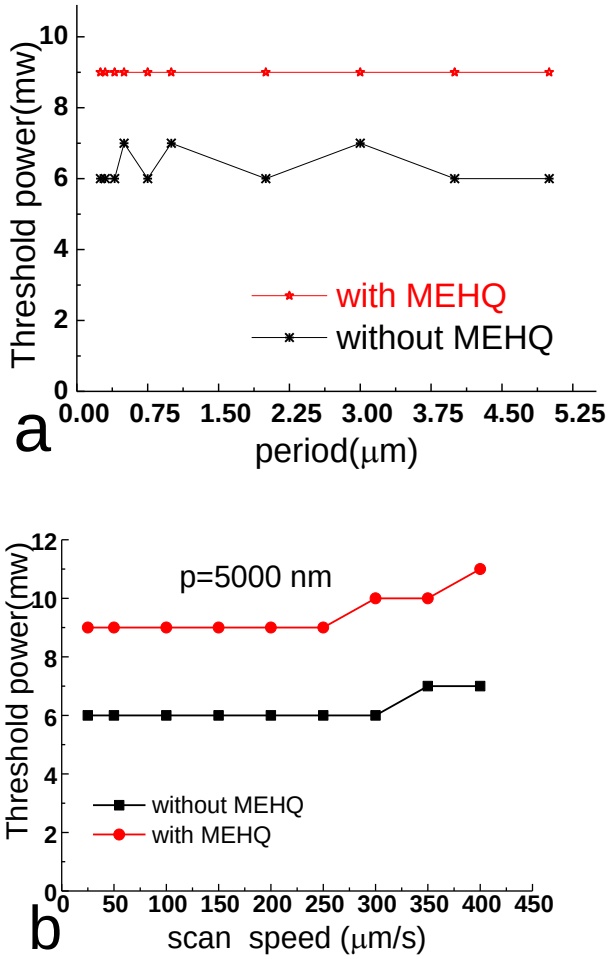

Figure 3.3: In two resists (a) Threshold power as a function of period (scan speed is 100 µm/s), and (b) Threshold power as a function of scan speed (the period of lines is 5000 nm).

Present in Figure 3.3, it is clear that, the threshold power of the resists containing MEHQ is much stable than the one without inhibitor; when the scan speed is over 250 µm/s, the threshold power increased. In other words, the threshold energy is quasi-independent from the period in the presence of inhibitor meaning this photoresist is less sensitive to proximity effect.

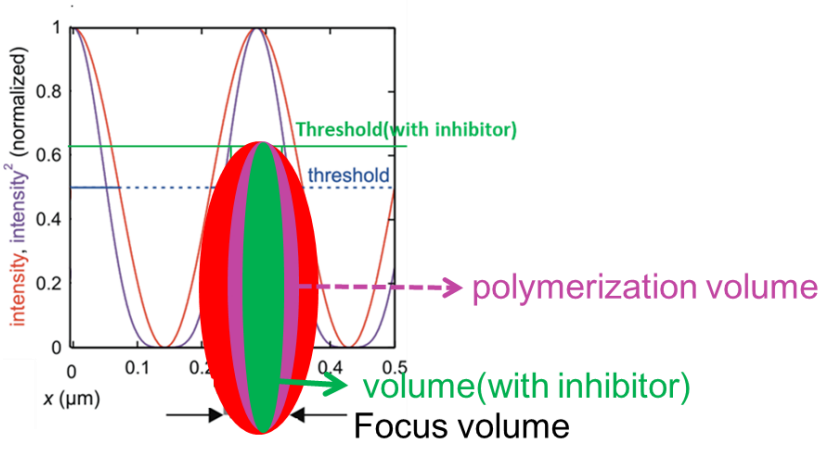

Figure 3.4: Schematic diagram of the voxel size and laser intensity: diffraction-limited intensity grating (red) and the squared intensity (purple) is two-photon exposure [95,167].

As schematized in Figure 3.4 the polymerization occurs in the focal volume of the beam, where the intensity is high enough to generate a high quantity of radicals. Indeed, radicals will react first with oxygen and inhibitors before PETA. This means that the polymerization can start only when and where the concentration of radicals is higher than this of inhibitors. Therefore, when adding inhibitors the threshold energy to start polymerization will increase. Considering the spatial distribution of light intensity within the focal point, the volume where the polymerization reaction can occur will be confinement. This chemical confinement of the reaction volume is important as much as the quantity of inhibitor increase.

Controlling the threshold energy provides a promising mean of improving the spatial resolution for TPP nanofabrication [168]. However, the threshold energy is a subtitle combination between the laser powers, the irradiation time, the concentration of inhibitors, the viscosity or diffusion of reactive species, and their reactivity with PETA. A fine control of these parameters would allow obtaining high spatial resolution of TPP nanofabrication. This is why we will investigate in the next part some of these parameters.

3.1.2. Influence of MEHQ on the resolution of the structures as-prepared *via* TPP-DLW

In this section, the investigation on the influence of MEHQ on the resolution of the structures fabricated by TPP-DLW was carried out. SEM images and measurements of linewidth were present as follows:

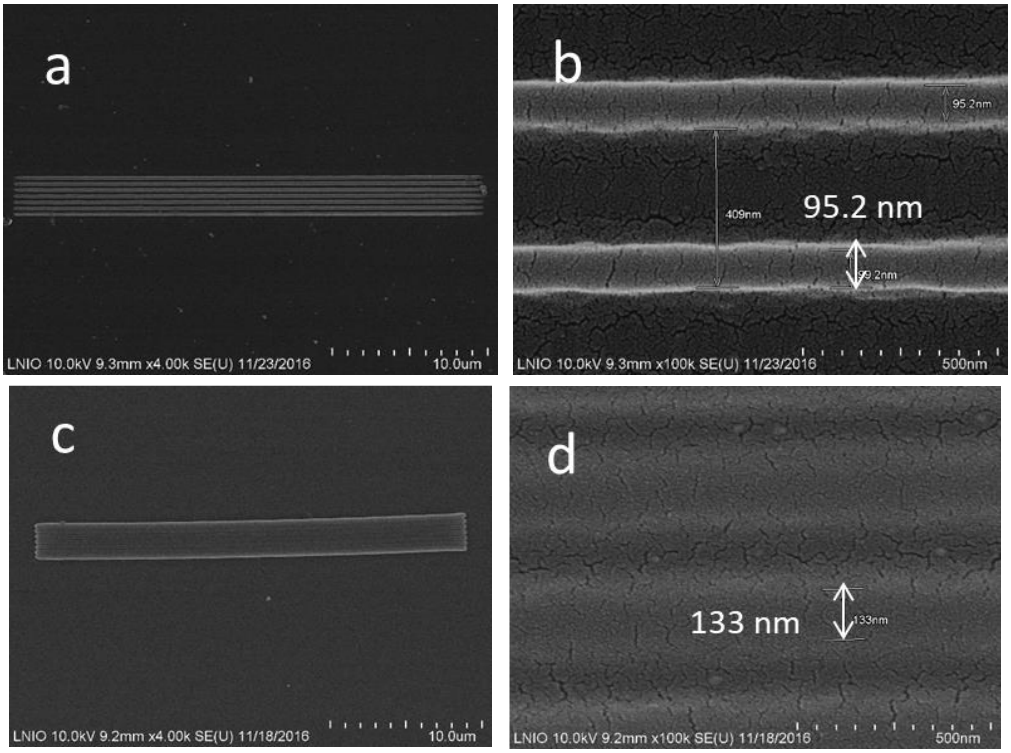

Figure 3.5: SEM images of the 2D lines in a period of 400 nm fabricated in a scan speed of 100 um/s

As for an instance, presented in Figure 3.5, the lines obtained with addition of MEHQ are thinner than those without inhibitor, where the former ones are with a linewidth of 95 nm, compared with the latter of 133 nm. Moreover, in the as-prepared 3D woodpiles *via* TPP-DLW, the smallest period can be achieved at 300 nm with a linewidth of 65 nm in the presence of MEHQ (see Figure 3.6); to the comparison, the smallest period in the absence of MEHQ is 350 nm, with a linewidth of 80 nm (see Figure 3.7). Briefly speaking, with addition of inhibitor, the resolution of 2D lines is markedly improved.

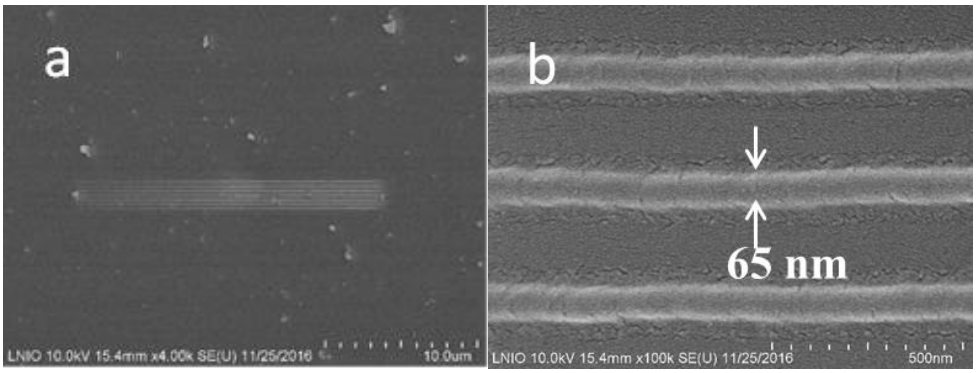

Figure 3.6: SEM images of the 2D lines in a period of 300 nm fabricated with addition of MEHQ (10 wt.%): (a) whole (b) detail

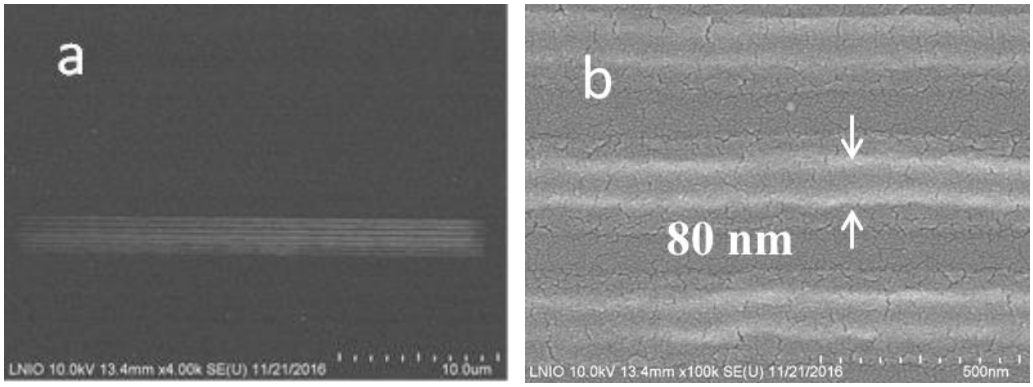

Figure 3.7: SEM images of the 2D lines in a period of 350 nm fabricated without addition of MEHQ: (a) whole (b) detail

Further investigation has also been put forward in the fabrication of 3D structures using two resists. Thus, woodpile structures in different periods (250 nm-1000 nm) were produced at scan speed of 100 µm/s under different laser power (8-14 mw). As a result, the smallest period in the case containing MEHQ is achieved in 250 nm with a line width of 80 nm (presented in Figure 3.8). By contrast, the smallest period in the fabrication without addition of MEHQ is obtained in 350 nm while with a line width around 85 nm (shown in Figure 3.9). Besides, the smallest linewidth can reach to 65 nm (see Figure 3.10), in a period of 350 nm in the presence of inhibitor, which is never reported in the fabrication of 3D structures *via* TPP-DLW using a single laser with a wavelength of 780 nm. It can be comparable to what has been achieved by DLW-STED that 3D woodpiles with interlayer period 400 nm were obtained by using two lasers (λ=810 nm is used for intriguing the polymerization and λ= 532 nm is used as depletion beam) [108].

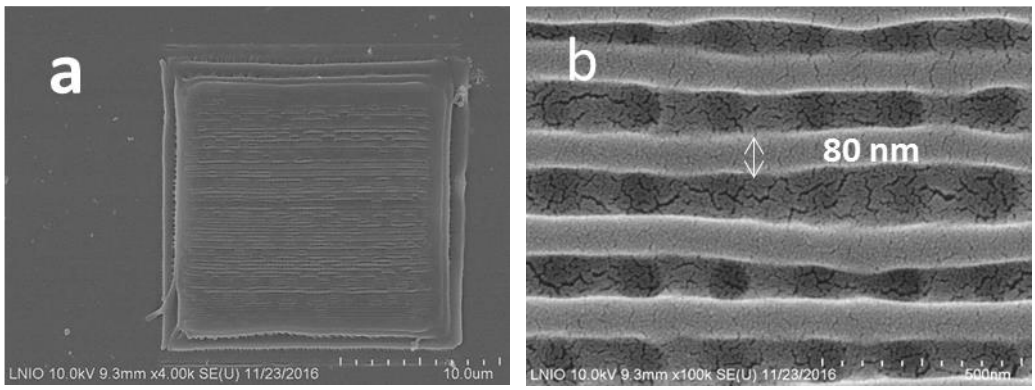

Figure 3.8: SEM images of woodpile fabricated in the presence of MEHQ in a period of 250 nm with a line width of 80 nm: (a) whole (b) detail

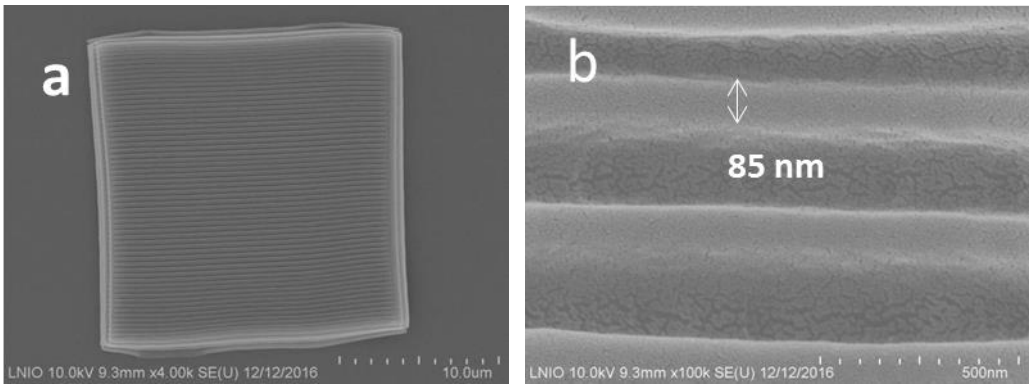

Figure 3.9: SEM images of woodpile fabricated without MEHQ in a period of 350 nm: (a) whole (b) detail

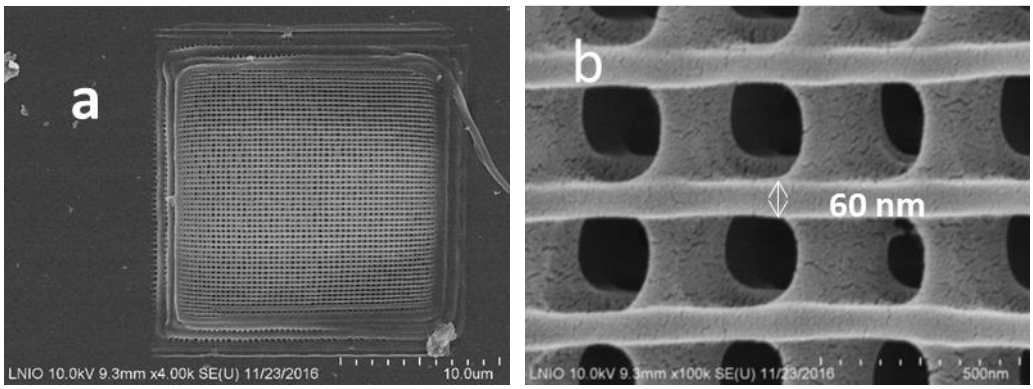

Figure 3.10: SEM images of woodpile fabricated in the presence of MEHQ in a period of 350 nm: (a) whole (b) detail

To sum up, it is obviously clear that, with addition of MEHQ, the resolution of 2D and 3D structures is significantly improved, in accord with the reported record [82] which shows 80-100 nm features were achieved with the addition of a quencher (2-(dimethylamino)ethyl methacrylate, DMAEMA) *via* TPP-DLW using a 800 nm laser. However, it is interesting to mention that in our work, the smallest period of 3D structures obtained can be attained at 250 nm even with a line width of 80 nm. Furthermore, the smallest line width can be achieved at 60 nm in a period of 350 nm.

3.1.3. Influence of MEHQ on the kinetics of polymerization

For the sake of clarifying the influence of MEHQ on the resolution of the structures, it is of importance to have a clear mind on the ongoing of the MEHQ during the polymerization.

Up to now, it was known that the resolution was improved with addition of MEHQ *via* TPP-DLW, shown in Figure 3.11.

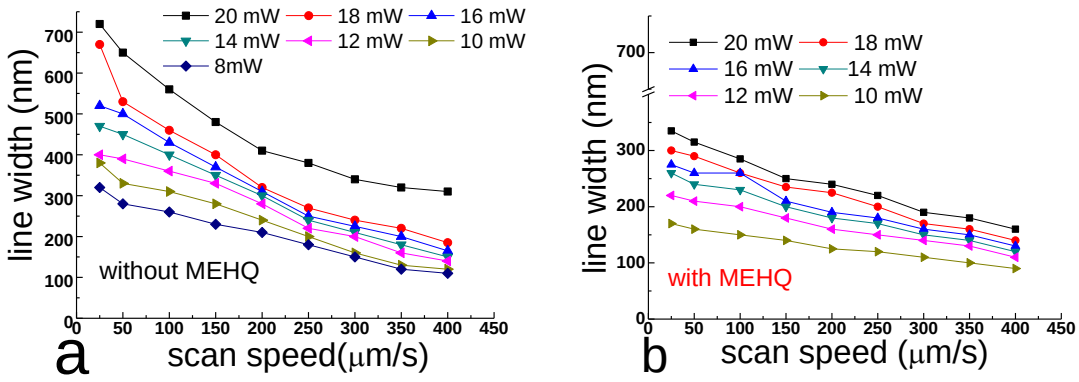

Figure 3.11: line width as a function scan speed for different laser powers with a period of 5000 nm (a) without MEHQ and (b) with MEHQ(10 wt.%)

In TPP procedure, under the exposure of laser, the polymer voxel, with a spheroid shape, grows as a function of the incident energy. The volume of the polymerized voxel can be described as follows:

$$V = \frac{4}{3}\pi pq^2 = \frac{1}{2}\pi L^3 \qquad (3\text{-}23),$$

where q is equatorial radius, which is line width L/2 in our case and p is polar radius which is 3 times of q. Thus, the volume of voxel as a function of exposure time can be obtained, shown in Figure 3.12.

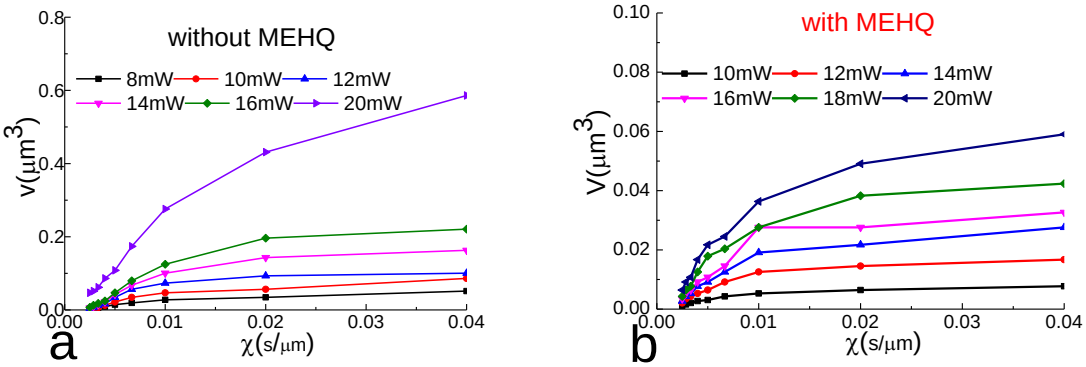

Figure 3.12: Voxel volume as a function of inverse scan speed for different laser powers with a period of 5000 nm by (a) without MEHQ and (b) with MEHQ (10 wt.%)

The volume as a function of exposure time can be described as follows [168]:

$$V = A(1 - e^{-B\chi}) \qquad (3\text{-}24),$$

where V is the voxel volume, $\mathcal{X}$ is the exposure time here proportional to the scan speed, A and B are the fitting parameters. The polymer growth rate is then given by the product of these two parameters, i.e. R_P= A*B. According to the fitting parameters, R_p was calculated and presented in Figure 3.13 as a function of incident laser power in logarithmic scale.

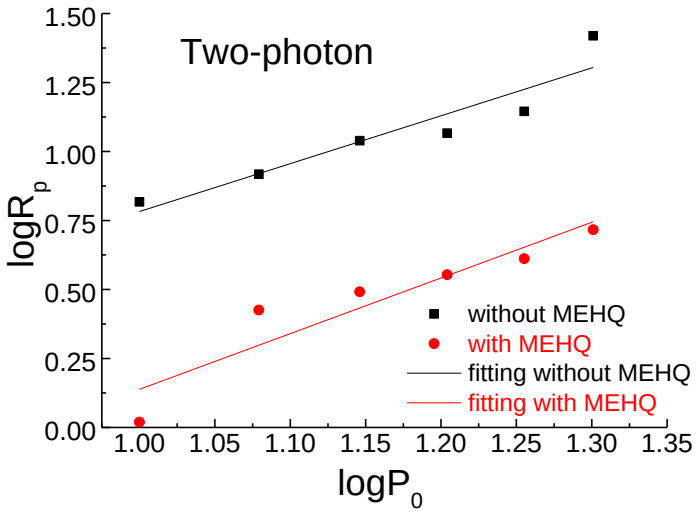

Figure 3.13: $\log R_p$ as a function of $\log P_0$ under two-photon excitation of the two resists (with and without MEHQ).

The curves were fitted, and the fitting equation is for the one with MEHQ:

$$\log R_p = 2.02 \log P_0 - 1.88 \qquad (3\text{-}25)$$

The slope is equal to N/α, with N = 2 (see equation 3-22). Thus, α ~ 1 means that the termination is monomolecular. However for the curve without MEHQ:

$$\log R_p = 1.73 \log P_0 - 0.95 \qquad (3\text{-}26)$$

α ~ 1.2 meaning that both mono and bimolecular terminations could occur simultaneously [169, 170].

In order to confirm the trend observed during polymerization at two-photon activation, the investigations on the decomposition and conversion rate of photo initiator and monomer respectively under one-photon excitation were carried out and corresponding results are presented in Figures 3.14 and 3.15.

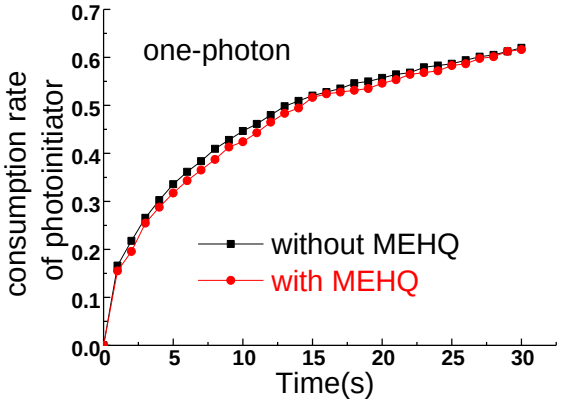

Figure 3.14: Curves of the consumption rate of the photo initiator (Irg. 819) as a function of irradiation time of two formulations: with and without MEHQ. The intensity of the lamp is 4500 mW. cm^{-2}.

The kinetics of initiator consumption is the same in the presence and absence of MEHQ. This result indicates that MEHQ does not affect the photoreactivity of the initiator.

As follows, the conversion rate of photo polymerization under exposure at different intensities in two resins is also measured, presented in Figure 3.15. From it, it is clear that the conversion rate of monomer is less than that of the one without inhibitor regardless of the intensity, besides, the final conversion rate tended to increase when the intensity is high. This can be attributed to the higher activity of initiator with a higher intensity.

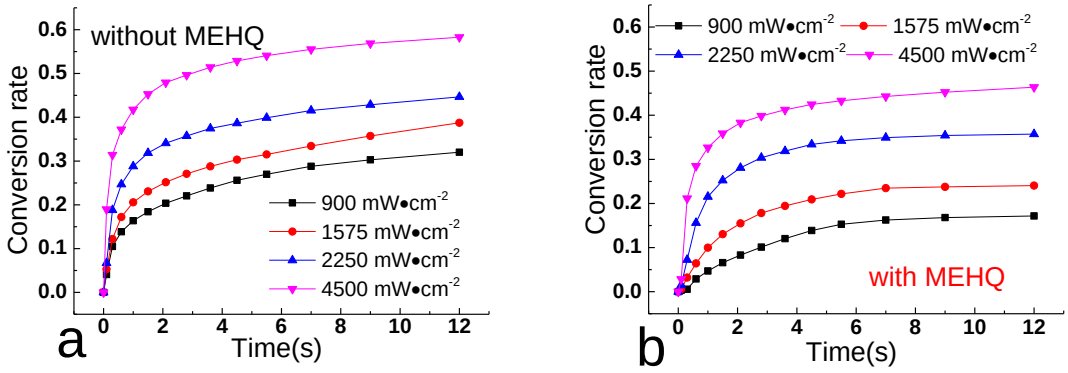

Figure 3.15: Conversion rate as a function of time in different intensity in two resists: (a) without MEHQ and (b) with MEHQ.

On the base of the calculation of $R_p/[M]$, referred in chapter 2, the curves of the log R_p as a function of $\log I_0$ were obtained and presented in Figure 3.16.

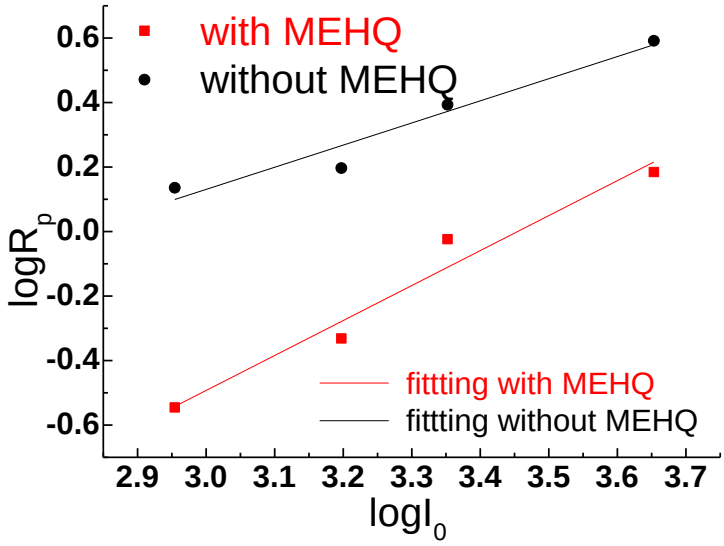

Figure 3.16: $\log R_p$ as a function of $\log I_0$ under one photon excitation of the two resists (with and without MEHQ).

The fitting equation for the curve with MEHQ is:

$$\log R_p = 1.08 \log I_0 - 3.58 \qquad (3\text{-}27)$$

The slope is equal to N/α, with N = 1 (see equation 3-20). Thus, α ~ 1 means that the termination is monomolecular. However for the curve without MEHQ:

$$\log R_p = 0.68 \log I_0 - 1.93 \qquad (3\text{-}28)$$

α ~ 1.5 meaning that both mono and bimolecular terminations could occur simultaneously [169,170]. The results here are consistent with those obtained by two-photon excitation. More particularly, the presence of MEHQ seems to favor a monomolecular termination process.

There are several possible inhibition mechanisms in free radical polymerization, listed below:

$$R^{\bullet} + Q \xrightarrow{K_q} R + Q^{\bullet} \text{ or } RQ^{\bullet} \qquad (3\text{-}29)$$

$$RM_m^{\bullet} + Q \xrightarrow{K_q} RM_m + Q^{\bullet} \text{ or } RM_m Q^{\bullet} \qquad (3\text{-}30)$$

$$PI^{*} + Q \xrightarrow{K_q} PI + Q^{\bullet} \text{ or } PIQ^{\bullet} \qquad (3\text{-}31),$$

where $R^{\bullet}$ is a primary radical generated after dissociation of PI, Q is the inhibitor or quencher, $Q^{\bullet}, RQ^{\bullet}, RM_mQ^{\bullet}$ are the inhibitor radicals, PI^* is the excited PI. The equation (3-31) is negligible, as the consumption rate of PI has not changed in the presence of MEHQ (see Figure 3.14).

Making the assumption that, the inhibitor radicals neither reinitiate polymerization nor reform the quencher Q, the equations (3-29) and (3-30) can be considered as additional routes of termination of reactive radicals. The following equations can be obtained as below, depending on the mechanism of termination:

Monomolecular:

$$\frac{d[RM_m^{\bullet}]}{dt} = R_i - K_{tm}[RM_m^{\bullet}] - K_q[Q][RM_m^{\bullet}] = 0 \qquad (3\text{-}32)$$

Bimolecular:

$$\frac{d[RM_m^{\bullet}]}{dt} = R_i - 2K_{tb}[RM_m^{\bullet}]^2 - K_q[Q][RM_m^{\bullet}] = 0 \qquad (3\text{-}33)$$

where k_q is the constant rate for quenching reaction, $[RM_m^{\bullet}]$ is the concentration of radicals generated from the initiation and propagation steps.

According to the equation (3-18), for monomolecular termination and one photon excitation, the polymerization rate in the presence of inhibitor can be written as follow:

$$R_p = \frac{K_p}{K_{tm}+K_q[Q]}[M]\Phi_i I_0\left(1 - e^{(-2.3A)}\right) \qquad (3\text{-}34)$$

For bimolecular termination, when the quenching effect is very strong which in our case here, $K_q[Q][RM_m^{\bullet}]$ dominates $2K_{tb}[RM_m^{\bullet}]^2$, the equation (3-33) becomes:

$$\frac{d[RM_m^{\bullet}]}{dt} = R_i - K_q[Q][RM_m^{\bullet}] = 0 \qquad (3\text{-}35)$$

$$R_p = \frac{K_p}{K_q[Q]}[M]\Phi_i I_0\left(1 - e^{(-2.3A)}\right) \qquad (3\text{-}36)$$

According to equations (3-32) and (3-34), if high amount of inhibitor is used, R_p will be proportional to I_0 in one photon excitation and I_0^2 or P_0^2 in 2-photon excitation. The value of R_p will decrease in the presence of MEHQ because of the new term $K_q[Q]$ that has to be considered in the kinetic model and because of the decrease of Φ_i. Indeed, according to the equation (3-27) a new route for reaction of $R^{\bullet}$ with Q indicates that the probability for the

reaction with the monomer decreases. Thus, Φ_i is expected to decrease in the presence of MEHQ.

Based on the consumption rate of PI and conversion rate of M in this work, combined to the mechanism referred in [157-171], it is proposed that, after incidence of light, the initiator can generate free radicals which may proceed in 2 different pathways:

- Quenching by MEHQ or oxygen;
- Reaction with the monomers in the resin to initiate polymerization.

Besides, MEHQ can also form MEHQ radicals as well, which affects the initiation and propagation steps of the reaction in three approaches:

1- by quenching the chain radicals;
2- by quenching the free radicals;
3- by chain transfer with the monomer to form additional radicals which cannot initiate polymerization.

To sum up, with the MEHQ involved in TPP-based DLW, the resolution of 2D lines and 3D woodpiles as-prepared was improved. To be clear, for 2D lines, the smallest linewidth of 65 nm is obtained in a period of 300 nm; for 3D woodpiles, the smallest linewidth of 60 nm is obtained in a period of 350 nm, and the smallest period of 250 nm, which is better than the reported smallest period of 400 nm with a resolution of 80 nm by TPP-DLW [92]. By investigation on the effects of the conversion rate, laser power and scan speed on the resolution, the termination mechanism in the case with MEHQ involved is boldly surmised that monomolecular termination is dominant; the quenching occurs not only between quencher and free radicals but also between quencher and chain radicals along with the H-transfer between MEHQ and monomer. In addition, owing to the termination mechanism varies with addition of MEHQ, the resolution is improved. In this light, it is expected to get a better resolution considering the quenching effect with an elaborate parameter selection.

3.2 Fabrication of 2D and 3D structures with addition of QDs by TPP-DLW

Quantum dots (QDs) films or layers have been extensively used for various photonic and electronic applications in recent decades. Three-dimensional (3D) nanostructures are the elegant fashion in micro optics, micro fluidics, biomedicine and imaging. In particular, 3D fluorescent nanostructures play an important role in detection and sensing as well as emitting systems. Since the multi-fold application of QDs, as well as the capability of the TPP-based

DLW to obtain 3D structures with nanometer size in arbitrary shape, the proposal to functionalize the structures utilizing TPP-DLW containing QDs is in a clear and ordered pattern. In this section, the characterization of the structures as-prepared containing QDs were presented.

2D lines containing QDs and for a reference, lines without QDs with a length of 30 µm in a period of 5 µm are fabricated in the same scanning speed and laser power, shown in Figure 3.17. It is interesting to find that, in the presence of QDs, the lines are thinner than the ones without QDs, which is not reported before. Indeed, the smallest period (300 nm) to get the resolved lines and the corresponding linewidth (75 nm) are clearly smaller in the presence of QDs than this without QDs (350 nm and 90 nm respectively), as shown in Figure 3.18.

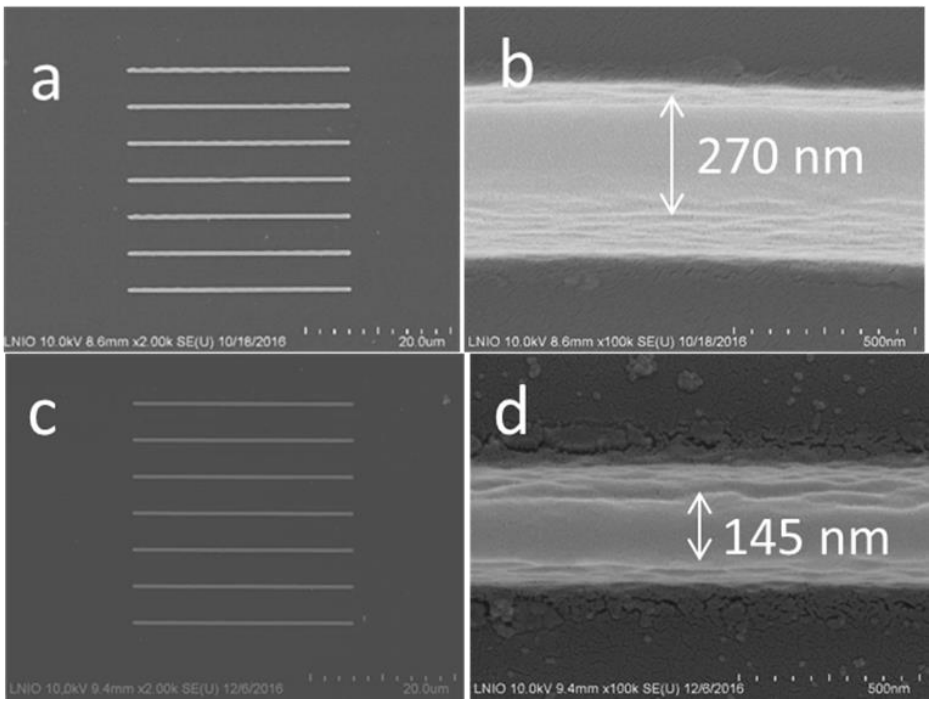

Figure 3.17: SEM images of polymer lines fabricated by TPP in the formulation without QDs (a and b) and in the presence of QDs (c and d).

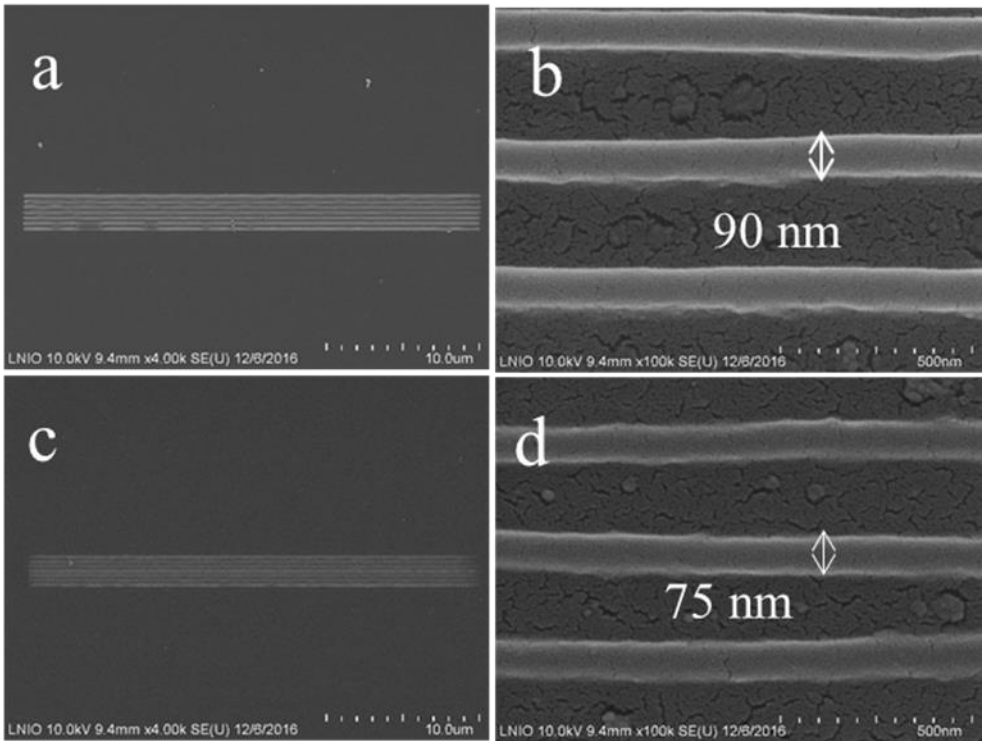

Figure 3.18: SEM images of polymer lines fabricated by TPP in the formulation without QDs (a and b) at 7 mw and in the presence of QDs (c and d) at 9 mw in a same scanning speed of 100 μm/s.

It appears clearly that the linewidth in the presence of QDs is quiet smaller than the one without QDs. Similar trend can be seen in the case of 3D structures obtained with both resists, shown in Figure 3.20. Indeed, the woodpile containing QDs with an interlayer period of 350 nm as-prepared shows clear resolution comparing to the one obtained in the absence of QDs. Moreover, the smallest period to reach available resolution in the issue of woodpiles fabrication containing QDs is 400 nm, by comparison, in the absence of QDs, the smallest period is 500 nm shown in Figure 3.21. This can be also clearly seen from Figure 3.19, which shows the variation of polymer linewidth with time for the two resists at different laser powers. This phenomenon has never been reported before. Given to this, it is a new way to get a better resolution of structures fabricated by TPP-DLW. Additionally, due to the unique properties of QDs, this way is very promising to envisage nanoscale functionalization with different color emitting QDs [123].

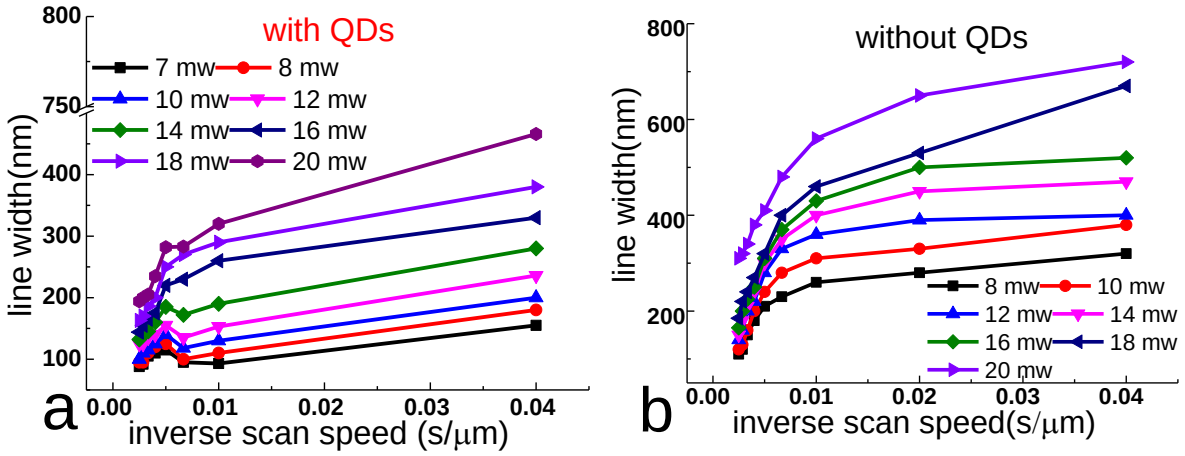

Figure 3.19: Curves of the line width as a function of inverse scanning speed under different laser power used for polymerization: (a) with QDs and (b) without QDs.

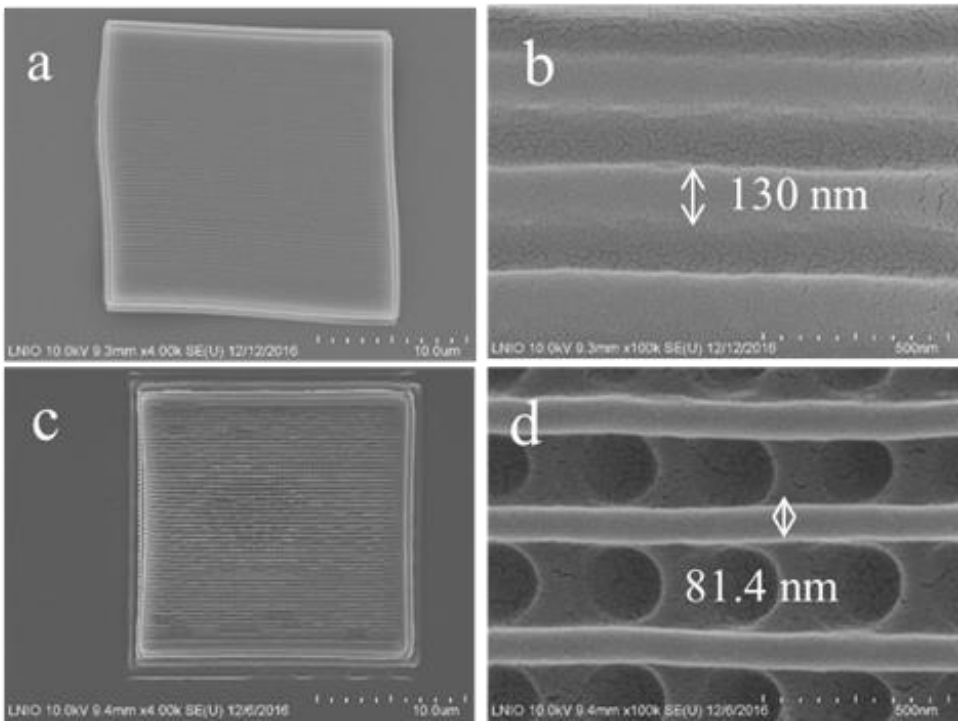

Figure 3.20: SEM images of woodpile in a period of 350 nm fabricated at 8 mw by TPP-DLW in a scanning speed of 100 μm/s (a, b) without QDs; (c, d) with QDs.

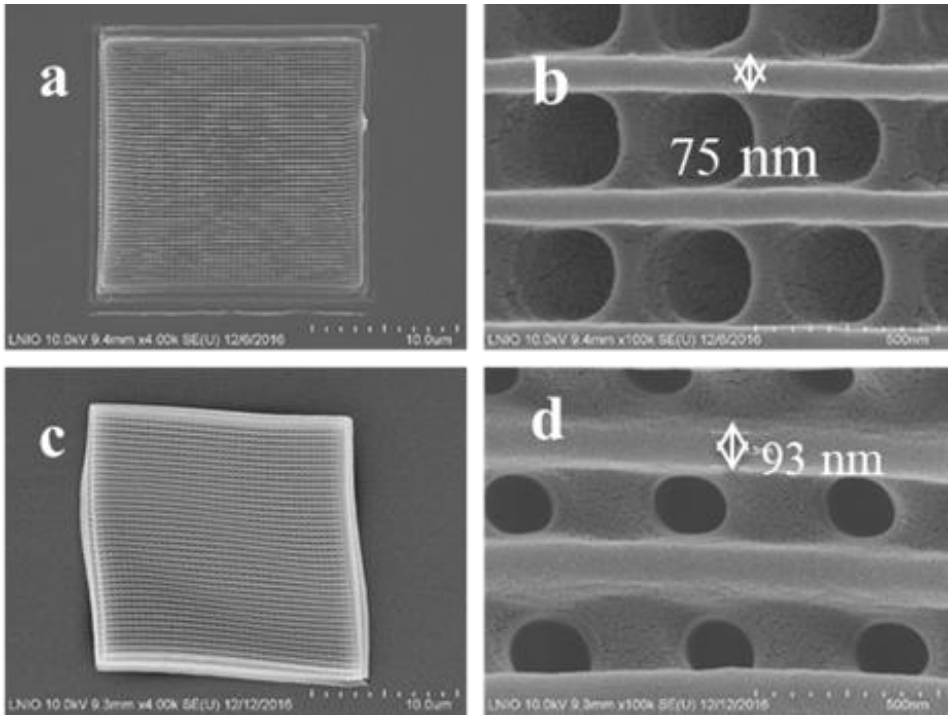

Figure 3.21: SEM images of woodpile fabricated by the TPP-based DLW at a scanning speed of 100 µm/s: (a and b) in a period of 400 nm fabricated with QDs at 8mw (c and d) in a period of 500 nm fabricated without QDs at 6 mw.

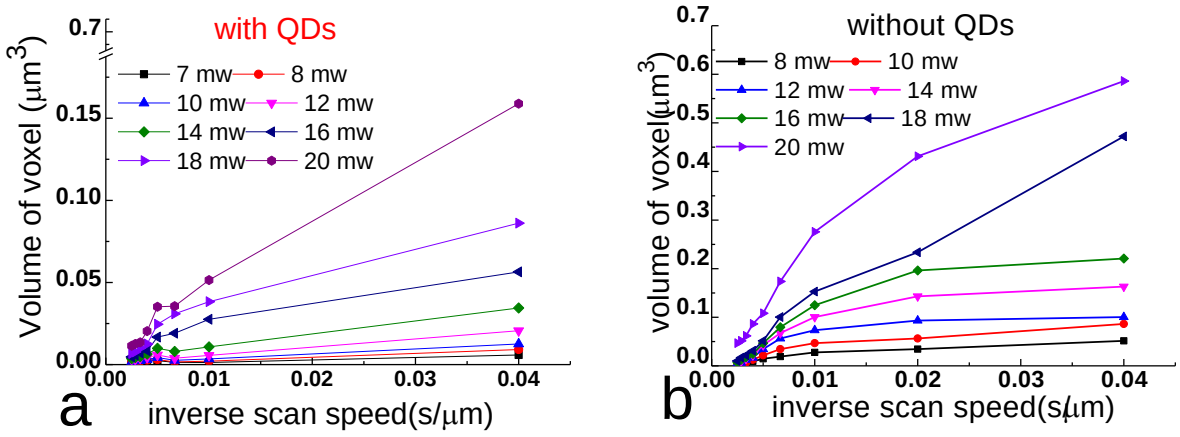

Figure 3.22: Volumes of polymer voxel obtained by TPP as a function of inverse scan speed for the two resists (a) with QDs and (b) without QDs.

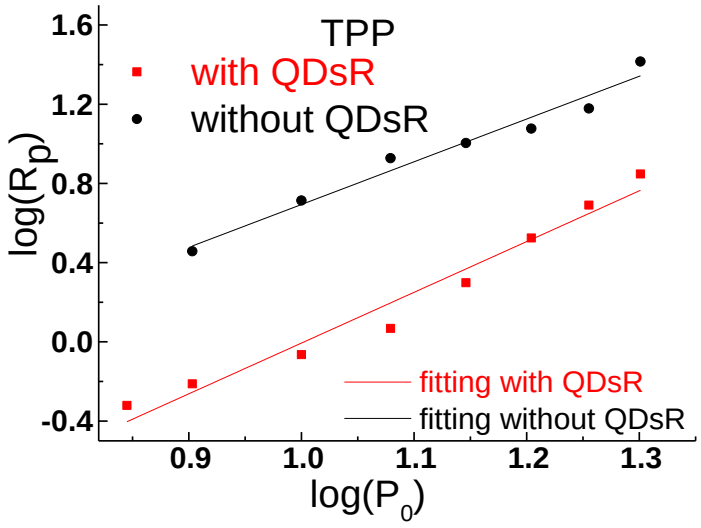

Figure 3.23: $\log R_p$ as a function of $\log P_0$ for both resists (with and without QDs) under two-photon excitation

For the sake of clarifying the influence of QDs on the resolution of the structures, it is of importance to have a clear mind on the ongoing of the QDs during the polymerization. The calculated voxel volume (according to equation 3-23) as a function of exposure time is shown in Figure 3.22. Then the growth rate or polymerization rate (R_p) is calculated after fitting the equation (3-24) as done in the previous section. $\log R_p = f(\log P_0)$ for both resists is presented in presented in Figure 3.23. The curves were fitted, and the fitting equation is for the one without QDs:

$$\log R_p = 1.63 \log P_0 - 0.82 \qquad (3\text{-}37)$$

The slope is equal to N/α, with N = 2 (see equation 3-22). Thus, α ~ 1.23 means that both mono and bimolecular terminations could occur simultaneously. However for the curve with QDs:

$$\log R_p = 2.13 \log P_0 - 2.11 \qquad (3\text{-}38)$$

α ~ 1 which means the termination performed an inclination to monomolecular termination in the presence of QDs [169]. Given to $R_p \propto I^{(N/\alpha)}$, where α is the determination coefficient constant of termination, N is the order of absorption which is supposed to be 2 [168-170].

In order to confirm the trend observed during polymerization at two-photon activation, the investigations on the decomposition and conversion rate of photo initiator and monomer respectively under one-photon excitation were carried out and corresponding results are presented in Figure 3.24.

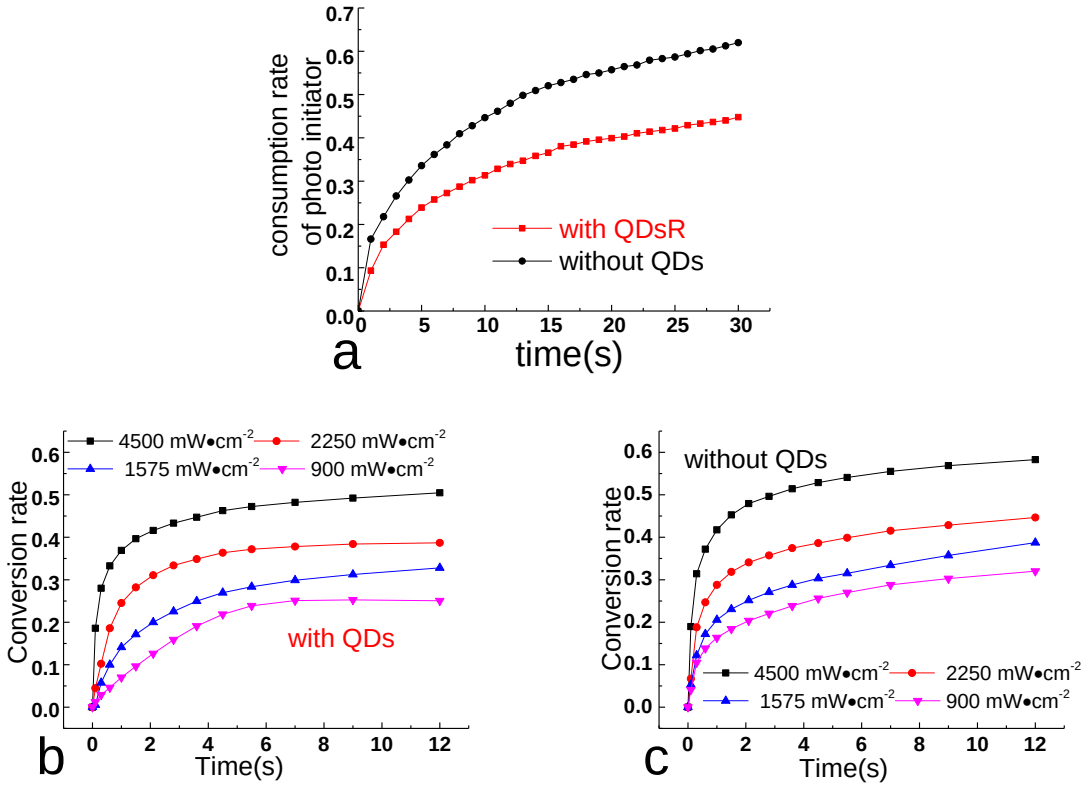

Figure 3.24: (a) The consumption rate of photo initiator as a function of time for both resists (presence/absence of QDs), (b and c) Comparisons of the conversion rate of monomer under different intensities for both resists.

In the presence of QDs, the decomposition rate of the initiator decreased from 62% to 44.8%. In addition, whatever the exposure intensity, the conversion rate of monomer is lower in the presence of QDs than that of the one without QDs. Both observations indicate that the generation of radicals might be locally influenced by the presence of QDs. Indeed, during excitation with UV lamp (main peak at 365 nm), QDs will absorb a part of the incident light decreasing thus the number of photons absorbed by the photoinitiator which in turn leads to lower amount of generated radicals. Another explanation could be related to a possible inhibition of radicals by QDs leading to fewer active radicals aimed to precede the

polymerization [172]. However, these conjectures should be proved in the future work. Besides, the polymerization rate Rp can be obtained, seen in Figure 3.25.

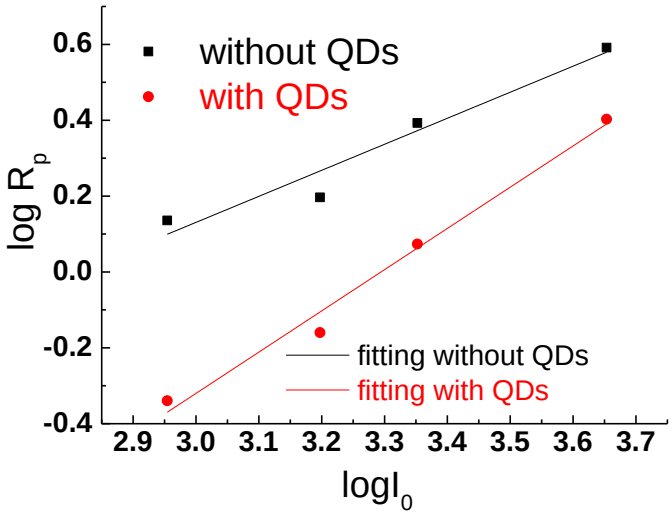

Figure 3.25: logRp as a function of $\log I_0$ for both resists under one-photon excitation.

The fitting equation for the curve without QDs is:

$$\log R_p = 0.69 \log I_0 - 1.93 \qquad (3\text{-}39)$$

The slope is equal to N/α, with N = 1 (see equation 3-20). Thus, $\alpha \sim 1.5$ means that both mono and bimolecular terminations could occur simultaneously without QDs. However for the curve with QDs:

$$\log R_p = 1.08 \log I_0 - 3.58 \qquad (3\text{-}40)$$

Once again here $\alpha \sim 1$ means that the termination is monomolecular. This result is consistent with the one obtained under two-photon excitation.

In the presence of QDs, the monomolecular termination is more favorable to occur, regardless of the routine of excitation. During the polymerization, there coexist two main radicals with different reaction liabilities: free radicals with random mobility to be reacted or terminated, and trapped radicals which makes inaccessible to the further reaction. Normally, the trapped radicals perform the monomolecular termination [173]. This mode of termination is considered as a virtual decrease in radical mobility, which means under the same excitation, in the presence of QDs, particular population of radicals turn to be trapped fast resulting in

the termination of the polymerization other than to grow a longer polymer chain or network. Hence, the final structure achieved presents to be in a finer resolution compared to the one without addition of QDs. Other factors could be responsible for this improved resolution in the presence of QDs. Indeed, due to the two photon absorption of QDs, the intensity of absorbed light by the PI is expected to decrease, leading thus to a local decrease of R_p. A possible interaction between QDs and excited PI could be responsible for the local decrease of generated radicals and thus R_p.

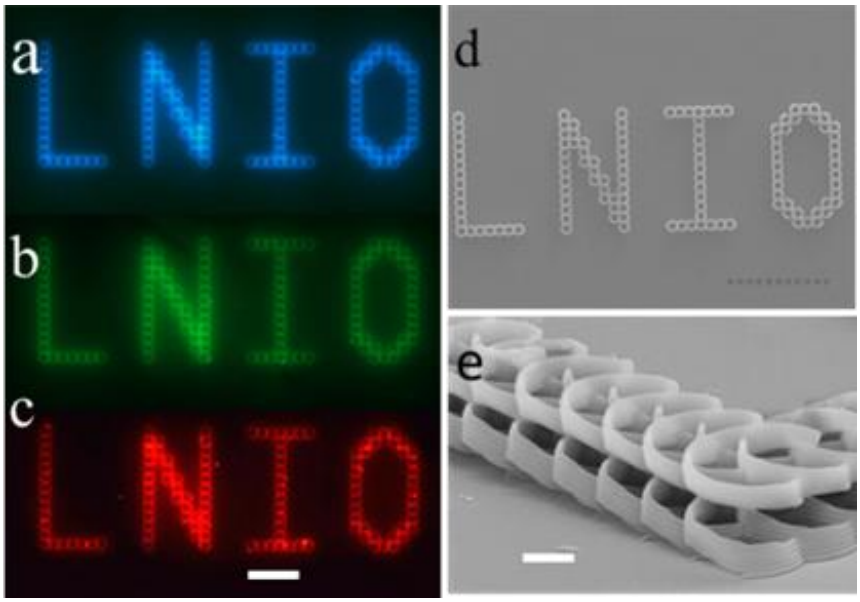

Figure 3.26: (a, b and c) Photoluminescence images of QD-containing 3D microstructures showing emission at 460 nm, 510 nm, and 613 nm, respectively. (d and e) Top view and side view SEM images of the corresponding microstructures. Scale bares are 10 µm, 50 µm and 2 µm respectively.

With the purpose for future application, it is necessary to assure the capability of fluorescence. As shown in Figure 3.26, under the excitation of a 404 nm laser, the grids and characters showed blue, red and green emission, respectively. On the basis of those previous observations, the emission intensity of the woodpiles containing QDs-red, was measured under different laser powers. It is obvious that the emission intensity increases with the increasing of laser power used for fabrication, as shown in Figure 3.27. This result can be simply explained by the increase of the polymer volume and thus the number of QDs. It shows however that there is no significant photo bleaching or diffusion of QDs from the irradiated areas to the dark areas as it was reported by Barichard et al. [174] in the issue of

holographic recording. Thus, our 3D micro and nanostructures contained QDs fabricated by TPP-DLW can still be photoluminescent.

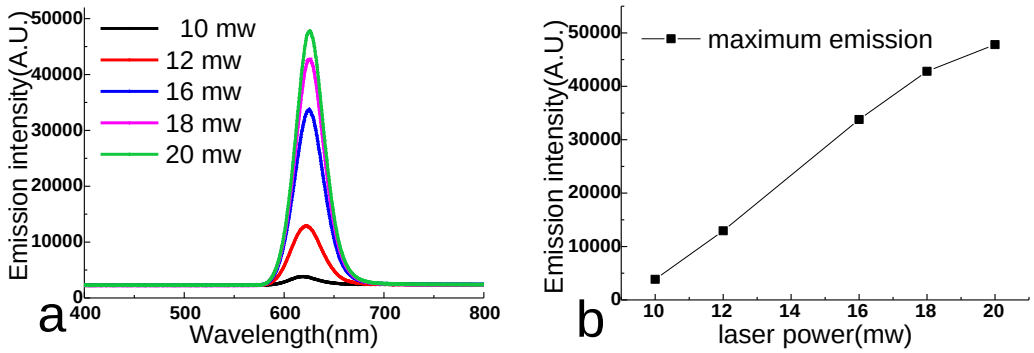

Figure 3.27: (a) Emission intensity of the woodpiles containing red-emitting QDs fabricated at different laser powers; (b) the maximum emission intensity as a function of laser power used.

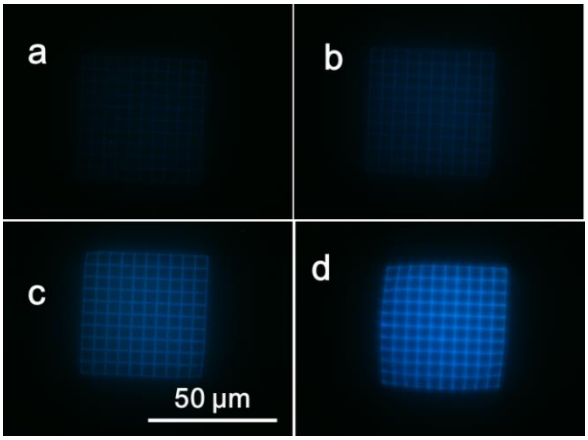

Figure 3.28: Fluorescent images of grids containing QDsB with z-direction height of 0.5 µm, 5 µm 10 µm and 15 µm respectively under a radiation of blue laser at wavelength of 405 nm.

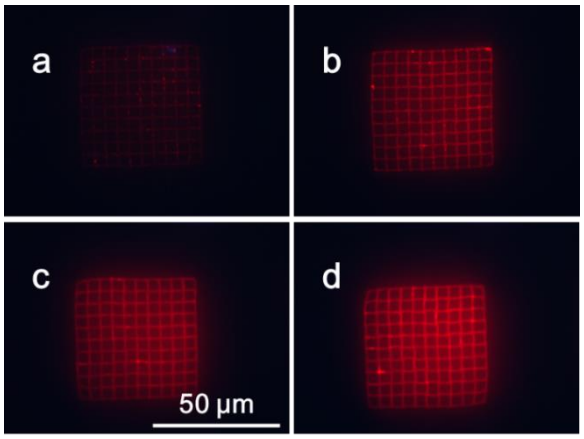

Figure 3.29: Fluorescent images of grids containing QDs R with z-direction height of 0.5 μm, 5 μm 10 μm and 15 μm respectively under a radiation of blue laser at wavelength of 405 nm.

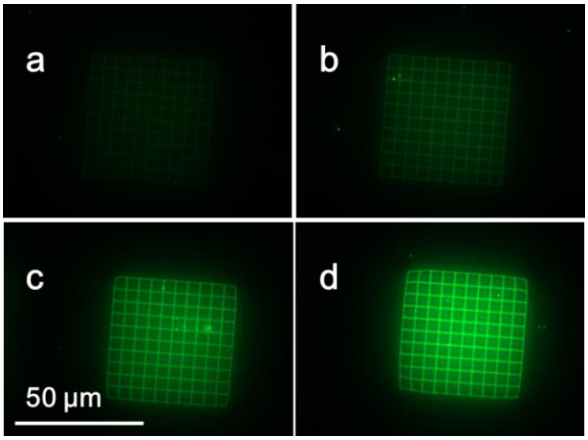

Figure 3.30: Fluorescent images of grids containing QDs R with z-direction height of 0.5 μm, 5 μm 10 μm and 15 μm respectively under a radiation of blue laser at wavelength of 405 nm.

Moreover, Figure 3.28, Figure 3.29 and Figure 3.30 present the photoluminescence images of the polymer grids with varied height containing QDs. From which, it is clear that, as the height increased, the emission became stronger. Given all that, it is proved the structures containing QDs fabricated by TPP-DLW can still be photo-luminescent and their emission properties can also be predicted according to the geometry size, which gives a light on the numerous applications envisioned. Furthermore, it shows the light on the clear mind on sorting out the optimal writing process parameter before the fabrication.

3.3 Conclusion

In this chapter, at the beginning, the fabrication of 2D lines and 3D woodpiles with addition of inhibitor was fabricated *via* TPP-DLW, as well as the investigation of the influence of inhibitor on the resolution of the as-prepared structures were studied. The results showed that with MEHQ involved in TPP-DLW, the resolution was significantly improved; especially in 3D woodpiles, the smallest linewidth is 60 nm while the period is 350 nm, and the smallest period is 250 nm with a linewidth of 80 nm. The investigation of the influence of MEHQ on the polymerization kinetics was also carried out. There are several assumptions based on resolution measurement, FTIR and UV spectra measurements: the termination mechanism with the presence of MEHQ during TPP-DLW may be varied, specifically,

monomolecular termination is dominant; the quenching occurs in three ways, quenching between MEHQ and free radicals, quenching between MEHQ and chain radicals, and chain transfer between MEHQ and monomer. The resolution is improved somehow attributed to the quenching mechanism varied with addition of MEHQ.

Secondly, regarding to the numerous applications of hybrid 3D luminescent structures, in this section, 3D structures were fabricated with the utilization of QDs-containing polymer resins *via* TPP-DLW. The capability to fabricate 3D luminescent nanostructures containing quantum dots with 80 nm resolution was demonstrated. The influence of the QDs and laser power on the resolution of the as-prepared structures was also investigated. It is turned out that, the presence of QDs improves the spatial resolution where the feature size of the polymer lines can reach 75 nm. According to the FTIR and UV spectra measurements that show remarkable decrease in the polymerization rate of the photoresists in the presence of QDs, the improved resolution might be attributed to the two photon absorption of QDs during writing leading to less photon absorbed by the photo initiator. On the other hand, in the presence of QDs, the radicals inclined to perform monomolecular termination which somehow favors the improved resolution of the as-prepared structures. Moreover, the photoluminescence images and emission spectra show stable local emission from the as-prepared structures containing QDs. Besides, the emission intensity of the structures does not show any significant photobleaching and varies only with volume of the polymer nanostructure. In this sense, the spatial positioning, the size of the active polymer nanostructure and its fluorescence properties can be controllable in the case of TPP-based direct laser writing, which affords a path for some promising applications where the local integration of a single Nano-emitter with a fine control of its spatial positioning is still an unresolved challenge.

Chapter4. Integration of QDs with plasmonic and photonic structures *via* TPP-DLW

4.1 Introduction

This chapter deals with the applications of the QDs-containing photopolymers. In a context of a partnership with other PhD students (Hongshi Chen, Dandan Ge and Aurélie Broussier) in the "Laboratoire de Nanotechnologie et Instrumentation Optique" (LNIO), I have been working on the integration of QDs with plasmonic structures (such as Ag nanowire, Au gratings and Au nanocubes) and tipped fibers. This chapter presents the first obtained results based on the use of photosensitive resins containing QDs such as PETA-QDsR-IRG and PETA-QDsG-IRG. As shown in the chapter 3, it is possible to get stable 3D structures containing QDs with controllable size and shape. Considering the topical challenge to integrate, on demand and in a controlled way, QDs with plasmonic structures or other photonic structures, there is with great promise to use resins containing QDs *via* TPP-DLW.

Let us stress that the results shown in this chapter are just some primary attempts to be pursed with future investigations and studies through other projects or thesis in LNIO.

4.2 QDs coupling with Ag-nanowires

In contrast to dielectric waveguides, the fundamental plasmon mode of silver nanowires (Ag NWs) remains strongly localized to the wire, contributed to that the mode indices scale conversely with the wire diameter [175-177]. Accordingly, this strong field localization of surface plasmon (SP) mode makes possible strong interaction between Ag NWs with quantum emitters [158, 159]. It is known that the emission properties of quantum emitter can be remarkably modified by the proximity of NWs. Theoretically speaking, once quantum emitter gets excited, there are three desexcitation-decay routes. The first way is a radiative path direct optical emission into free-space modes. Second, owing to ohmic losses, the emitter might be damped non-radiatively, by non-radiative energy transfer into metal (quenching). Last but not the least; the nanowire might probably capture the light issued from QDs spontaneous radiation to excite guided surface plasmon (SP) modes of the nanowire. In fact, as the spontaneous emission rate in to SPs can far outdo the non-radiative rate and radiative rate. Consequently, the coupling to SP and total decay rate can be enhanced compared to that of the uncoupled emitters [175].

With the development of the emerging technologies, on-chip integration of solid-state photonic systems plays an important role, which lies much on the efficiency of light-matter interaction. Waveguide-based scheme offers strongly confined SPPs mode where the photon detection can be integrated on chips. On behalves of both QDs and NWs, the coupling QDs to NWs has received much attention as hybrid system for future quantum plasmonic circuitry platforms [175], single-photon source [159], plasmonic nanolaser [176], quantum switch [177], and nanoantennas [178].

Among variety of researches, the most frequent method is by chemical growth of QDs deposited on the NWs [160], which makes the localization of QDs random and not controllable.

In this section, the polymerizable resin containing QDs was utilized: PETA-QDsR-IRG and PETA-QDsG-IRG by TPP-DLW; it was possible to integrate QDs to silver NWs in the required position with given geometry or size.

This work has been done in collaboration with Aurélie Broussier and Stefano Pierini, two LNIO PhD students who work on nanoscale energy transfer in hybrid nanoplasmonics and integration of nanosources.

Ag NWs were deposited on the substrate by spin coating followed by DLW of resins containing QDs. The first attempt is to get a polymer dot containing QDs G at one end of nanowire. Then, at the other end of the nanowire, another dot containing QDs R would be deposited *via* TPP-DLW. In this context, the final goal is to obtain the red emission by energy transfer between a donor (QDs G, emitting in green) and an acceptor (QDs R, emitting in red) *via* metal NW surface plasmons, when the green dot is excited with the blue light (405 nm), opening a new route to energy transfer in nanophotonics, involving important studies such as measurement of the propagation distance of the surface plasmons and the investigation of the parameters such as incidence excitation energy, incident polarization, coupling efficiency, etc.

The SEM images of a nanowire deposited on glass substrate with QDs are presented in Figure 4.1.

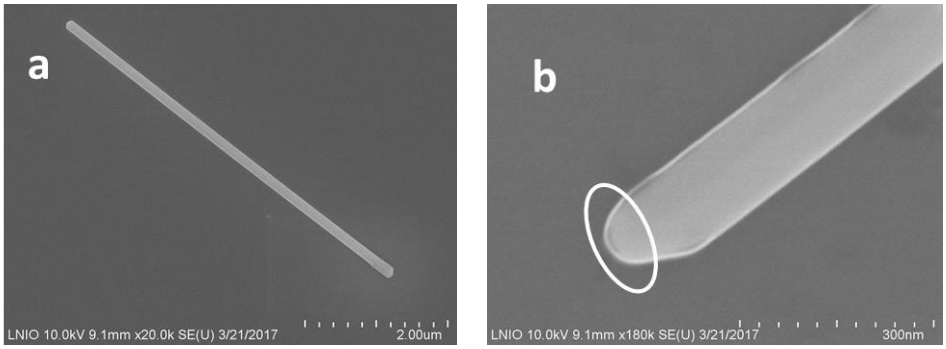

Figure 4.1: SEM images of an Ag NW: (a) 5 m long wire and (b) zoom in of the extremity.

4.2.1. Surface plasmon launching

As a first step, in order to confirm that energy transfer is possible *via* surface plasmon propagation on the wire, the set-up shown in Figure 4.2 was implemented. Two different lasers are introduced, one is with the wavelength of 633 nm, and another is with 533 nm. A linearly polarized focused beam is used in normal incidence to illuminate an extremity of NW in order to launch the surface plasmons.

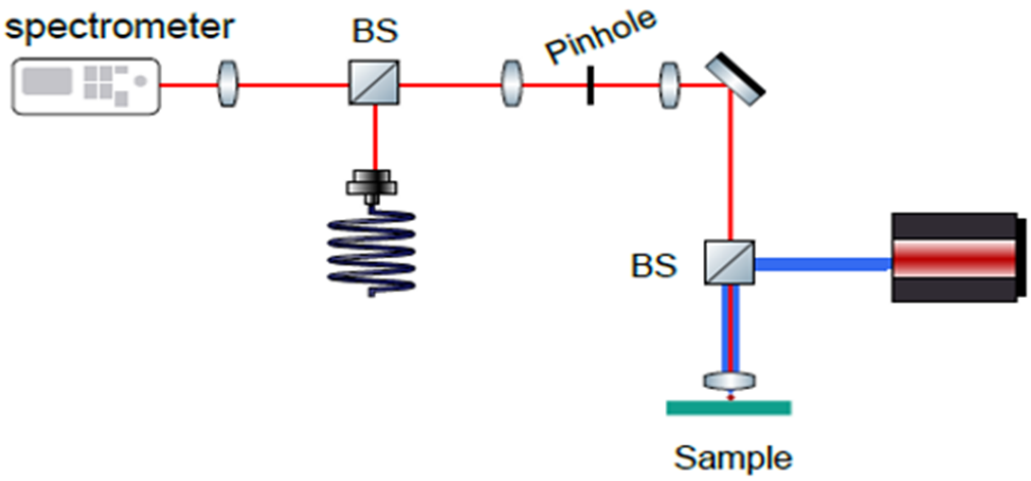

Figure 4.2: The optical set-up developed to study the surface plasmon launching in Ag NWs.

It should be stressed that the illuminated nanoscale extremity (see Figure 4.1b) is expected to lead to a large angular scattering spectrum, making possible surface plasmon launching by matching the plasmon dispersion function. In other words, scattering from the NW extremity is likely to produce desired large in-plane wave vectors allowing for plasmon launching. In addition, the intrinsic polarization anisotropy of isolated indium phosphide (InP) nanowire was demonstrated to lead in striking anisotropy in the photoluminescence intensity

recorded parallel and perpendicular to the long axis of a nanowire [179]. Then it is of importance to confirm the polarization anisotropy of Ag NW in our case.

Y polarized 633 nm laser with a power of 26.7 µw was introduced onto the end of 15 µm AgNW (see Figure 4.3). A full field image (bright and dark) permits the observation of scattering. From Figure 4.3, it is clear that by this excitation, the other end of the NW can be excited, which means the energy can be transferred by the nanowire, from an extremity to the other one, through surface plasmon propagation. Since a surface plasmon a longitudinal surface wave, it requires incident field component along its wavevector. In this figure, this component was significant (Y incident polarization). In order to confirm that surface plasmons are involved an X-oriented NW was selected and illuminated under the same condition as for Figure 4.3. Figure 4.4 shows the observed optical images. It turns out that energy cannot transfer by nanowire due to the orientation selectivity of nanowire; the longitudinal surface wave could not get excited.

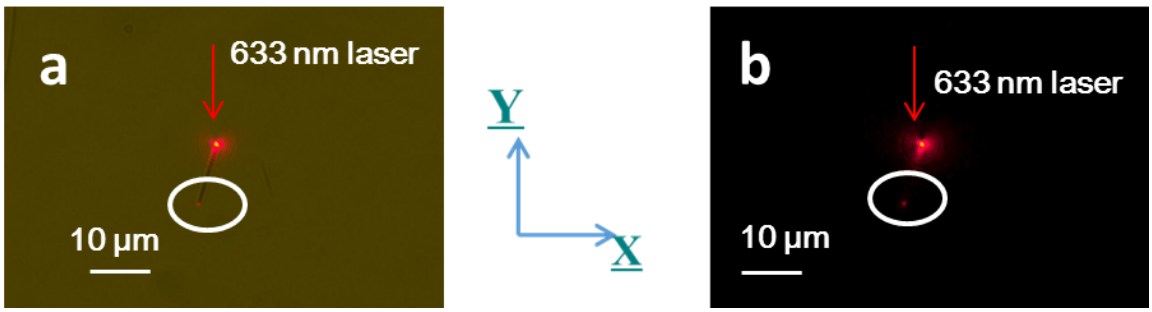

Figure 4.3: Optical images of an Ag NW under a local excitation of a 633 nm laser with a Y polarized light (a) bright and (b) dark. The arrow points out the incident laser beam. The circle highlights light scattering at the output extremity.

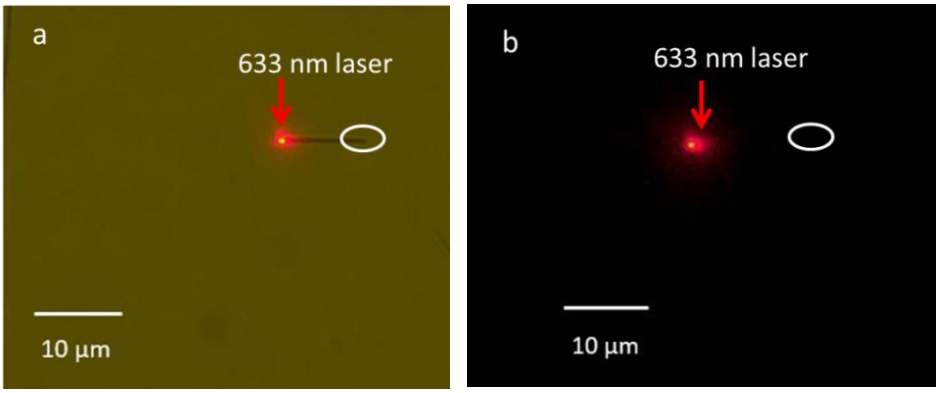

Figure 4.4: Optical images of an X-oriented Ag NW under a local excitation of 633 nm laser with a Y-polarized light (a) bright field and (b) dark field; the arrow points out the incident laser beam. The circle highlights light scattering at the output extremity.

A 532 nm wavelength laser with an excitation power of 6.7 µw was also used to excite one end of AgNW under the same conditions as for Figure 4.3 and 4.4 (see Figure 4.5). In Figure 4.5, clearly-observed emission at the other NW extremity is probably the signature of energy transfer by surface plasmon propagation. It was also proved that nanowire exhibits orientation selectivity at this wavelength.

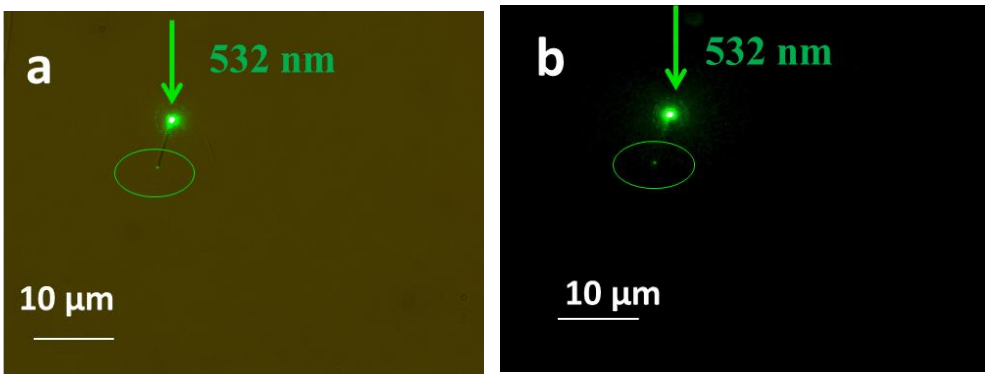

Figure 4.5: Optic images of an AgNW under a λ =532 nm excitation. (a) bright field and (b) dark field.

In conclusion, Ag nanowires can support propagating surface plasmons in both wavelengths. Regarding to this, it is notable that the NW orientation relative to the incident polarization direction plays an important role in energy transfer.

4.2.2. Size dependent-on the laser parameters

In order to define the photonic parameters for the integration of nanometric polymer dots that contain QDs on the extremity of AgNW, it is necessary to study the size dependent-on the laser parameters. Figure 4.6 shows the diameter (as measured by SEM) of polymer dots integrated on glass substrate as a function of laser (a) power and exposure time (b).

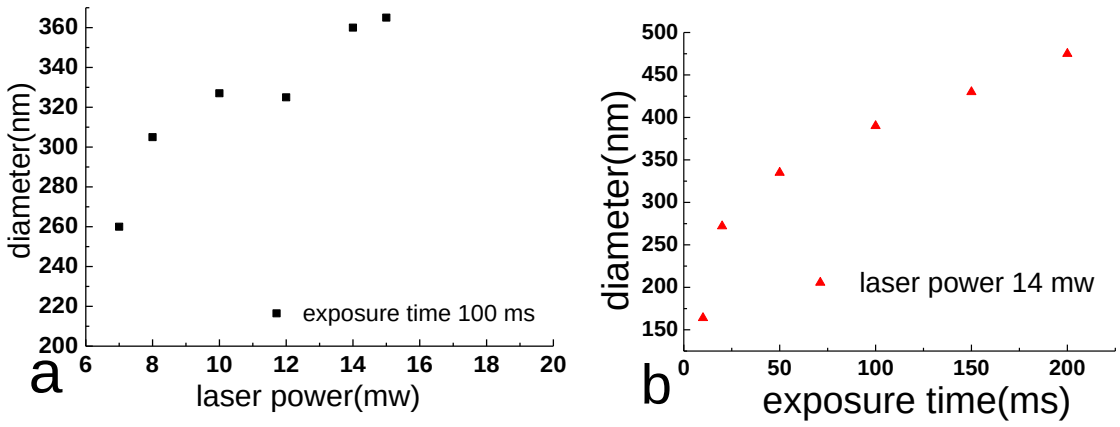

Figure 4.6: diameter of the dot fabricated outside the nanowire as a function of laser power and exposure time.

From Figure 4.6, it is clear that, under the same time of exposure, the diameter of the dot increased as the laser power increased. On the other hand, with the same laser power, the diameter increased when the exposure time rose. SEM images of QDs-containing polymer dots are shown in Figure 4.7 and Figure 4.8.

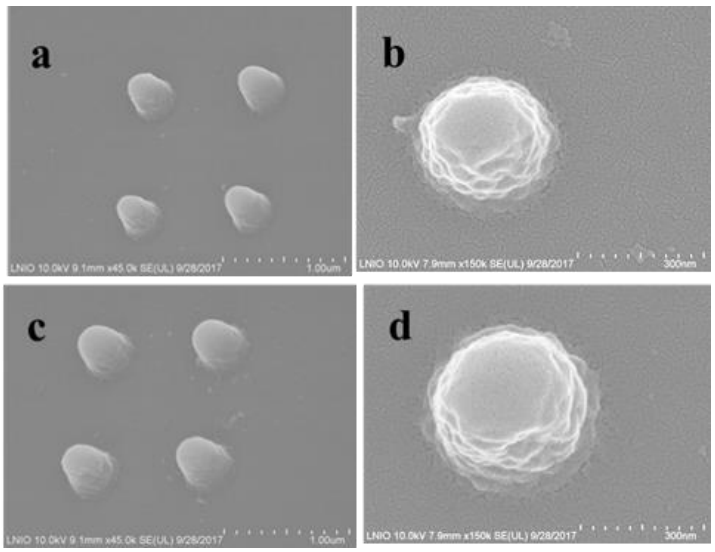

Figure 4.7: The dots containing QDs G fabricated with the same exposure time of 100ms (a and b) at laser power 7 mw; Diameter=260 nm; (c and d) laser power 14 mw; Diameter=360 nm.

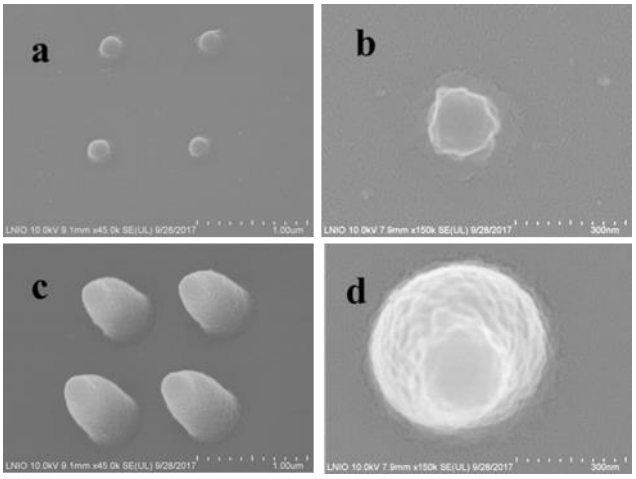

Figure 4.8: The polymer dots containing QDs G fabricated with the same exposure power of 14 mw (a and b) with exposure time of 30 ms; Diameter = 160 nm; (c and d) with exposure time of 200 ms; Diameter = 490 nm.

4.2.3. Study of the energy threshold to be used for the integration of QDs on AgNWs

As the SNWs can absorb a part of the incident light will be used for the integration by TPP, it is necessary to study the influence of AgNW on the laser parameters already identified in the previous section. First a pulsed laser (λ=780 nm) was introduced to expose on the AgNW without adding the photopolymer. It quickly turned out that the nanowire got burned when the incident laser energy is very strong. For instance, present in Figure 4.9, under 14 mw exposure, the nanowire was burned when the exposure time was over 80 s, however, when the exposure time was 75 s, the NW kept intact.

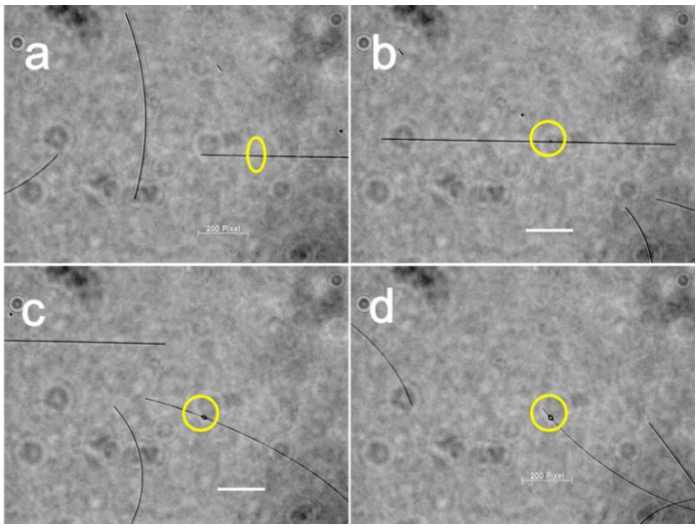

Figure 4.9: Optical images of Ag NW under exposure power at14 mw with exposure time: (a) 75s, (b) 80 s (c) 85 s and (d) 90 s. The circles highlight the position where the laser is exposed.

As a result, we had to manage this threshold of damage for avoiding any modification of the nanowire under pulsed laser excitation.

Besides, it was interesting to find out that, the threshold energy of photopolymerization was modified by the presence of the NWs. The local energy enhancement in the system containing NW and QDs can be shown in Figure 4.10. Without nanowire, the threshold energy of QDs-containing photo resist, here is PETA-QDs G-IRG, is at least twice higher than that located on the nanowire.

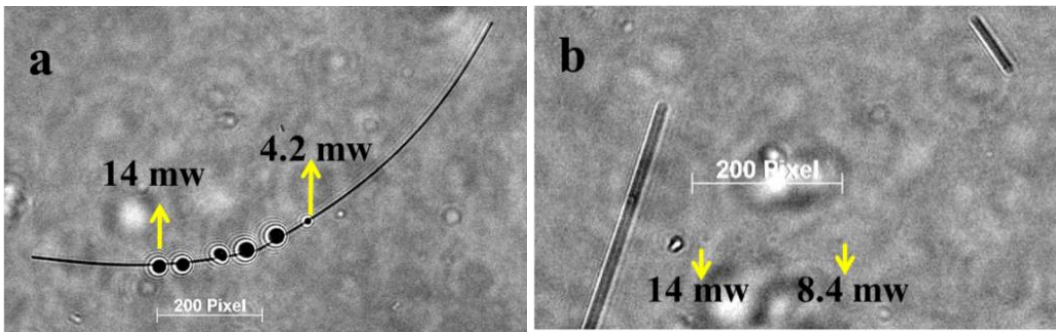

Figure 4.10: Optical images of polymer dots containing QDsG under the same exposure time of 5 ms: (a) on the Ag NW and (b) out of Ag NW. 200 pixel= 20 µm.

In Figure 4.10.a power and exposure time were set to keep the incident energy below the photopolymerization threshold. In that way no polymerization is expected as it can be seen in Figure 4.10.b. On the contrary, above the nanowire, polymer dot were clearly integrated, suggesting an enhancement effect which is may be attributed to the presence of nanowires. The local dose for photopolymerization may be increased due to the optical near-field plasmon enhancement [123] and/or the local heating. In this sense, it is of interest to do the investigation on the enhancement effect in the future work to make precise fabrication of polymer dot.

These preliminary observations show that the incidence laser power should be in the certain range in order to get a dot containing QDs without ruining the nanowire as well. These images also demonstrated that the size of the dot is dependent on the incidence laser power and exposure time. This dependence is discussed in the following section.

4.2.4. First promising results

As far as the hybrid plasmonic structures are concerned, it is of significance to have a clear mind not only on the location of the nano-emitter but also the size which plays an important role in the coupling efficiency. As mentioned above, *via* TPP-DLW, it is possible

to obtain the dot with controllable size and location in a simple manner by using the photosensitive resins containing QDs.

As the first trial, on one end of a nanowire, a dot containing QDs G is located *via* TPP-DLW using PETA-QDsG-IRG. In Figure 4.11, on the end of the Ag-NW, there is a dot with QDs-G showing green emitting color. However, since the location of nanowire is by random, and there is polarization in each different nanowire, so far, it is not available to observe the signal from the empty end of the nanowire (with no QDs). In this regard, the future efforts should be in the investigation on the controllable size of dot with single QD, the excitation laser energy, polarization and orientation of nanowire, coupling efficiency of QDs with nanowire, etc.

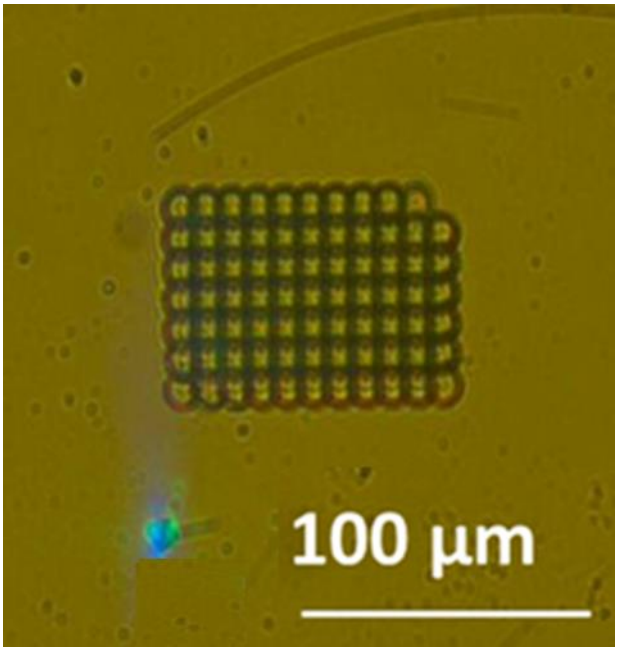

Figure 4.11: Optical image of AgNW with QDs-G in one end (the QDs are under 405 nm laser exposure).The nanowire is highlighted by the arrow. Structure above is to test QD-containing polymer pattern made for adjusting the parameters.

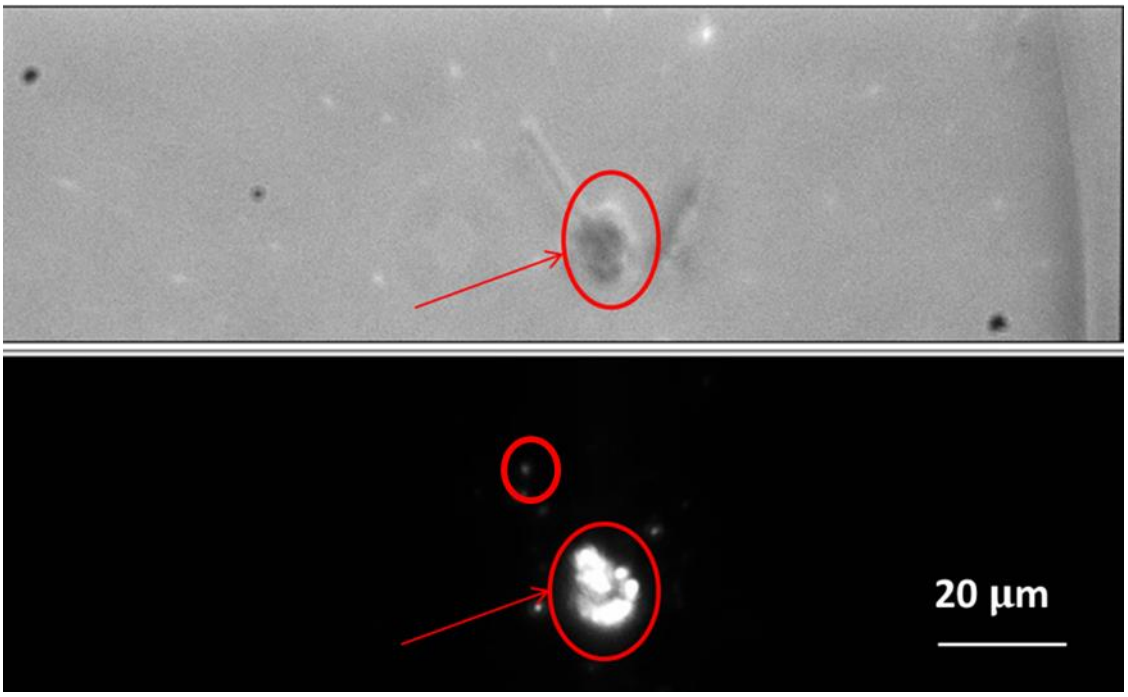

Figure 4.12: Top: optical image of a QD-containing polymer dot integrated at one extremity of an Ag NW. Arrows point out both dot and NW. Bottom: filtered photoluminescence image (green light). A blue laser beam was focused onto the polymer dot. The circles highlight the NW extremity.

Efforts were pursued, resulting in the results presented in Figure 4.12. Figure 4.12 (top) shows an optical image of a nanowire and QD-containing polymer dot that was integrated at one NW extremity. Both of them are highlighted by the arrows. Figure 4.12 (bottom) is the photoluminescence image of the same object. A laser spot at λ=405 nm was focused right on the polymer dot. While this incident wavelength cannot directly launch the surface plasmon, it is absorbed by the QDs that got excited and de-excited through green emission. This emission can couple with plasmons, resulting in surface plasmons that scatter at the other extremity. In Figure 4.12 (bottom) the incident light was cut by a spectral filter that stops wavelengths < 450 nm. Bright spot in the figure correspond thus to green emission, as confirmed by Figure 4.13 that shows the photoluminescence spectrum measured at the polymer dot and at the NW extremity highlighted by the circle. Emission from the QDs centered at 540 nm is clearly visible.

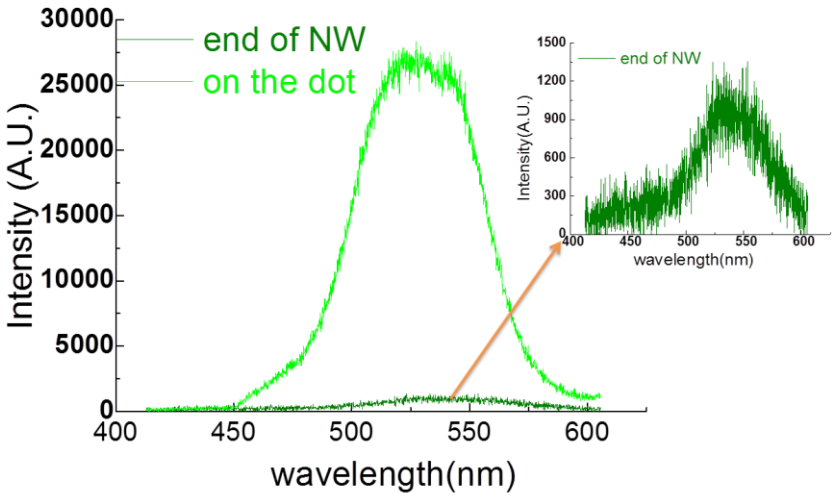

Figure 4. 13. Photoluminescence spectra taken at the polymer dot and at the other NW extremity. A confocal configuration was used: the signal comes from 3 microns size zone.

Although some doubts remain (role of the background from QDs still attached on the substrate or the NW despite the rinsing, direct scattering form the polymer dot,..) these preliminary results encourage the LNIO to work further on this subject.

To summarize, by exploiting the QDs-containing polymerizable resins *via* TPP-DLW, is one simple method to have a good control of the localization of QDs-emitters while coupled with nanowires. This provides an exciting possibility to create a platform to integrate SP-based passive elements and QDs-based active elements which can be favorable to the future nanoscale photonics.

4.3 Fibered probe nanotips containing QDs

In recent decades, extensive researches have been focused on scanning probe microscope (SPM). For example, as a member of SPM family, an atomic force microscope (AFM) has evolved into direct measurements of intermolecular forces with atomic-resolution characterization due to its low internal dissipation, high quality factor (Q-factor), self-sensing, which can be broadly applied such as in electronics, semiconductors, biology [15, 180]. Besides, it is routinely used for mapping the surface topography with resolution beyond the optical limit. Scanning near-field optical microscopy (SNOM), which can provide surface information with a lateral resolution of a few tens of nanometers, has been utilized, for example, for the fundamental understanding of surface plasmon in nano-structured metallic

surfaces [181]. In all these microscopes, the pivotal part is the tip, which will interact with the samples.

Active light emitting molecules that are locally integrated at the extremity of SNOM probes have for long given rise to many research works. The motivation is to avoid the background due to the incident light (emission for molecules is an inelastic process) and to exploit the physics of the nanoemitters (lifetime, orientation, quantum yield…).

For instance, semiconductor nanocrystals, quantum dots were used to functionalize AFM tips, which may be useful for fluorescence resonance energy transfer (FRET) microscope [182]. With such active molecules, near field information can be collected as the interaction between probe and sample near field occurs. As a significant example, the local density of state of a metal nanostructure was imaged through the modification of the lifetime of a nanoemitter localized at a fibered SNOM probe [183]. In general, active probe could be used as local photonic source in sensing and mapping systems.

Fabricating active SNOM probes based on active nanoemitters is still a challenge. In general, the probe tips are fabricated by various methods, such as mechanical pulling method or melt-stretching method [184], mechanical polishing [185], chemical etching [186], focused ion beam [187], electron beam lithography [188], and pulsed laser ablation [189], etc. Probe tips fabricated by mechanical machining methods can be with low optical transmission efficiency, and low reproducibility and uncontrollability of shape. Although the latter lithography methods can be controlled precision in shape, however, the procedure is time consuming and complicated. As known that most probes used frequently are based on optical fibers. The integration of nanoemitters on the fibered tip is still in challenge of the random localization of QDs, low stability of QDs on the tip and the low-resolution of the probe tip containing QDs.

Besides, it has been reported that polymer tip integrated at the fiber end can greatly increase the optical throughput [181], which can be made into optical nanosensors and detection [190]. Direct photopolymerization at the extremity of optical fiber is very useful for fabricating tip on the core surface of fiber due to its simple setup, low laser intensity and short exposure time like few seconds. The challenge is to integrate QDs on SNOM probe or fiber tip. Since the polymerization could be triggered by near-field energy, it is possible to use photosensitive resins containing QDs to obtain a probe containing QDs.

As the first step for the project aiming to get active SNOM probe, we had to confirm the feasibility of the resin PETA-QDsR-IRG selected for this application using a simple approach.

The preliminary study was done with Hongshi Chen, a LNIO PhD student who works on new active tips for SNOM. A drop of the resin was deposited on the end of a cleaved single mode optical fiber (diameter = 125 µm). A laser beam (λ=405 nm) for one-photo polymerization launched into the other fiber end, was guided by the fiber to the end where the resin is deposited. After exposure, the resin is polymerized. Then acetone and isopropanol are used for removing the remaining resin. As following, the tip is obtained.

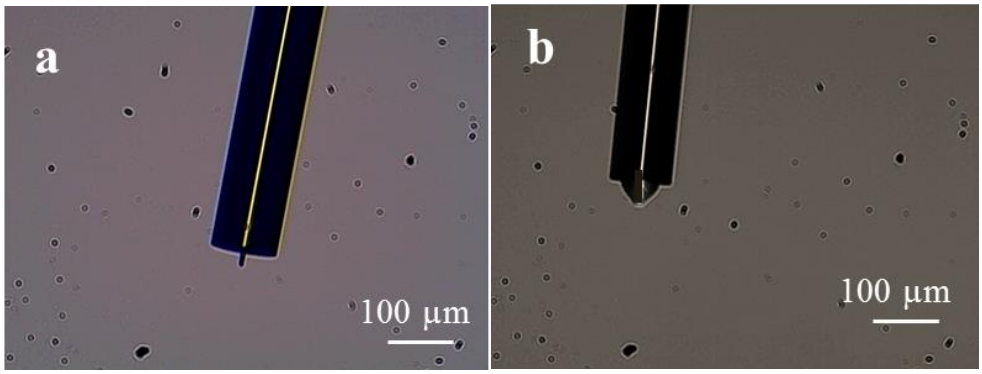

Figure 4.14: Optical images of QDs-containing polymer tips fabricated at the extremity of an optical fiber (a) exposure under 20 µw for 1/15 s and (b) exposure under 2 µw for 10 s.

In Figure 4.14, polymer tips obtained under different exposure time were shown. From this, it is clear that by controlling the exposure, the shape of the tip can be controllable. About the parameter optimization, there are several researches been reported studies [184]. In this section, we just show some examples. In order to confirm the presence of QDs inside the tips, a 405 nm laser is launched into the tip (from the other cleaved fiber extremity), and the red emission could be clearly observed from Figure 4.15, which can also be seen from the top view images, shown in Figure 4.16. More else, the emission spectrum from the tip is also obtained (shown in Figure 4.17), it shows the emission peak is around 613 nm.

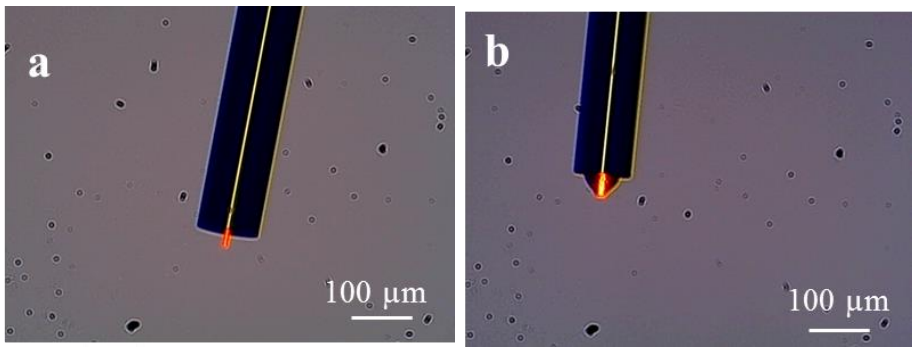

Figure 4.15: Fluorescent images of QDs-containing polymer tips fabricated at the extremity of an optical fiber (a) exposure under 20 µw for 1/15 s and (b) exposure under 2 µw for 10 s.

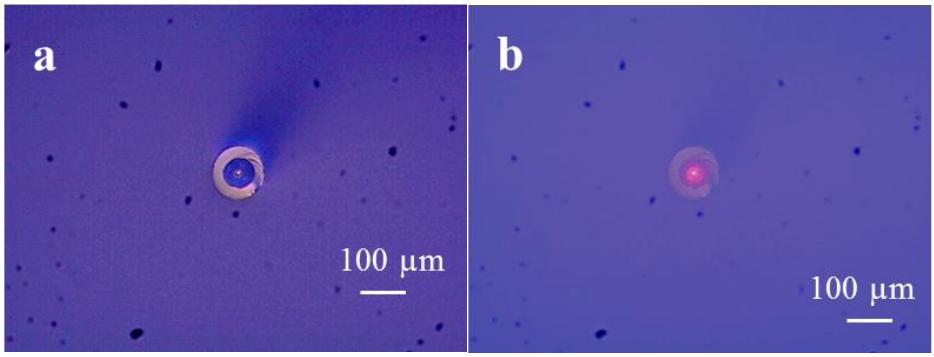

Figure 4.16: Optical images of the tip from top view: (a) without excitation (b) under excitation by a 405 nm laser.

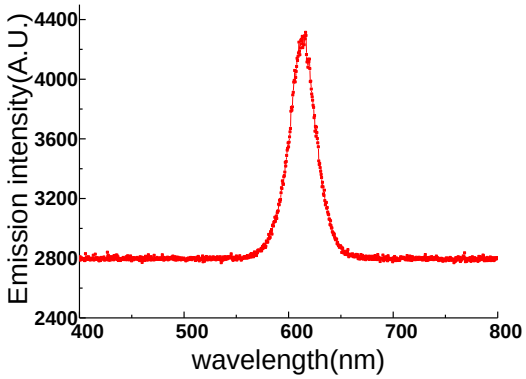

Figure 4.17: Emission spectrum of the tip under excitation by a 405 nm laser.

In order to improve the spatial localization of the QDs, a two-step exposure was done. A first tip was made with a polymer that does not contain any QDs. Then, from this first tip, a second tip was grown with a photopolymer containing both QDs and inhibitor (MEHQ) which was developed in the chapter 3. Result of this 2-step procedure is shown in Figure 4.18 and Figure 4.19. A small light-emitting dot (typical size below 200 nm) is integrated at the extremity of the polymer tip. This promising approach is currently explored by Hongshi Chen who installed on a SPM head for first tests of optical imaging based on fluorescent tips.

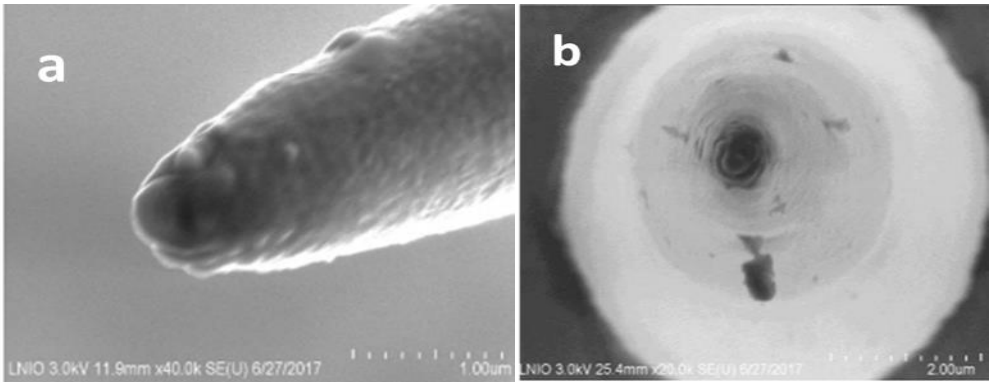

Figure 4.18: SEM images of the polymer tips *via* 2-step exposure (a) side view and (b) top view.

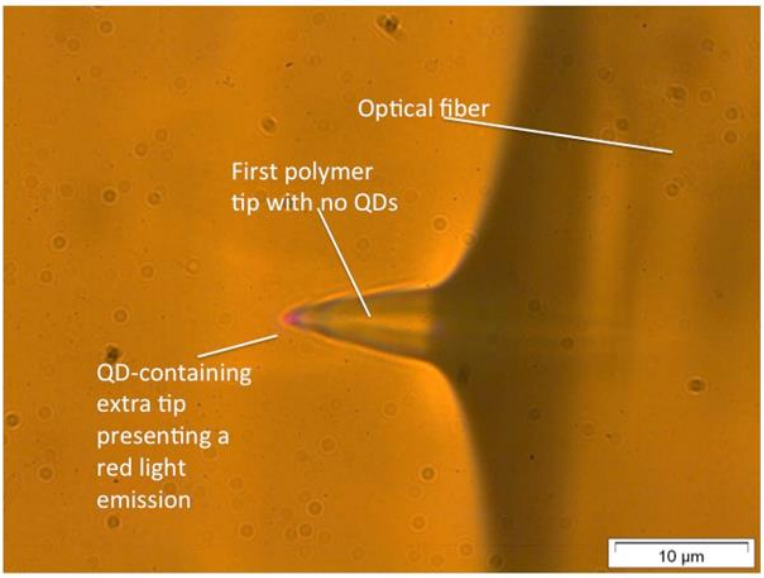

Figure 4.19: Fluorescence from an extra tip under excitation by a 405 nm laser.

An ultimate method is currently also investigated: polymerization will be performed at the extremity of a SNOM aperture probe. The probe optical near-field will be used for locally triggering the photo polymerization, resulting (hopefully) in a nanometric polymer dot at the end of the SNOM probe. This dot should contain one or a few QDs

In brief, the polymerizable resin containing QDs can be used in the fabrication of fiber tips, which may be applicable for example in SNOM and probe-assisted FRET. Further investigations about the fabrication and procedures or parameter optimization or functionalization or integration with other devices should be done in the concern of development of science and technology. The final goal is to integrate a single photon source

by polymerization with proper parameters such as exposure time, exposure energy, laser wavelength and resin compositions.

4.4 QDs coupling with gratings

In the field of optics, it is attractive that by surface plasmon which can help us to concentrate and channel light using sub wavelength structures. In this way, the photonic circuits with miniaturized scale can be achieved. As to build such a circuit, waveguides is one of the ineligible elements [138]. Besides, nanophotonic waveguides are adequate components for engineering photon emission and scattering attributed to the strong confinement of photons to one-dimensional geometry [191-193]. Recent researches on QDs coupling to waveguide gratings have demonstrated the modified optical radiation and enhancement of luminescence *via* SPPs [194]. It sheds a light onto the idea of localization of light emitter inside an optical medium with a photonic band gap to modify the luminescent behavior.

Regard of the application on the on-chip information processing, it is crucial to take control of the photon emission by single emitter. Nowadays, in majority, the localization of QDs is by depositing on a substrate. In this case, the location of QDs is by random and the geometry as well as the size is stochastic. Moreover, the growing films containing QDs might lead to low efficiency or high dark counts [195, 196]. In this section, due to the virtue of direct laser writing, the QDs can be located in designed place on the nanowire with certain geometry and scale. Furthermore, indistinguishable photons can be negligible toward on-chip optical quantum computation.

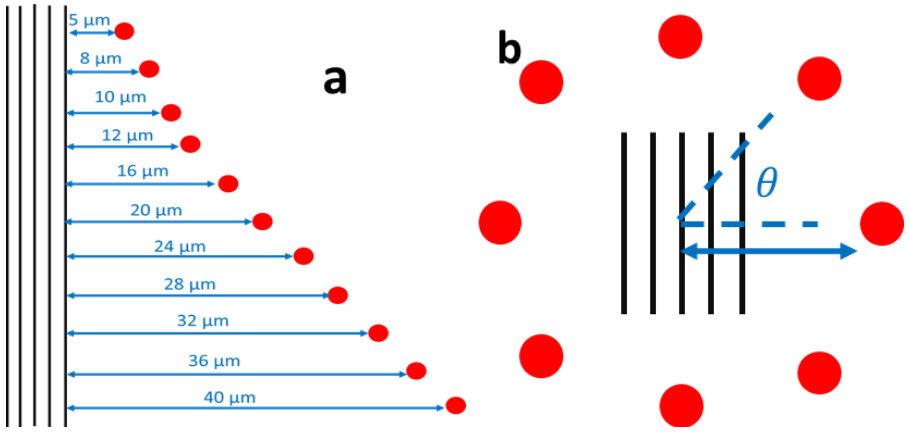

Figure 4.20: designed location of QDs to the gold gratings

This work has been done in collaboration with Aurélie Broussier. Gratings are designed for launching propagating surface plasmons and fabricated by EBL; the procedures are

mentioned in chapter 2. The QDs can be placed *via* TPP-DLW with the utilization of QDs-containing resins at different distances from the gratings, as shown in Figure 4.20.a, or in varied direction to the gratings (Figure 4.20.b). Figure 4.21 presented the SEM image of the gratings made by EBL.

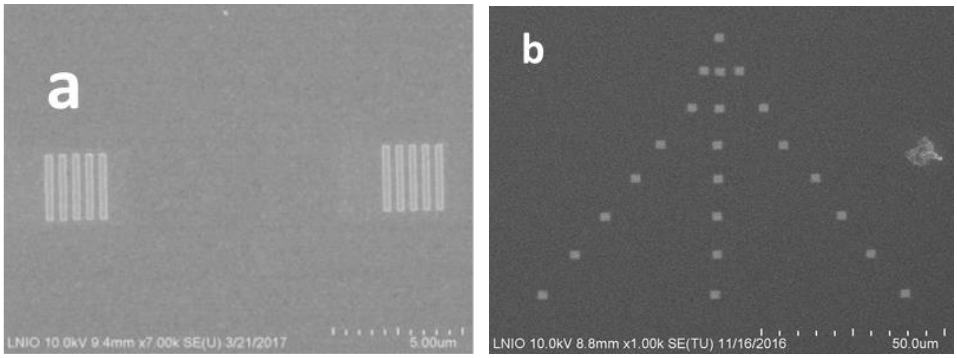

Figure 4.21: SEM image of the as-prepared gratings (a) zoomed on and (b) whole

The goal is to control energy transfer between the grating and QDs through surface plasmon propagation: the grating launchers the surface plasmons that propagates on the metal film in order to excite the QDs that emit light.

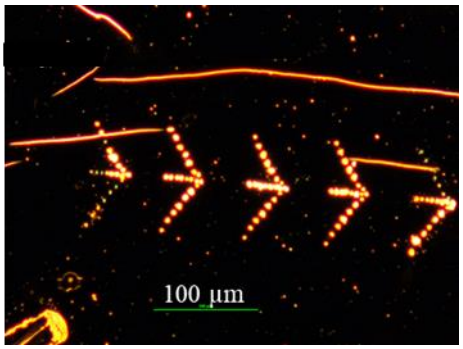

Figure 4.22: Optical image of gratings with QDs located on

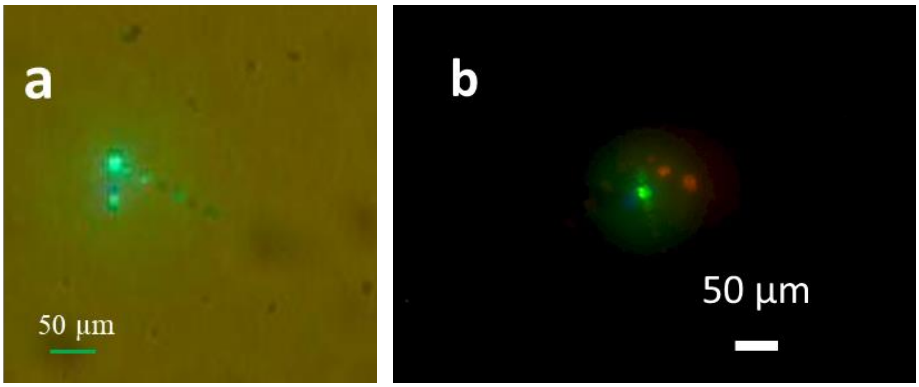

Figure 4.23: Fluorescent image of the gratings with two kinds of QDs located on: (a) QDsG (b) QDSG and QDsR

The gratings with QDs located on were shown in Figure 4.22. The fluorescent image can be present in Figure 4.23 under exposure of a 405 nm laser. It can be seen that, the green and red emission can be obtained which demonstrated the successful localization of QDs.

So far, no coupling was observed. This could be by reason of wrong configuration parameters (period of grating, thickness of Au layer, distance between gratings, size of QDs emitters, etc.), excitation laser power and polarization. Since then, it is necessary to do simulation investigation focused to achieve the optimized configurations of this hybrid structures, the available excitation laser power and the polarization angle. All these could be realized in the future studies. In this work, we showed great opportunity to precise location of QDs-nanoemitters on the metal gratings *via* TPP-DLW with the formulation of photosensitive polymer resins containing QDs.

4.5 Photosensitive resins containing QDs in the fabrication of hybrid plasmonic structures

Fast development of information and communication technologies, higher bandwidth and greater energy efficiency is drastically required in response to the increasing storage of optical data. In this regard, variable and considerable optical functionalities in a small chip are in desperate need which calls for fast development of the integrated optics and nanophotonics. As an essential part of the nanophotonics, the efficient integration of optical nanosources which is quite qualified to activate specific parts on the circuit is highly required [197, 198]. Recently, great interest has been devoted in the fabrication of hybrid plasmonic nanoemitters, which consists of metal nanostructure and adjoining components such as organic dye molecules or quantum dots [199-202]. In this sense, over the past decade, the effects between metal nanostructures and external molecules have been investigated. Plasmon-induced polymerization has been demonstrated to occur as a result of coupling of hybrid plasmonic structures leading to the creation of hybrid nanomaterials with modified optical properties [203, 204].

Attributed to the promising optical behaviors such as coherent coupling, optical gain, solar energy conversion, photocatalysis and nonlinear optical interactions, hybrid nanomaterials has drawn great attention in nanooptics. The reported results show the coupling reaction can be controlled by the selective size, shape, and composition and polarization state [205, 206].

Additionally, QDs-containing hybrid polymer-metal structures presenting anisotropic spatial distribution [123]. In this ref, two-color anisotropic nanoemitters was fabricated based on plasmonic TPP with photosensitive resin containing QDs. Great challenges remain in reliably integration of multi-colors nanoemitters in nanooptic and nanophotonic circuit. In this sense, it is of interest to fabricate nanoemitters in specific locations *via* TPP-DLW, which enables the location of emitters in specific locations, for example shown in Figure 4.24. Besides, the size, emission properties can also be controlled during fabrication.

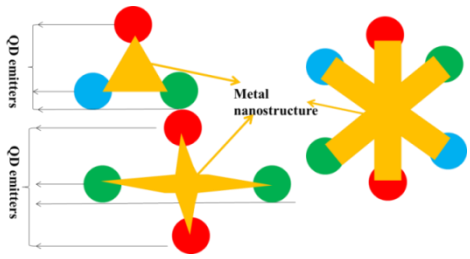

Figure 4.24: Sketch of multi-color emitters with metal nanostructures

As for beginning, the first step is to confirm the reliability of polymerization. PETA grafted red QDs with 1 wt.% Irgacure 819 and Au nano-cubes were used for polymerization. This work was done in collaboration with Dandan Ge, a PhD student who is working on new hybrid nanosources, and Sylvie Marguet (CEA Sacaly) who fabricated the nano-cubes.

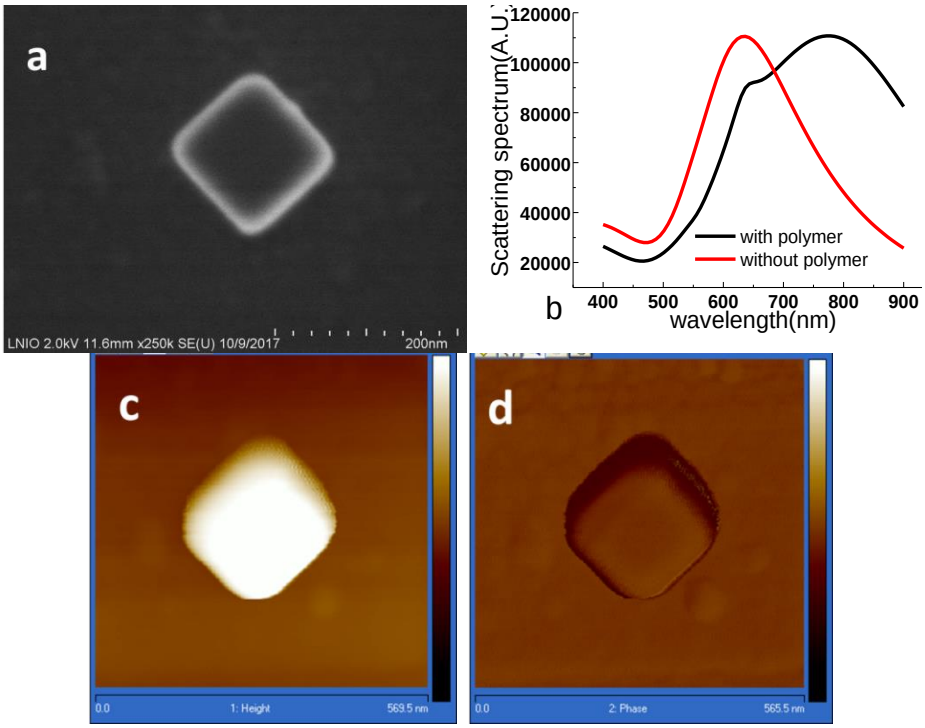

Figure 4.25: a: SEM image of the studied nano-cube; b: Scattering spectrum of a single cube on glass (with and without surrounding polymer); c: Topography image of the studied cube; d: phase image of the studied cube.

Figure 4.25.a shows SEM image of studied single nano-cube as well as scattering spectra of a single cube on glass (with and without photopolymer). As shown in Figure 4.25.b, the spectral position of the plasmonic resonance is suitable for near-field TPP at λ=780 nm.

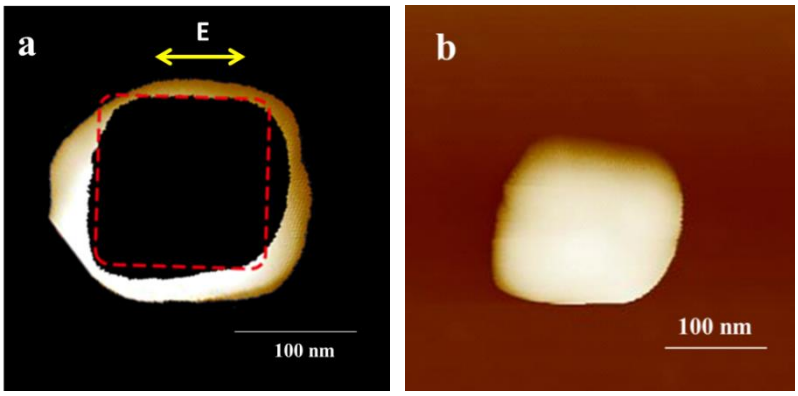

Figure 4.26: Images of the obtained polymer around the nano-cube. The plasmonic two-photon polymerization was carried out at λ= 730 nm, under an objective of 40x0.6

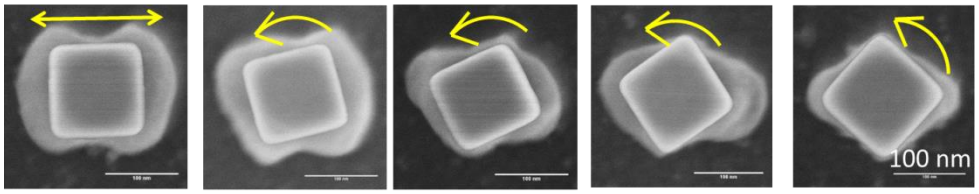

Figure 4.27: Images of the obtained polymer around the nano-cube. The plasmonic two-photon polymerization was carried out at λ= 730 nm, under an objective of 40x0.6

Figure 4.26 and Figure 4.27 shows a first result of the polymer integrated in the vicinity of an Au nan-ocube, which confirms the realization of photopolymerization. More precisely, Figure 4.26.b is the AFM image of the cube taken before photopolymerization, while Figure 4.26.a is the AFM image of the same studied cube taken after photopolymerization. We extracted Figure 4.26.b from Figure4.26.a (dark central zone) to highlight the integrated polymer that is expected to contain QDs. Moreover, from Figure 4.27, it was obvious to see the integration of QD-containing polymer at specific locations of the nanocubes. Photoluminescence experiments are in progress.

The future work is going to be focused on the location of nanoemitters with precise size, shape and number of QDs following by the investigation on the selective polarization of incidence laser in order to successfully obtain multi-color emitters. Considering the superior virtue of flexible localizing polymerization *via* TPP-DLW, it gives great opportunity to be the integration of hybrid plasmonic structures.

4.6 *Conclusion*

In this section, the integration of QDs with plasmonic and photonic structures such as nanowire, fiber tips, metal gratings, and nanocubes was realized *via* TPP-DLW by using photosensitive resins containing QDs. We demonstrated that the QDs can be located as expected with controllable size. In the future, the investigation on the light emission, the coupling efficiency and energy transfer mechanism might be the key issue considering the promising application in plasmonics and photonics.

Chapter 5. Conclusions and perspectives

This thesis aims at the fabrication 3D/2D functional structures with improved resolution *via* TPP-based DLW. Among the considerable routes to improve the resolution, chemical routes were investigated in this thesis by addition some specific inhibitors of free radicals.

Firstly, the investigation was devoted in the influence of MEHQ on the resolution of the structures obtained *via* TPP-DLW. Photochemical and kinetics studies were done at both one and two photon excitations in order to understand the contribution of MEHQ on the polymerization mechanism at both macro and microscale respectively. The results showed that with MEHQ involved in TPP-DLW, the resolution of 2D lines and 3D woodpiles as-prepared is improved, especially in 3D woodpiles; the smallest linewidth is 60 nm while the period is 350 nm, and the smallest period is 250 nm with a linewidth of 80 nm. This improvement of resolution is attributed to a significant increase of the threshold energy of polymerization and change in the termination mechanism of the polymerization. More particularly, with the presence of MEHQ, radical chains seem to perform monomolecular termination.

Secondly, hybrid 3D QDs-containing polymer structures have been showing fascinating application such as in optics and plasmonics. QDs-containing polymer structures were fabricated *via* TPP-DLW. The interesting results showed that the spatial resolution of 2D and 3D structures is significantly improved with the presence of QDs. This interesting behavior that has never been reported before was deeply studied in this work. The influence of the QDs and laser power on the resolution of the as-prepared structures was then investigated. The feature size of the fabricated polymer lines could reach 75 nm. According to the FTIR and UV spectra which show remarkable decrease in the polymerization rate of the photo resists containing QDs, among as the investigation on the relationship between the laser power and polymer growth, the improved resolution in the issue of the fabrication containing QDs might be attributed to the absorption of QDs during writing leading to less photon absorbed by the initiator, on the other hand, with the presence of QDs, the radicals inclined to perform monomolecular termination which somehow favors the improved resolution of the as-prepared structures. Moreover, the fluorescent images and emission spectra show stable local emission from the as-prepared structures containing QDs. Besides, the emission intensity of the structures varies with the writing laser power. In this sense, the size of the

structure and fluorescent properties can be controllable in the case of TPP-based direct laser writing, which affords a path for the future investigations and applications.

In chapter 4, the integration of QDs with plasmonic and photonic structures such as nanowire, fiber tips, metal gratings, and nano-cubes was realized *via* TPP-DLW by using the photopolymerizable resins containing QDs developed in chapter 3. We demonstrated that the QDs could be integrated as expected with controllable size. In the future, the investigation on the light emission, the coupling efficiency and energy transfer mechanism might be the key issue considering the promising application in plasmonics and photonics.

As for future perspectives, considerable applications can be done. By exploiting the QDs-containing polymerizable resins *via* TPP-DLW is one simple method to have a good control of the localization of QDs-emitters while coupled with nanowires, metal gratings, waveguide. This provides an exciting possibility to create a platform to integrate SP-based passive elements and QDs-based active elements which can be favorable to the future nanoscale photonics. Additionally, regarding to the demand of high resolution in imaging technologies and sensors, nano-scale tip containing QDs is promising which might support the mapping in SNOM, FRET and AFM.

Chapter 6. French Summary

6.1 Introduction

L'écriture laser directe par polymérisation à deux photons (ELD-PDP) de résines photosensibles est basée sur un processus non linéaire qui permet une stéréolithographie optique et une écriture directe de haute résolution de structures 3D. L'atout principal est l'absorption à deux photons par les résines photosensibles. Un faisceau laser infrarouge femto-seconde est concentré dans le volume de la résine déposée sur le substrat de silicium ou de verre. En balayant le faisceau dans l'espace, des structures tridimensionnelles peuvent être fabriquées. Cette technique peut servir à fabriquer divers micro-systèmes polymères comme des systèmes micro-fluidiques, biomédicaux, optiques, mécaniques et micro électroniques [21]. Cependant, un challenge réside en ce qui concerne la résolution : jusqu'à présent, la résolution est toujours 1 ou 2 ordres de grandeur inférieure à celle permise par d'autres techniques telles que la lithographie électronique (EBL).

Compte tenu de la limite de résolution de ELD-PDP, il existe plusieurs solutions. Par exemple, un schéma de puissance minimum et la durée d'exposition minimale (MPMT) a été proposée pour réduire au minimum les voxels, ce qui veut dire réduire la puissance du laser utilisée et la durée d'exposition. Toutefois, cette procédure fait face à la difficulté de contrôler les conditions d'exposition laser afin d'obtenir les dimensions désirées [10, 11]. En outre, l'approche STED (déplétion par émission stimulée) est efficace pour réduire la taille de la fonction des structures fabriquées [12]. Toutefois, dans le cas du STED, deux faisceaux sont utilisés, ce qui exige le contrôle précis des systèmes impliqués [13]. Par ailleurs, l'utilisation de molécules inhibitrices s'est avérée bénéfique pour une meilleure résolution [14-16]. I. Sakellari [82] ont rapporté des structures de « tas de bois » avec une période 400 nm fabriquées en utilisant cette approche.

Dans cette thèse, un inhibiteur de photo polymérisation a été étudié et utilisé dans le but d'améliorer la résolution des structures 2D et 3D par un faisceau ELD-PDP, qui est censé être concurrentiel à celui de la STED-ELD. Des études de l'influence de cet inhibiteur et l'effet des conditions d'écriture (puissance du laser, vitesse d'écriture, etc.) sur la cinétique de polymérisation et la résolution ont été réalisées.

En outre, la fonctionnalisation de la structure 3D fabriquée par ELD-PDP a été étudiée pendant cette thèse. Les boîtes quantiques semi-conductrices luminescentes (BQs) ont donné lieu, ces 10 dernières années, à des travaux considérables en raison de leurs propriétés optiques uniques, dans de nombreux domaines incluant le diagnostic, les capteurs, et la nanophotonique/plasmonique [175-178]. Dans cette thèse nous traitons de la fabrication de structures 2D et 3D contenant des BQs *via* ELD basée sur la PDP. En particulier, nous étudions l'influence des BQs sur la résolution et des propriétés fluorescentes des structures finales. Enfin, nous présentons des résultats préliminaires de couplage de structures polymères contenant des BQs avec des systèmes plasmoniques et photoniques.

6.2 Partie Expérimentale

6.2.1. Description des résines utilisées

Pour fabriquer des structures 3D, nous avons utilisé deux résines photosensibles. Elles sont nommées PI et PMI et sont toutes les deux basées sur l'utilisation du Pentaérythritol triacrylate (PETA) comme monomère et du Bis (2, 4,6-trimethylbenzoyl)-phenylphosphineoxyde (ou IRGACURE 819) comme photoamorceur 2-photon. PMI contient un inhibiteur, le 4-methoxyphenol (MEHQ). La Table 6.1 récapitule les différents composés des deux résines. De plus, pour les structures fluorescentes, les résines contenant des BQs sont utilisées. La résine est greffée avec les BQs. Les BQs peuvent émettre à des longueurs d'onde différentes (510 nm, 460 nm, 610 nm et 590 nm). La Table 6.2 énumère les différentes compositions des résines contenant des BQs.

Table 6.1 Composé chimique, rôle et % massique de chaque constituant des résines

	Nom chimique	Acronyme	Rôle	% massique
Résine PI				
	Pentaérythritol triacrylate	PETA	Monomère	99
	Bis(2,4,6-trimethylbenzoyl) -phenylphosphineoxyde	IRGACURE 819	Photoamorceur	1
Résine PMI				
	Pentaérythritol triacrylate	PETA	Monomère	89
	Bis(2,4,6-trimethylbenzoyl) -phenylphosphineoxyde	IRGACURE 819	Photoamorceur	1
	4-methoxyphenol	MEHQ	Inhibiteur	10

Table 6.2 les résines contenant des BQs

	Longueur d'onde (Absorption)	Longueur d'onde (Emission)
Résine PETA_BQsR	350-550 nm	620 nm
Résine PETA_BQsG	350-470 nm	501 nm
Résine PETA_BQsB	350-450 nm	460 nm

6.2.2. Procédure de microfabrication

Nettoyage du substrat

Le nettoyage du substrat est une partie importante afin d'obtenir une surface sans poussière préservant ainsi la réponse de la résine. Différentes étapes doivent être achevées pour une bonne adhésion entre le substrat et la résine. Premièrement, le substrat est nettoyé dans de l'acétone, ensuite il est rincé avec de l'isopropanol. La désorption de l'isopropanol est achevée par séchage suite à un flux d'azote.

Lithographie à deux photons "Nanoscribe"

Toutes les 2D/3D structures sont fabriquées par ELD basée sur la PDP à l'aide du système commercial Nanoscribe qui permet la fabrication de structures polymères complexes. Le système est équipé d'une source laser qui émet des impulsions laser ultra-courtes (<120fs) à une fréquence de 100 MHz avec une longueur d'onde de 780 nm. L'inscription directe d'un dessin 3D se fait *via* un logiciel d'écriture qui synchronise le mouvement de l'échantillon avec l'intensité du laser. Le déplacement de l'échantillon par rapport au faisceau d'écriture (qui lui est fixe) se fait en associant une étape de balayage piézoélectrique (zone de débattement : 300×300×300 mm^3) avec une platine motorisée (zone de débattement de 130×100 mm^2). Après avoir traversé un filtre spatial et un système optique de collimation, le faisceau laser étendu et parallèle est couplé à un objectif de microscope à immersion d'huile d'indice 1.518 (grossissement ×100 et NA: 1.4) qui permet sa focalisation à l'interface haute du substrat se trouvant en contact avec la résine. Le système Nanoscribe offre la possibilité de positionner automatiquement le point focal du laser à l'interface substrat-photopolymère.

Une fois l'interface identifiée, il est possible de commencer l'écriture à une certaine position. L'identification de cette interface est essentielle pour s'assurer que la polymérisation a lieu au contact du substrat. Si ce contact n'est pas établi, les structures seront éliminées avec le reste de la résine au cours du développement. La précision du système de positionnement autofocus en z est de ±10 nm. Ce positionnement se fait selon un déplacement en z de l'objectif de focalisation. Le contrôle de la puissance du laser peut se

faire directement *via* l'ordinateur avec possibilité de la moduler au moment de l'exposition de la résine. Le système permet également de visualiser en direct la polymérisation à l'aide d'une une caméra et d'une source LED rouge (longueurs d'onde auxquelles les résines sont transparentes), située au-dessus du porte échantillon. En effet, la réticulation du polymère entraine un changement de son indice de réfraction permettant ainsi de visualiser la structure.

Développement

Après structuration, le développement appliqué est choisi selon le type de résine photosensible utilisée. Les zones non-irradiées sont éliminées par rinçage à l'acétone pendant 10 minutes puis à l'isopropanol pendant 5 minutes.

6.2.3. Caractérisation

Microscope optique et Microscope Electronique à Balayage (MEB) :

Les images optiques en champ sombre et champ clair sont obtenues à l'aide d'un microscope optique « Nikon Eclipse LV100 », équipé par 5 objectives « ZEISS » : 5x (ouverture numérique (ON) = 0,15); 10x (ON = 0,25); 20x (ON = 0,45); 50x (ON = 0,8); et 100x (ON = 0,9).

Les images MEB sont prises à l'aide d'un microscope Hitachi S18, avec une tension d'accélération de 10 KV. Les échantillons sont préalablement métallisés avec une couche de 5 nm d'or/palladium. Cette couche est déposée avec le système de dépôt « SC7640 SPUTTER Coater » en appliquant une tension de 1,75 KV et une durée de métallisation de 80 secondes. Le but du dépôt d'une telle couche est d'apporter à l'échantillon une haute conductivité lors de l'observation afin d'éviter le piégeage des charges qui nuirait à la qualité des images MEB.

Fluorescence

Un microscope inversé est utilisé dans cette thèse pour exciter et aussi collecter le signal fluorescence de QD. La longueur d'onde d'excitation est 405 nm. Un filtre spectral rejette cette longueur d'onde pour l'imagerie de fluorescence.

6.3 Fabrication de nanostructures 3D par ELD-PDP

6.3.1. Influence du MEHQ sur la résolution des nanostructures 2D et 3D fabriquées par ELD-PDP

L'utilisation d'un inhibiteur moléculaire au cours de la polymérisation s'est avérée bénéfique pour une meilleure résolution [80, 81]. Dans ce travail, MEHQ est donc utilisé

comme inhibiteur pour favoriser un confinement chimique du volume réactionnel. Cette molécule a donc été ajoutée à la formation photopolymérisable à deux photons.

Sur la base de cette formulation, la fabrication de lignes à différentes périodes (de 250 nm à 5000 nm) avec des puissances laser dans la gamme (0-20 mw) et des vitesses de balayage dans la gamme (25-400 μm / s) a été réalisée dans le but d'étudier la résolution des structures obtenues avec ajout de MEHQ afin d'évaluer l'influence de MEHQ sur la résolution atteinte.

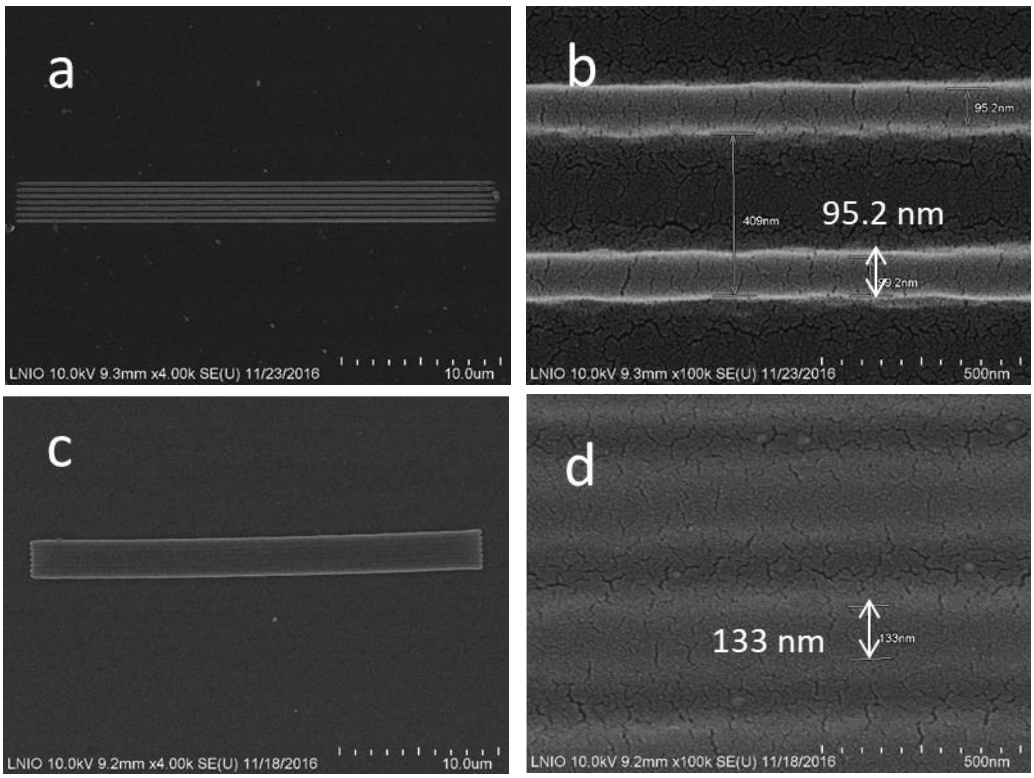

Figure 6.1 : Images MEB des lignes ayant période de 400 nm fabriquées à une vitesse de balayage de 100 μm/s: (a) et (b) avec MEHQ ; (c) et (d) sans MEHQ.

Sur la Figure 6.1, les lignées obtenues par ajout de MEHQ sont plus minces que celles sans inhibiteur : largeur de ligne de 95 nm au lieu 133 nm. En outre, avec MEHQ, la plus petite période atteinte est de 300 nm avec une largeur de ligne de 65 nm, (voir Figure 6.2) ; pour comparaison, la plus petite période sans MEHQ est de 350 nm, avec une largeur de ligne de 80 nm. Avec ajout de l'inhibiteur, la résolution des lignes 2D est nettement améliorée, ce qui est en accord avec les résultats rapportés dans d'autres références [80, 81].

Sur les Figures 6.2 et 6.3, les lignes obtenues avec addition de MEHQ sont plus fines que celles sans inhibiteur, où les premières ont une largeur de ligne de 95 nm, par rapport à la dernière de 133 nm. De plus, dans les tas de bois 3D préparés par EDL-DPD, la plus petite

période peut être atteinte à 300 nm avec une largeur de ligne de 65 nm en présence de MEHQ (voir Figure 6.4). Pour comparaison, la plus petite période en l'absence de MEHQ est de 350 nm, avec une largeur de ligne de 80 nm (voir Figure 6.5). En bref, avec l'ajout d'inhibiteur, la résolution des lignes 2D est nettement améliorée.

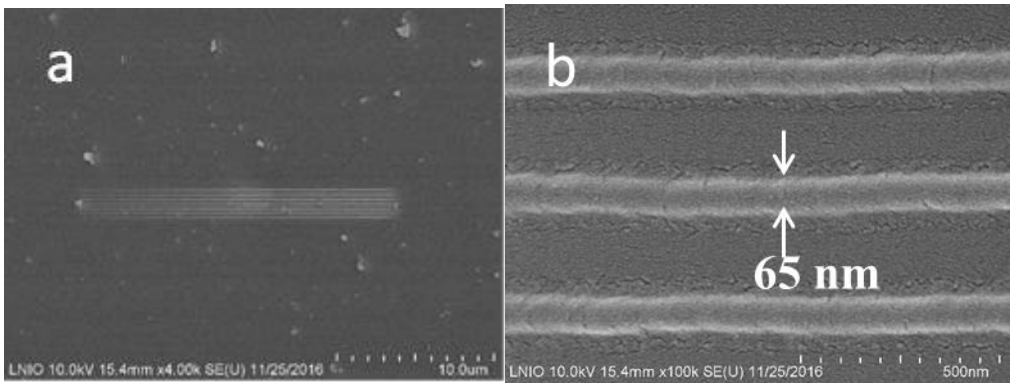

Figure 6.2 : MEB images des lignes 2D dans une période de 300 nm fabriquées avec ajout de MEHQ: (a) pattern entier (b) détail.

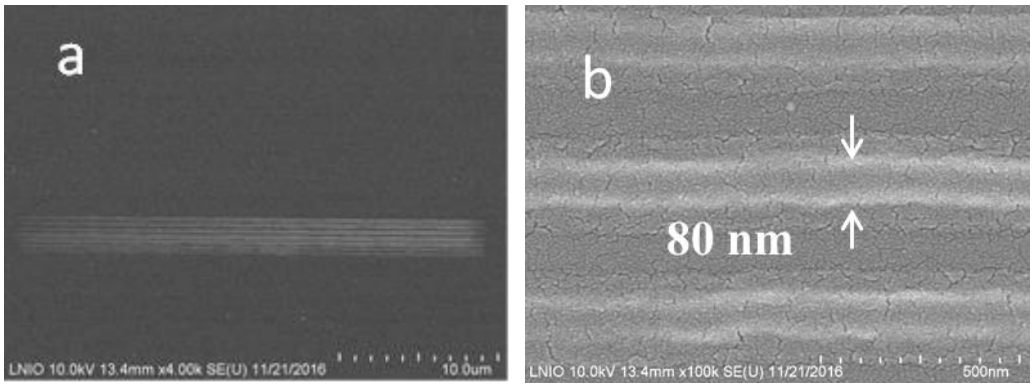

Figure 6.3 : MEB images des lignes 2D dans une période de 350 nm fabriquées sans MEHQ: (a) pattern entier (b) détail.

Une étude plus poussée a également été entreprise concernant les structures 3D. Ainsi, des structures de tas de bois à différentes périodes (250 nm-1000 nm) ont été produites à une vitesse de balayage de 100 µm/s sous une puissance laser différente (8-14 mW). Pour ces structures, la plus petite période dans le cas contenant MEHQ est atteinte : 250 nm avec une largeur de ligne de 80 nm (présentée Figure 6.4). En revanche, la plus petite période de la fabrication sans addition de MEHQ est obtenue à 350 nm alors que la largeur de la ligne est d'environ 85 nm (voir Figure 6.5). Par ailleurs, la plus petite largeur de ligne peut atteindre 60 nm (voir Figure 6.6), en une période de 350 nm en présence d'inhibiteur, ce qui constitue une première dans le domaine de fabrication de structures 3D par ELD-PDP utilisant un seul

laser de longueur d'onde 780 nm. Ce résultat peut être comparé à ce qui a été réalisé par STED-ELD : des tas de bois 3D avec une période intercalaire 400 nm ont été obtenues en utilisant deux lasers (une longueur d'onde de 810 nm est utilisée pour amorcer la polymérisation et $\lambda = 532$ nm est utilisé comme faisceau de déplétion) [98].

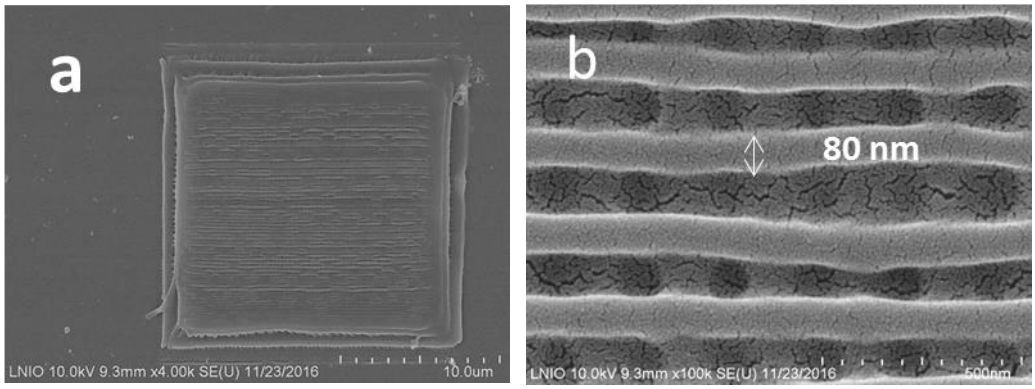

Figure 6.4 : MEB images des tas de bois 3D dans une période de 250 nm fabriqués avec MEHQ: (a) tas de bois (b) détail.

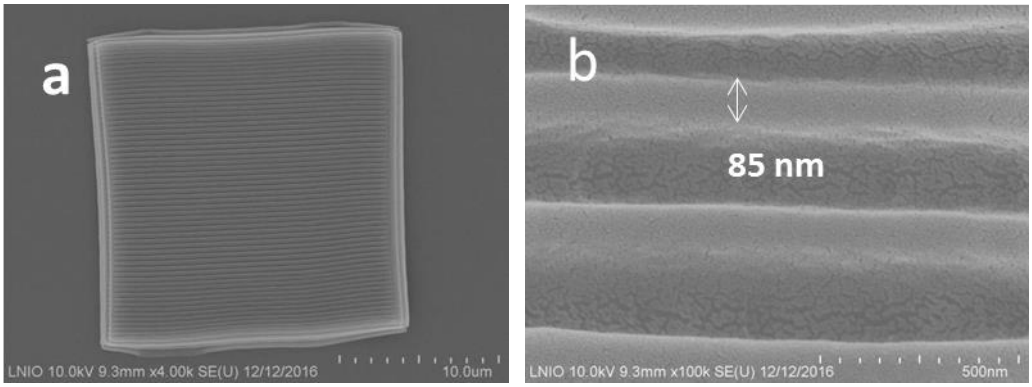

Figure 6.5 : MEB images des tas de bois 3D dans une période de 350 nm fabriqués sans MEHQ: (a) tas de bois (b) détail.

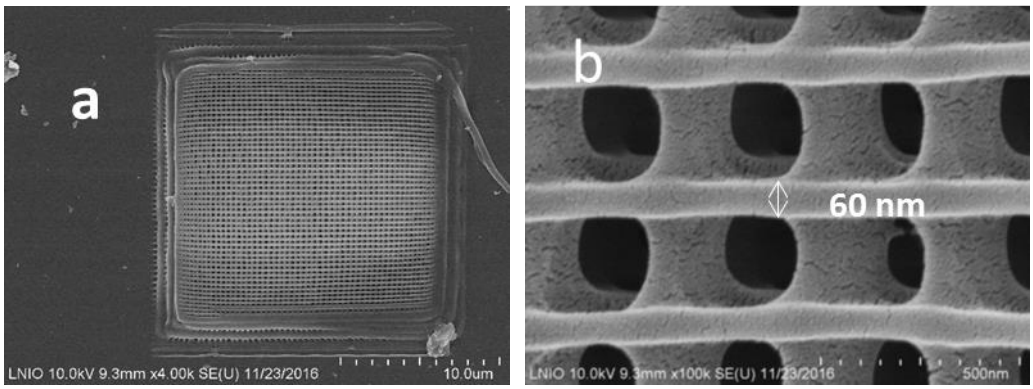

Figure 6.6 : MEB images des tas de bois 3D dans une période de 350 nm fabriqués avec MEHQ: (a) tas de bois entier (b) détail.

Pour clarifier l'influence de MEHQ sur la résolution des structures, des études plus poussées ont été entreprises. Jusqu'à présent, il était connu que la résolution était améliorée avec l'ajout de MEHQ par EDL-PDP. Cette observation montrée dans la Figure 6.7 a été notée quel que soit la puissance de laser et vitesse d'écriture.

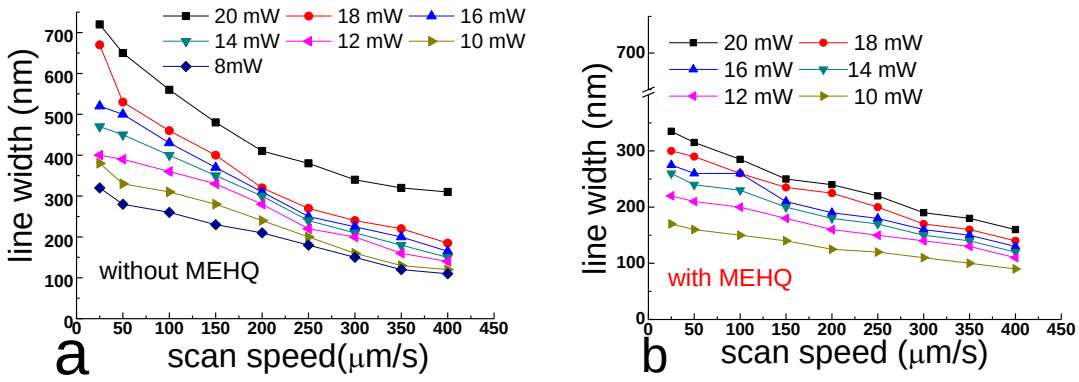

Figure 6.7 : Largeur de ligne en fonction de la vitesse de balayage pour différentes puissances laser avec une période de 5000 nm (a) sans MEHQ et (b) avec MEHQ

Dans la procédure PDP, sous l'exposition du laser, le voxel de polymère qui se développe pendant l'exposition de la résine au faisceau laser correspond à un sphéroïde dont le volume peut être décrit comme suit :

$$V = \frac{4}{3}\pi pq^2 = \frac{1}{2}\pi L^3 \qquad (6\text{-}1)$$

Où q est le rayon équatorial du faisceau, qui est la largeur de ligne $L/2$ et p est le rayon polaire qui est 3 fois plus grand que q. Ainsi, le volume du voxel en fonction du temps d'exposition peut être obtenu (cf Figure 6.8).

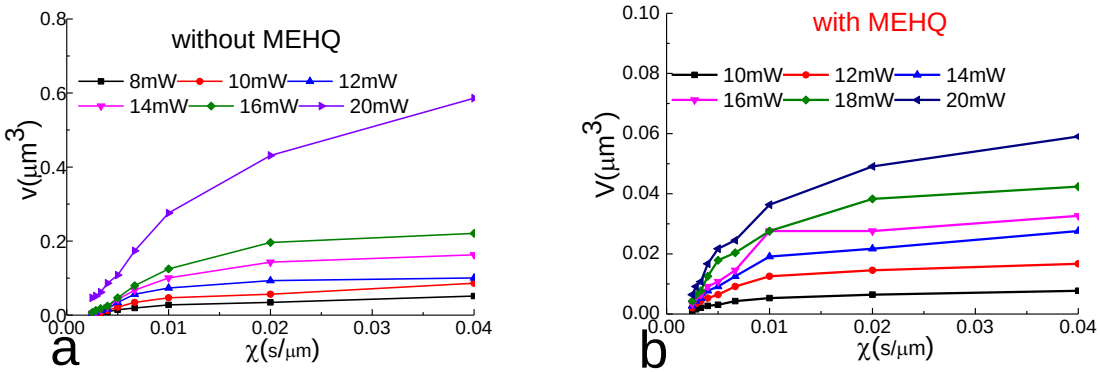

Figure 6.8 : Volume de voxel polymerisé en fonction de la vitesse de balayage inverse pour différentes puissances laser avec une période de 5000 nm par (a) sans MEHQ et (b) avec MEHQ

Le volume du voxel polymère en fonction du temps d'exposition peut être décrit comme suit [168]:

$$V = A(1 - e^{-BX}) \qquad (6\text{-}2)$$

où V est le volume de voxel, X est le temps d'exposition ici proportionnel à la vitesse de balayage, A et B sont les paramètres d'ajustement. Le taux de croissance du polymère est ensuite donné par le produit de ces deux paramètres, c'est-à-dire $R_P = A * B$. Selon les paramètres d'ajustement, Rp peut être obtenu, ce qui est présenté sur la Figure 6.9. Les courbes ont été ajustées, et les équations d'ajustement sont:

$$\log R_p = 2.02 \log P_0 - 1.88 \qquad (6\text{-}3)$$

Le coefficient directeur de cette droite correspond à N/α, avec N = 2 (voir équation 3-22). Ainsi, $\alpha \sim 1$ ce qui veut dire que la terminaison de la polymérisation est mono-moléculaire. En revanche, en l'absence du MEHQ:

$$\log R_p = 1.73 \log P_0 - 0.95 \qquad (6\text{-}4)$$

$\alpha \sim 1.2$ ce qui veut dire que les modes de terminaison mono et bimoléculaire peuvent avoir lieu simultanément [168-170].

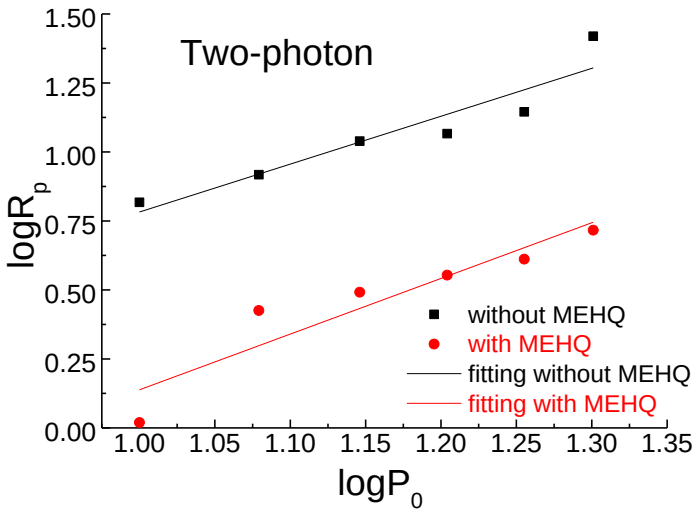

Figure 6.9 : logRp en fonction de $\log P_0$ des deux résines (avec et sans inhibiteur) photopolymérisées à deux photons.

Afin de confirmer la tendance observée lors de la polymérisation à l'activation des deux photons, les études sur le taux de conversion de l'initiateur et du monomère respectivement

sous excitation monophotonique ont été effectuées et les résultats correspondants sont présentés à la Figure 6.10.

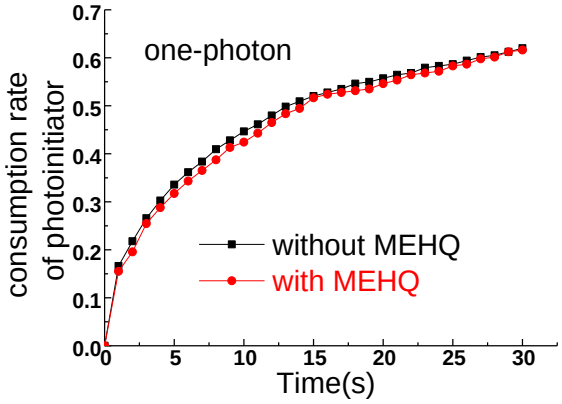

Figure 6.10 : Courbes du taux de consommation du photoamorceur dans deux résines : avec et sans MEHQ

Il apparait clairement d'après la figure 6.10 que la présence de MEHQ ne change pas la cinétique de consommation du photoamorceur. Ainsi, il est raisonnable de considérer que le MEHQ n'influence pas la photoréactivité du photoamorceur. Le taux de conversion de photopolymérisation en fonction du temps d'exposition à une lampe UV (365 nm) des deux résines est également mesuré (Figure 6.11). Cette figure montre que quel que soit l'intensité d'exposition, avec l'ajout de MEHQ, la réaction de polymérisation est plus lente.

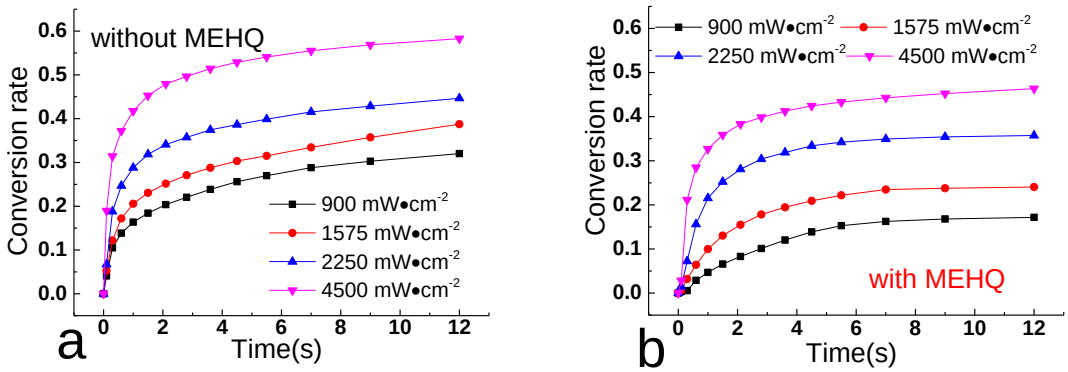

Figure 6.11 : Taux de conversion du monomère en fonction du temps d'exposition du photopolymère à une lampe UV (365 nm) de différentes intensités : (a) formulation sans MEHQ et (b) formulation avec MEHQ

En se basant sur le calcul de la vitesse de polymérisation of $R_p/[M]$ (voir chapitre 2), la variation de log R_p en fonction de logI_0 a été obtenue pour les deux résines (avec et sans inhibiteur) et présentée en Figure 6.12.

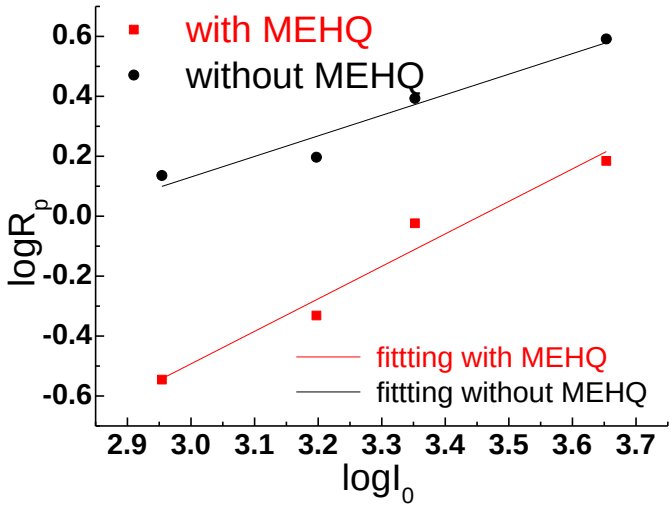

Figure 6.12 : log R_p en fonction de log I_0 des deux résines étudiées sous excitation à un photon

L'équation de droite correspondante en présence de MEHQ est :

$$\log R_p = 1.08 \log I_0 - 3.58 \qquad (6\text{-}5)$$

Le coefficient directeur de cette droite correspond à N/α, avec N = 2 (voir équation 3-22). Ainsi, α ~ 1 ce qui veut dire que la terminaison de la polymérisation est mono-moléculaire. En revanche, en l'absence du MEHQ:

$$\log R_p = 0.68 \log I_0 - 1.93 \qquad (6\text{-}6)$$

α ~ 1.5 ce qui veut dire que la terminaison peut se faire également suivant deux modes (biomoléculaire et mono-moléculaire) [169,170].

Les résultats obtenus ici sont cohérents avec ceux obtenus par photopolymérisation à deux photons. Ainsi, quel que soit le mode d'activation (un ou deux photons), la présence de MEHQ semble favoriser une terminaison monomoléculaire.

Pour résumer, avec la présence du MEHQ lors de l'ELD-PDP, la résolution des lignes 2D et des tas de bois 3D a été améliorée. En ce qui concerne les lignes 2D, la plus petite largeur de ligne de 65 nm est obtenue sur une période de 300 nm. Pour les tas de bois 3D, la

largeur de ligne la plus petite de 60 nm est obtenue sur une période de 350 nm et la plus petite période de 250 nm, meilleure que la plus petite période rapportée dans la littérature (400 nm avec une résolution de 80 nm) en utilisant ELD-PDP [82]. En étudiant les effets du taux de conversion, de la puissance du laser et de la vitesse de balayage sur la résolution, le mécanisme de terminaison en présence du MEHQ est dominé par la terminaison mono-moléculaire. Ceci semble être un facteur favorable à l'amélioration de la résolution.

6.3.2. Influence des BQs sur la résolution des nanostructures 3D fabriquées par ELD-PDP

Les films polymères contenant des boîtes quantiques (BQs) ont été largement utilisés pour diverses applications photoniques et électroniques au cours des dernières décennies. Par ailleurs, les nanostructures tridimensionnelles (3D) ont constitué des solutions élégantes pour la micro-optique, la micro-fluidique, la biomédecine et l'imagerie. Dans ce contexte, l'approche consistant à fonctionnaliser les structures polymères réalisées par ELD-PDP par des BQs est extrêmement prometteuse. Dans ce sous-chapitre, la caractérisation de telles structures est présentée.

Les lignes 2D contenant des BQs et, pour référence, les lignes sans BQs d'une longueur de 30 μm sur une période de 5 μm sont fabriquées avec la même vitesse de balayage et la même puissance laser (Figure 6.13). Il est intéressant de constater qu'en présence de BQs, les lignes sont plus fines que celles sans BQs, ce qui n'a jamais été rapporté auparavant. En effet, la plus petite période (300 nm) pour obtenir les lignes résolues et la largeur de ligne correspondante (75 nm) sont nettement plus faibles en présence de BQs que celles sans BQs (respectivement 350 nm et 90 nm), comme le montre la Figure 6.14.

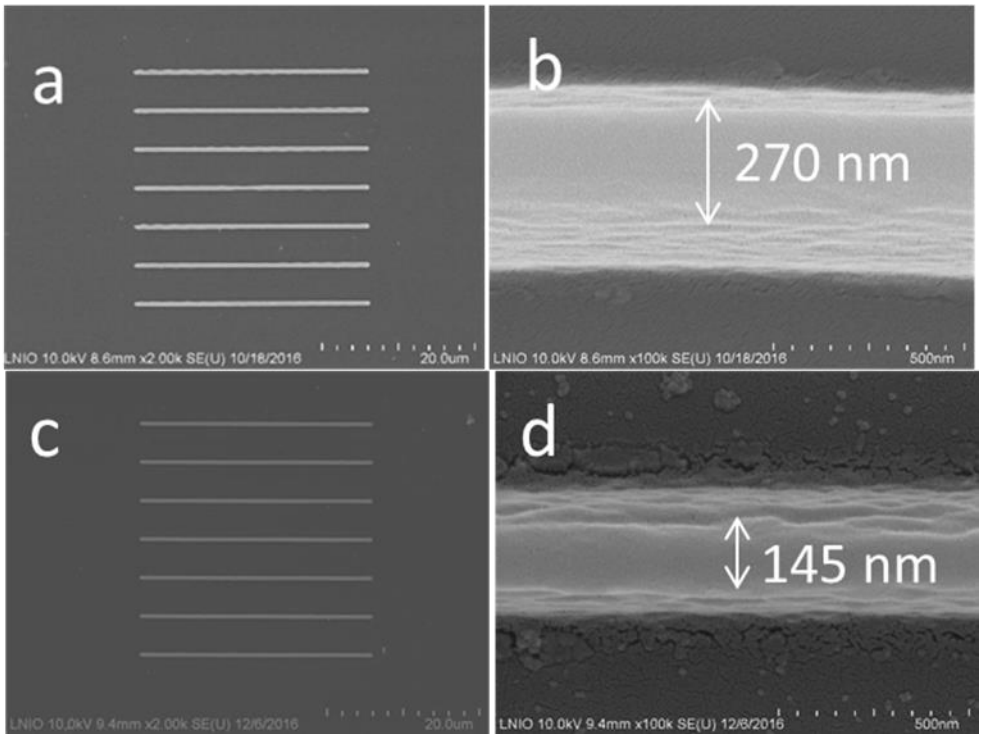

Figure 6.13 : Images MEB de lignes de polymère fabriquées par ELD-PDP (a et b) formulation sans BQs (c et d) en présence de BQs.

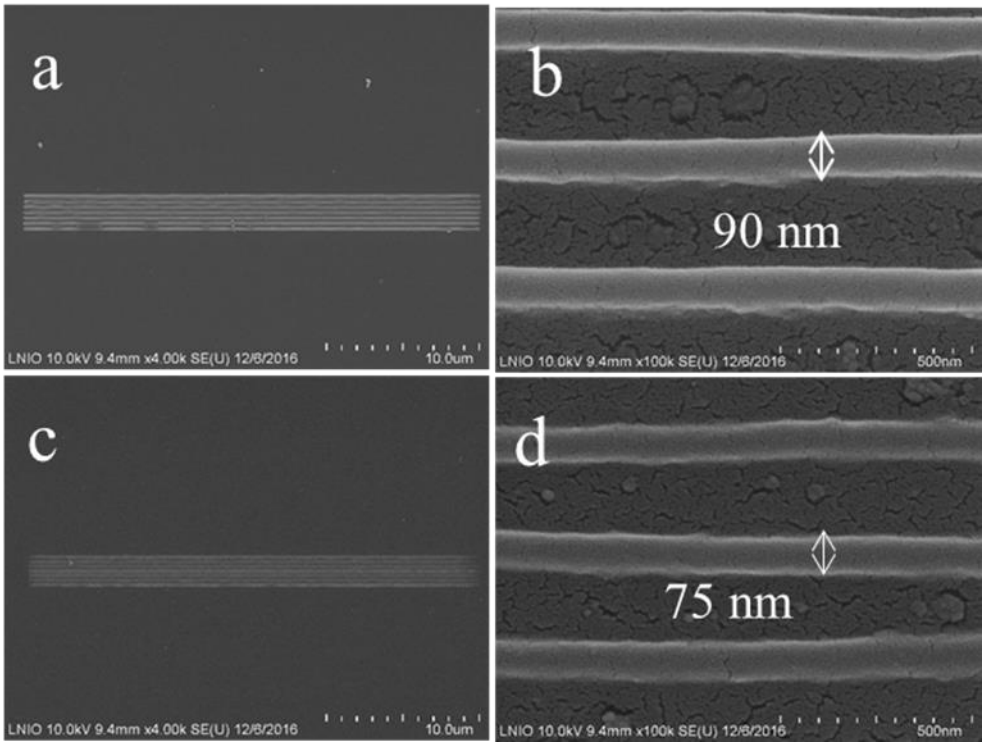

Figure 6.14 : Images MEB de lignes de polymère fabriquées par ELD-PDP à la même vitesse de balayage de 100 µm / s. (a et b) dans la formulation sans BQs sous une puissance laser de 7 mw (c et d) en présence de BQs sous une puissance laser de 9 mw.

Il apparaît clairement que la largeur de ligne en présence de BQ est plus faible que celle sans BQs. Une tendance similaire peut être observée dans le cas des structures 3D, comme le montre la figure 6.15. En effet, les structures tas de bois contenant des BQs avec une période inter couche de 350 nm présentent une meilleure résolution par rapport à celle obtenue en l'absence de BQs. La plus petite période avec BQs est de 400 nm, alors qu'elle de 500 nm sans BQs (Figure 6.16 et Figure 6.17). Cette tendance est confirmée par la Figure 6.15 qui montre la variation de la largeur de ligne du polymère en fonction de l'inverse de la vitesse pour les deux formulations, à différentes puissances laser. Ce phénomène n'a jamais été signalé auparavant dans la littérature. Ces résultats ouvrent la porte à une nouvelle façon d'obtenir une meilleure résolution des structures fabriquées par ELD-PDP. De plus, en raison des propriétés uniques des BQs, cette approche permet d'envisager la fonctionnalisation à l'échelle nanométrique avec différents BQs émettant différentes couleurs [114].

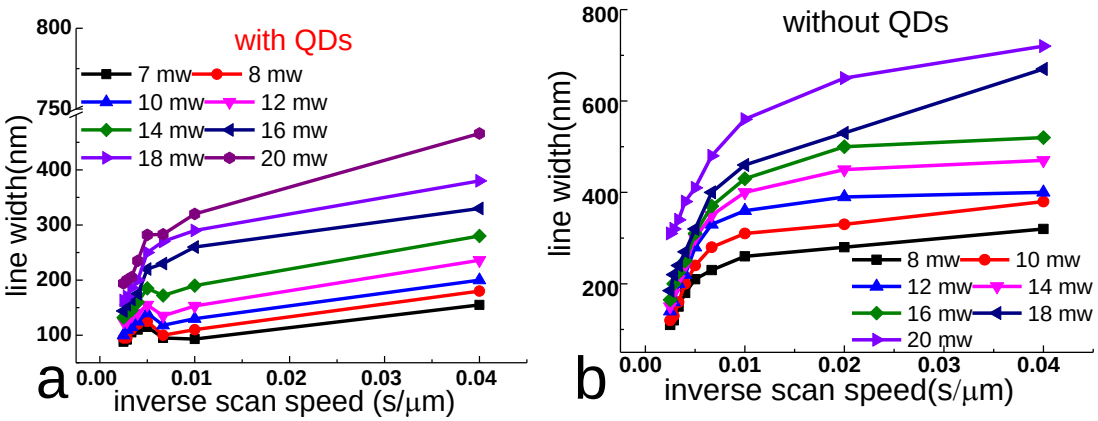

Figure 6.15 : Courbes de la largeur de ligne en fonction de la vitesse de balayage inverse sous différentes puissances laser utilisées pour la polymérisation: (a) avec BQs et (b) sans BQs.

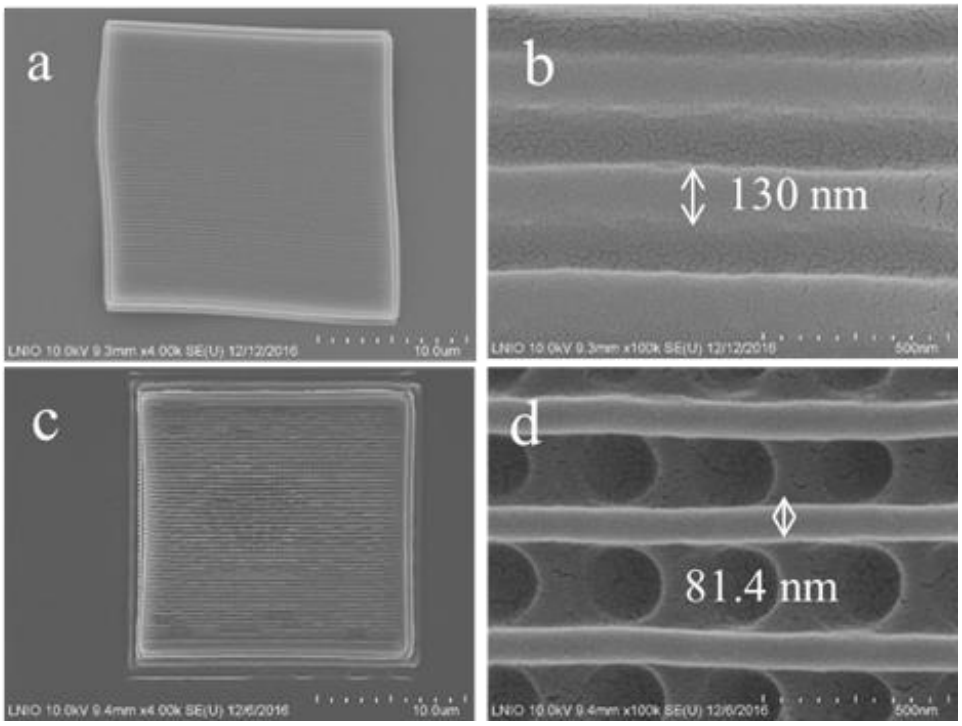

Figure 6.16 : Images MEB de tas de bois dans une période de 350 nm fabriqué à 8 mW par TPP-DLW à une vitesse de balayage de 100 um / s (a, b) sans BQs; (c, d) avec BQs

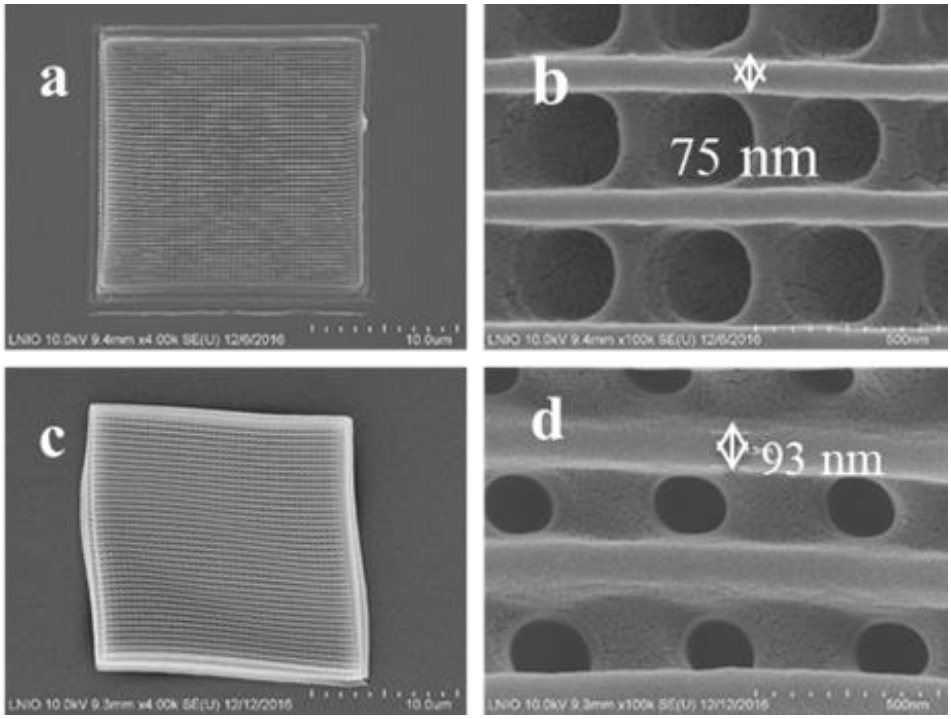

Figure 6.17 : Images MEB de woodpile par EDL-PDP obtenues à une vitesse de balayage de 100 µm / s: (a et b) sur une période de 400 nm fabriquées avec des BQs à 8mw (c et d) sur une période de 500 nm fabriquées sans BQs à 6 mw.

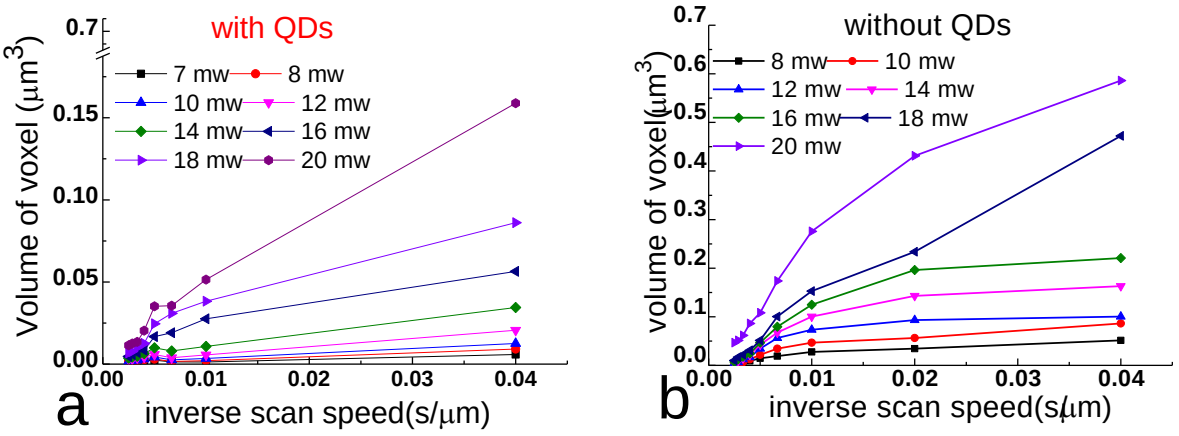

Figure 6.18 : Volumes du voxel polymère en fonction de l'inverse de la vitesse de balayage pour deux formulations (a) avec BQs et (b) sans BQs.

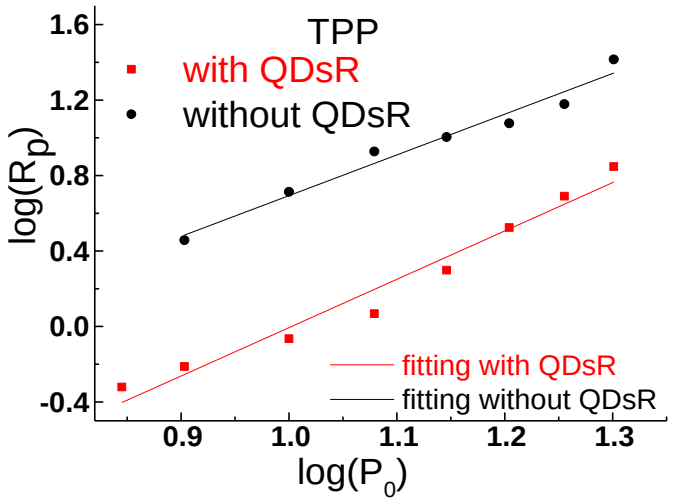

Figure 6.19 : logRp en fonction de $\log P_0$ des deux résines photopolymérisées à deux photons.

Afin de clarifier l'influence des BQs sur la résolution des structures, le volume de voxel calculé à partir des lignes en fonction du temps effectif d'exposition (inverse de la vitesse de balayage) est montré sur la Figure 6.18. Par ailleurs, le taux de croissance ou le taux de polymérisation (Rp) peut être obtenu, ce qui est présenté à la Figure 6.19. les équations de droite correspondant sont les suivantes :

Sans BQs :

$$\log R_p = 1.63 \log P_0 - 0.82 \qquad (6\text{-}7)$$

avec BQs :

$$\log R_p = 2.13 \log P_0 - 2.11 \qquad (6\text{-}8)$$

Étant donné $Rp \propto I^{(N / \alpha)}$, où α est la constante de détermination du coefficient de terminaison, N est l'ordre d'absorption supposé être 2 [168, 170]. Dans ce sens, $\log Rp \propto (N / \alpha) \log P_0$ en présence de BQs, α est presque égal à 1, ce qui signifie que la terminaison a effectué une transition vers la terminaison monomoléculaire. En comparaison, sans BQs, $1<\alpha<2$, en d'autres termes, la terminaison est censée compter comme une terminaison mixte, à savoir la terminaison bimoléculaire et monomoléculaire simultanée [169].

Afin de confirmer la tendance observée lors de la polymérisation à deux photons, les études sur la décomposition et le taux de conversion du photo initiateur à 2-photon et du monomère respectivement sous excitation monophotonique ont été effectuées et les résultats correspondants sont présentés sur la Figure 6.20.

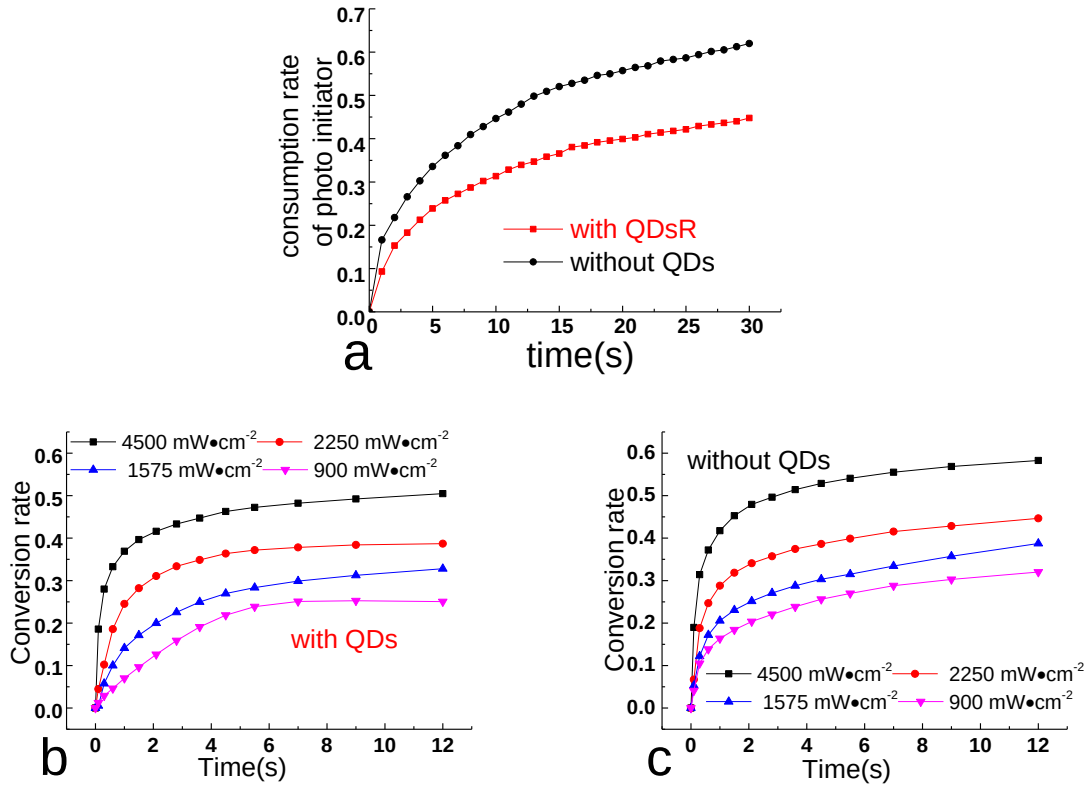

Figure 6.20 : (a) Taux de consommation du photo initiateur en fonction du temps pour les deux formulations (présence / absence de BQ), (b et c) Les comparaisons du taux de conversion de la polymérisation sous différentes intensités pour les deux formulations.

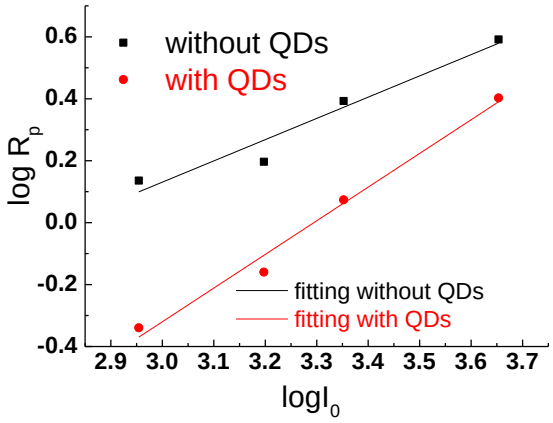

Figure 6.21 : logRp en fonction de $\log I_0$ des deux résines photopolymérisées à un photon

En présence de BQs, le taux de décomposition de l'initiateur a diminué de 62% à 44,8%. De plus, quel que soit l'intensité de l'exposition, le taux de conversion du monomère est plus faible en présence de BQ. Ces deux observations indiquent que la génération de radicaux pourrait être influencée localement par la présence de BQs. En effet, lors de l'excitation avec une lampe UV (pic principal à 365 nm), les BQs absorbent une partie de la lumière incidente diminuant ainsi le nombre de photons absorbés par le photoamorceur qui à son tour conduit à une quantité plus faible de radicaux générés. Une autre explication pourrait être liée à une éventuelle inhibition des radicaux par les BQs conduisant à moins de radicaux actifs visant à amorcer la polymérisation [172]. Cependant, ces conjectures devraient être prouvées par des travaux futurs. En outre, le taux de polymérisation Rp peut être obtenu, comme le montre la Figure 6.21. les équations de droites sont les suivantes :

Sans BQs :

$$\log R_p = 0.69 \log I_0 - 1.93 \qquad (6\text{-}9)$$

avec BQs :

$$\log R_p = 1.08 \log I_0 - 3.58 \qquad (6\text{-}10)$$

Là aussi, sous excitation monophotonique, en présence de BQs, lors de la terminaison, le mécanisme est passé de la terminaison mixte à la terminaison monomoléculaire, ce qui confirme la même tendance observée dans l'excitation à deux photons. Ainsi, il est probable que, lors de la polymérisation, quelle que soit le type d'excitation, la terminaison monomoléculaire est favorable grâce à la présence des BQs. Au cours de la polymérisation,

coexistent deux radicaux principaux avec des réactions différentes: radicaux libres à mobilité aléatoire, et radicaux piégés qui rendent impossible toute réaction ultérieure. Normalement, les radicaux piégés effectuent la terminaison monomoléculaire [173]. Cette dernière est considérée comme une diminution virtuelle de la mobilité radicale, ce qui signifie que sous excitation, en présence de BQs, une population particulière de radicaux devient piégée rapidement. Ainsi, la structure finale obtenue présente une résolution plus fine par rapport à celle sans ajout des BQs.

Dans le but d'une application future, il est nécessaire d'étudier la capacité de fluorescence des structures polymères obtenues. Comme le montre la Figure 6.22, sous l'excitation d'un laser à 404 nm, les grilles et les caractères ont montré des émissions bleues, rouges et vertes, respectivement.

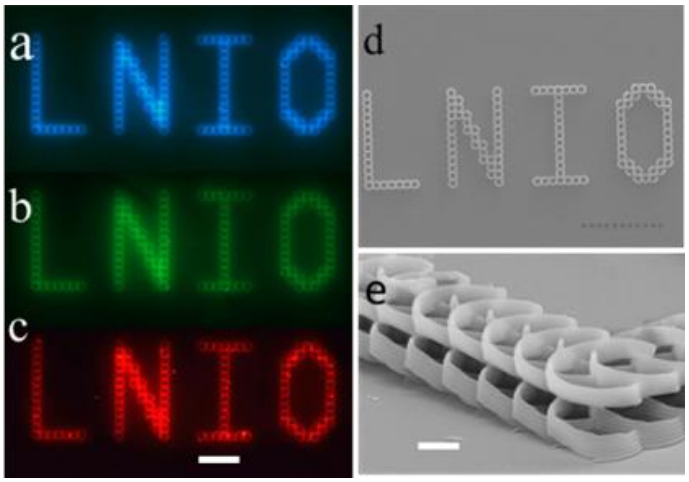

Figure 6.22 : (a, b et c) Images de fluorescence de microstructures 3D contenant des BQs montrant une émission à 460 nm, 510 nm et 613 nm, respectivement (d et e) Vues de dessus et de côté SEM des microstructures correspondantes. Les barres d'échelle sont, pour c, d, e respectivement de 10 μm, 50 μm et 2 μm.

Sur la base de ces observations, l'intensité d'émission des tas de bois fabriquées à plusieurs puissances, contenant du BQs-rouges, a été mesurée. Il est évident que l'intensité d'émission augmente avec l'augmentation de la puissance laser utilisée pour la fabrication, comme le montre la Figure 6.23. Ce résultat peut être simplement expliqué par l'augmentation du volume de polymère obtenu et donc du nombre de BQs piégés dans la matrice. Il montre par ailleurs qu'il n'y a pas de photo décoloration significative ou de diffusion de QDs des zones irradiées vers les zones sombres comme cela a été rapporté par Barichard et al. [174] dans la question de l'enregistrement holographique. Ainsi, nos micro et

nanostructures 3D fabriquées par ELD-PDP contiennent effectivement des émetteurs quantiques et peuvent encore être photo luminescentes.

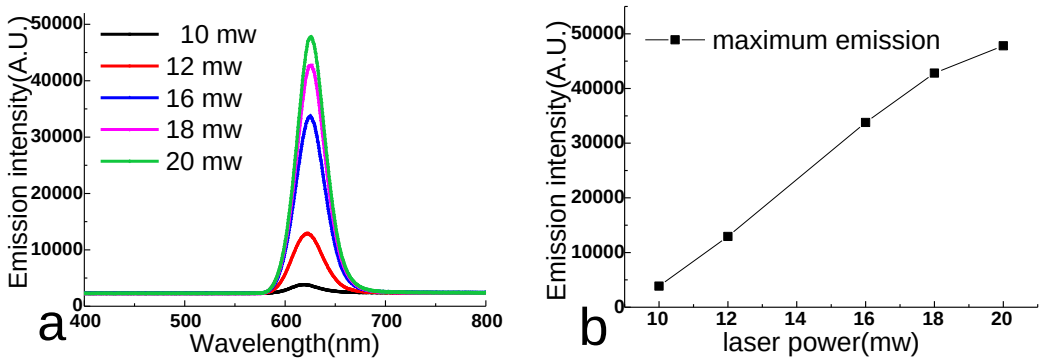

Figure 6.23 : (a) Intensité d'émission (excitation à 404 nm) des piles de bois contenant des boites quantiques à émission rouge fabriqués à différentes puissances laser; (b) l'intensité d'émission maximale en fonction de la puissance laser utilisée pour la fabrication.

6.3.3. Intégration de BQs avec des structures plasmoniques et photoniques *via* ELD-PDP

Les formulations photopolymerisables contenant des BQs étudiées ont été utilisées dans le but d'intégrer des zones émettrices de lumières à des composants plasmoniques et photoniques

En ce qui concerne les structures plasmoniques hybrides, il est important de contrôler non seulement la localisation du système actif émetteur de lumière mais aussi sur sa taille qui joue un rôle important sur l'efficacité du couplage avec les plasmons. Comme mentionné ci-dessus, *via* ELD-PDP, il est possible d'obtenir des points de polymères avec une taille et une localisation contrôlables d'une manière simple en utilisant les résines photosensibles contenant des BQs. Ce sous-chapitre traite des applications des photopolymères contenant des BQs. Dans le cadre d'un partenariat avec d'autres doctorants (Hongshi Chen, Dandan Ge et Aurélie Broussier) du Laboratoire de Nanotechnologie et Instrumentation Optique (LNIO), j'ai travaillé sur l'intégration de QDs avec des structures plasmoniques (nanofils d'argent, réseaux d'or et nanocubes d'or) et des fibres optiques.

Concernant les nanofils d'argent (NF-Ag), des premiers essais de ELD-PDP en utilisant PETA-BQsG-IRG ont été effectués à proximité des NFs. Sur la Figure 6.24, à l'extrémité

d'un petit NF-Ag, on peut observer un point polymère qui a été intégré et qui contient BQs-G dont l'émission verte (sous excitation bleue) est visible.

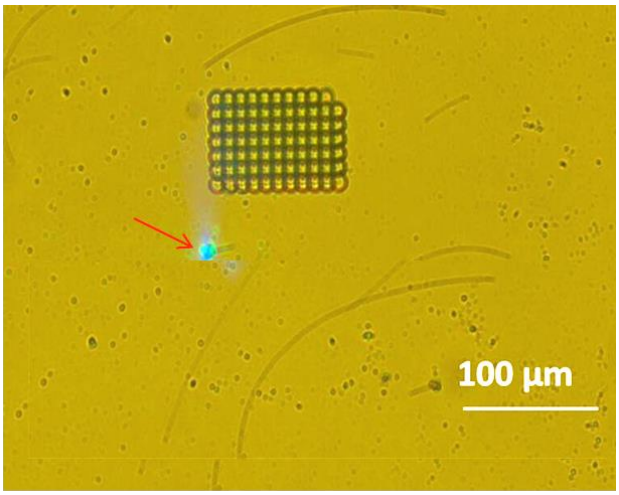

Figure 6.24 : Image optique de NF-Ag. Des BQs-G ont été intégrés à l'extrémité d'un NF court. (les BQ sont sous l'exposition de laser de 405 nm). Le nanofil et le point polymère sont mis en évidence par la flèche rouge. La structure en haut de l'image a été réalisée pour tester un motif polymère contenant des BQs et ajuster/définir les paramètres permettant d'obtenir le point polymère.

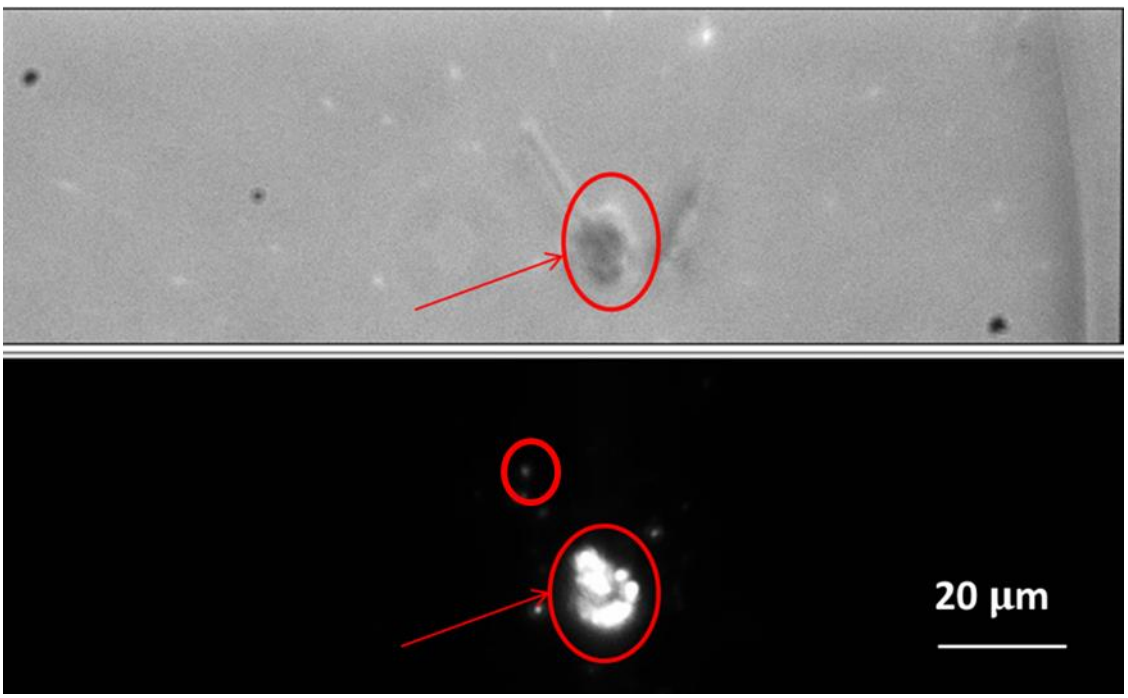

Figure 6.25 : En haut: image optique d'un point de polymère contenant BQ intégré à une extrémité d'un Ag NW. En bas: image de photoluminescence filtrée (lumière verte). Un faisceau laser bleu a été focalisé sur le point de polymère. Le cercle bleu met en évidence le

point de polymère intégré à une extrémité du NF-Ag. La flèche rouge indique l'autre extrémité.

Les efforts ont été poursuivis, ce qui a donné les résultats présentés à la Figure 6.25. La Figure 6.25 (en haut) montre une image optique d'un nanofil et d'un point de polymère (cercle bleu) contenant du BQ qui a été intégré à une extrémité du NF. La Figure 6.25 (en bas) est l'image de photoluminescence du même objet. Une tache laser à λ= 405 nm a été focalisée directement sur le point de polymère. Pour l'imagerie de la photoluminescence, la lumière incidente a été coupée par un filtre spectral qui arrête les longueurs d'onde <450 nm. Alors que cette longueur d'onde incidente ne peut pas lancer directement le plasmon de surface, elle est absorbée par les BQs qui se désexcitent en émettant de la lumière verte. Cette émission peut se coupler avec des plasmons, ce qui se traduit par un plasmon de surface qui se propage à l'autre extrémité et qui redevient radiatif par diffusion à l'autre extrémité. Dans la Figure 6.25 (en bas) le point lumineux (flèche rouge) sur la figure correspond à de l'émission verte située précisément à l'autre extrémité du NF. Ce point lumineux correspondrait à la diffusion évoquée ci-dessus et serait donc la signature d'un transfert d'énergie entre les QDs intégrés par PDP à l'extrémité du NF et l'autre extrémité du NF *via* le plasmon de surface. La Figure 6.26 confirme qu'il s'agit de la photoluminescence des BQs : il montre le spectre de photoluminescence mesuré au point de polymère et à l'extrémité NW. L'émission des QD centrés à 540 nm est clairement visible. Notons que ces spectres sont locaux car la détection est de type confocal : une zone d'environ 3 µm de taille est sélectionnée

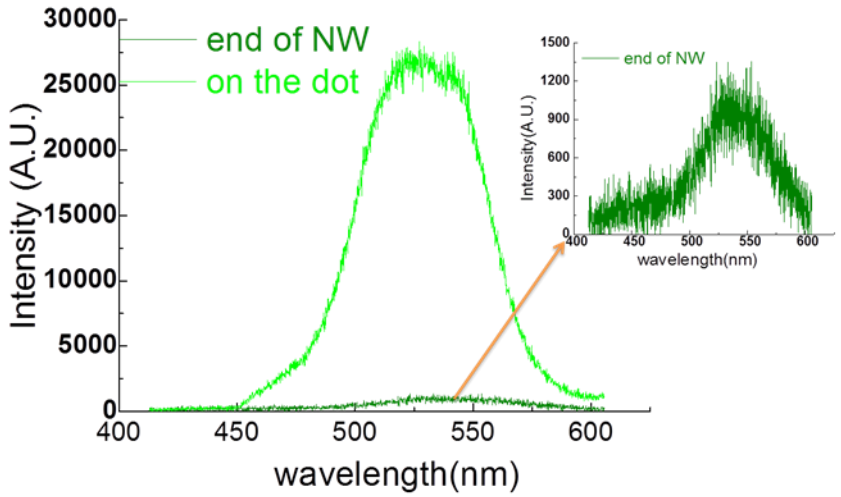

Figure 6. 26 : Spectres de photoluminescence pris au point de polymère (bleu) et à l'autre extrémité du NF, indiquée par une flèche rouge sur la figure 6.26. Une configuration confocale a été utilisée: le signal provient de la zone de taille de 3 microns

Les molécules photoluminescentes actives intégrées localement à l'extrémité des sondes SNOM ont longtemps donné lieu à de nombreux travaux de recherche. La motivation est d'éviter le fond dû à la lumière incidente (l'émission des molécules est un processus inélastique) et d'exploiter la physique des nano-émetteurs (durée de vie, orientation, rendement quantique ...). La résine polymérisable contenant des BQ peut être potentiellement utilisée dans la fabrication de pointes SNOM active. Une nouvelle approche de photopolymerisation en extrémité de fibre optique a été explorée. Il s'agit d'exploiter la méthode décrite ref. [181,186] pour intégrer une source de lumière en extrémité de fibre optique. Afin d'améliorer la localisation spatiale des BQs, une exposition en deux étapes a été réalisée. Une première intégration a été faite avec un polymère qui ne contient pas de BQ. Ensuite, à partir de cette première pointe, une seconde pointe a été obtenue avec un polymère contenant à la fois des BQs et un inhibiteur (MEHQ). Le résultat de cette procédure en deux étapes est illustré à la Figure 6.27. Un petit point émettant de la lumière (taille typique inférieure à 200 nm) est intégré à l'extrémité de la pointe polymère couplée à la fibre optique.

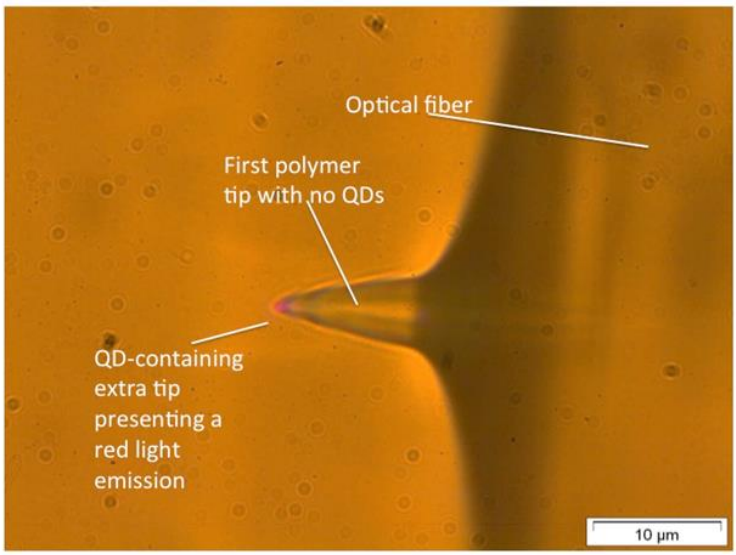

Figure 6.27 : Fluorescence d'une pointe supplémentaire sous excitation par un laser 405 nm.

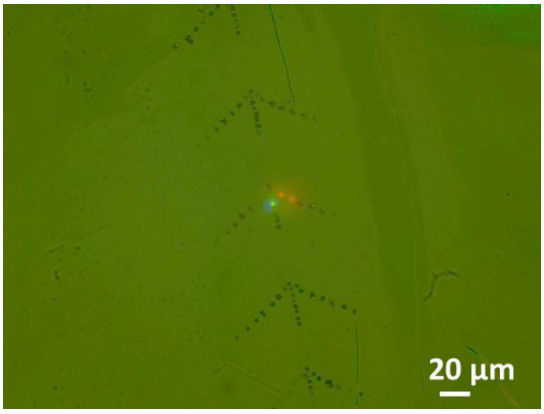

Figure 6.28: Image de fluorescence (excitation à 405 nm) de deux types de QD situés à proximité de réseaux métalliques sur or. Les points noirs correspondent aux plots de polymère contenant des QDs. Les réseaux de 2,5 micron de large (période=500 nm) sont situés sur la branche centrale des motifs en forme de flèche.

Une autre approche consiste à l'utilisation de réseaux en or destinés à lancer ou recevoir des plasmons de surface sur or. Afin d'étudier l'interaction de nano émetteurs avec cette structure en réseaux Les BQs peuvent être aussi placés via TPP-DLW avec l'utilisation de résines contenant des QDs à différentes distances des réseaux représentés sur la Figure 6.28. On peut voir que l'émission verte et rouge peut être obtenue, ce qui démontre la localisation réussie des BQs. Une étude de ce système hybride est en cours.

Concernant la nanoplasmonique hybride, la Figure 6.29 montre un premier résultat du polymère intégré au voisinage d'un nanocube d'or, ce qui confirme la réalisation de la photo polymérisation plasmonique à l'échelle nanométrique [197]. Plus précisément, la Figure 6.29.b est l'image AFM du cube prise avant la photopolymérisation. La Figure 6.29.a est l'image AFM du cube étudié prise après photopolymérisation. Nous avons supprimé la Figure 6.29.b de la Figure 6.28.a (zone centrale sombre) pour mettre en évidence le polymère intégré qui devrait contenir des BQ. Des expériences de photoluminescence sont en cours.

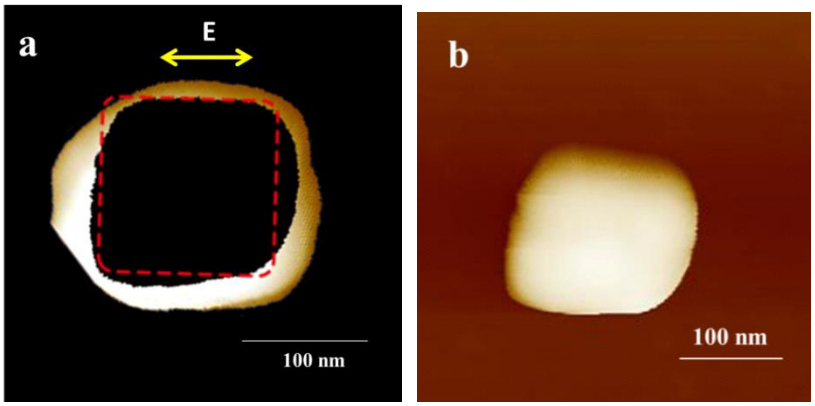

Figure 6.29: Images du polymère obtenu autour du nano-cube. La polymérisation plasmonique à deux photons a été réalisée à $\lambda = 700$ nm, sous un objectif de 40x0,6.

L'intégration de BQs avec des structures plamoniques et photoniques telles que des nanofils, des pointes de fibres, des réseaux métalliques et des nano-cubes a été réalisée *via* EDL-PDP en utilisant des résines photosensibles contenant des BQs. Nous avons démontré que les BQs peuvent être positionné de façon contrôlable. À l'avenir, l'étude de l'émission de lumière, de l'efficacité du couplage et du mécanisme de transfert d'énergie pourrait être la question clé compte tenu de l'application prometteuse en plasmonique et en photonique.

6.4 Conclusions

Cette thèse vise à la fabrication de structures fonctionnelles 3D ou 2D avec une résolution améliorée par ELD basée sur la PDP. Parmi les voies explorées pour améliorer la résolution, une solution chimique basée par l'ajout d'inhibiteur de polymérisation radicalaire dans ce travail a été explorée.

Tout d'abord, l'étude a été consacrée à l'influence de l'inhibiteur MEHQ sur la résolution des structures obtenues *via* ELD-PDP. Les résultats ont montré qu'avec le MEHQ impliqué dans ELD-PDP, la résolution de lignes 2D et de tas de bois 3D est améliorée, la plus petite largeur de ligne est de 60 nm. Le mécanisme de terminaison en présence de MEHQ est modifié, en particulier, la terminaison monomoléculaire est dominante.

Les structures polymères 3D contenant des BQs ont été fabriquées *via* ELD-PDP. Les résultats intéressants ont montré l'amélioration de la résolution des structures 2D et 3D en présence de BQs, ce qui n'avait jamais été montré auparavant. L'influence des BQs et de la puissance du laser sur la résolution des a été étudiée. La présence de BQs améliore la résolution des lignes de polymère. La spectroscopie FTIR et UV montre une diminution remarquable du taux de polymérisation des formulations photosensibles contenant des BQs. L'origine de résolution améliorée en présence de BQs a été discutée : les radicaux sont enclins à effectuer une terminaison monomoléculaire qui favorise un meilleur confinement spatial.

De plus, les images de fluorescence et les spectres d'émission montrent une émission locale stable à partir des structures contenant des BQs. En outre, l'intensité d'émission des structures varie avec la puissance du laser d'écriture. En ce sens, la taille de la structure et les propriétés fluorescentes peuvent être contrôlées dans le cas d'une écriture laser directe TPP, ce qui ouvre la voie à de futures investigations et applications.

Au chapitre 4, l'intégration des BQs avec des structures photoniques et plasmoniques telles que des nanofils d'argent, des fibres optiques, des réseaux métalliques plasmoniques et des nanocubes d'or a été réalisée *via* ELD-PDP en utilisant des résines photosensibles contenant des BQs. Nous avons démontré que les BQs peuvent être positionnées de façon contrôlée à différentes échelles. À l'avenir, l'étude de l'émission de lumière, de l'efficacité du couplage et du mécanisme de transfert d'énergie pourrait être la question clé compte tenu de l'application prometteuse en plasmonique et en photonique.

En ce qui concerne les perspectives futures, de nombreuses études et applications peuvent être envisagées. L'utilisation de systèmes polymérisables contenant des BQs *via* ELD-PDP est une approche simple pour avoir un bon contrôle de la localisation des émetteurs BQs pour un couplage optimum avec des nanofils, des réseaux métalliques, des guide d'ondes, etc. Cela offre de nombreuses perspectives pour créer une plate-forme pour intégrer des éléments photonique et plasmoniques passifs et des éléments actifs à base de BQs, ouvrant la porte à une nouvelle nanophotonique hybride.

References

[1] Henzie J., Barton J. E., Stender C. L. and Odom T. W. Large-area nanoscale patterning: chemistry meets fabrication. Acc. Chem. Res.2006, 39, 249–257.
[2] Fan H. J., Werner P. and Zacharias M. Semiconductor nanowires: from self-organization to patterned growth. Small 2006, 2, 700–717.
[3] Park S. H., Lim T. W., Yang D. Y., Kong H. J., Kim R. H. and Lee K. S. Fabrication of nano-precision PDMS replica using two photon photopolymerization and vacuum pressure difference technique. B. Korean Chem. Soc.2004, 25, 1119–1120.
[4] Sun H. B., Maeda M., Takada K., Chon J. W., Gu M. and Kawata S. Experimental investigation of single voxels for laser nanofabrication *via* two-photon photopolymerization. Appl. Phys. Lett.2003, 83, 819–821.
[5] Kawata S., Sun H. B., Tanaka T. and Takada K. Finer features for functional microdevices. Nat.2001, 412, 697–698.
[6] Serbin J., Egbert A., Ostendorf A. and Chichkov B. N. Femtosecond laser-induced two-photon polymerization of inorganic-organic hybrid materials for applications in photonics. Opt. Lett. 2003, 28, 301–303.
[7] Park S. H., Lim T. W., Yang D. Y., Kim R. H. and Lee K. S. Fabrication of a bunch of sub-30-nm nanofibers inside microchannels using photopolymerization *via* a long exposure technique. Appl. Phys. Lett.2006, 89, 173133.
[8] Maruo S., Nakamura O. and Kawata S. Three-dimensional microfabrication with two-photon-absorbed photopolymerization. Opt. Lett.1997, 22, 132–134.
[9] Sun H. B., Tanaka K. and Kawata S. Three-dimensional focal spots related to two-photon excitation. Appl. Phys. Lett.2002, 80, 3673–3675.
[10] Sun H. B. and Kawata S. Two-photon laser precision microfabrication and its applications to micro-nano devices and systems. J. Lightwave Technol.2003; 21(3):624-33.
[11] Sun H. B., Takada K. and Kawata S. Elastic force analysis of functional polymer submicron oscillators. Appl. Phys. Lett.2001, 79, 3173–3175.
[12] Borisov R. A., Dorojkina G. N., Koroteev N. I., Kozenkov V. M., Magnitskii S. A., Malakhov D. V., Tarasishin A. V. and Zheltikov A. M. Fabrication of three-dimensional periodic microstructures by means of two photon polymerization. Appl. Phys. B1998, 67, 765–767.
[13] Park S. H., Lee S. H., Yang D. Y., Kong H. J. and Lee K. S. Subregional slicing method to increase 3D nanofabrication efficiency in two-photon polymerization. Appl. Phys. Lett.2005, 87, 154108.
[14] Park S. H., Lim T. W., Yang D. Y., Yi S. W., Kong H. J. and Lee K. S. Direct nano-patterning methods using nonlinear absorption in photopolymerization induced by a femtosecond laser. J. Nonlinear Optic. Phys. Mat.2005, 14, 331–340.
[15] Lim T. W., Park S. H. and Yang D. Y. Contour offset algorithm (COA) for precise patterning in two-photon polymerization. Microelectron. Eng.2005, 77, 382–388.
[16] Yang H. K., Kim M. S., Kang S. W., Kim K. S., Lee K. S., Park S. H., Yang D. Y., Kong H. J., Sun H. B., Kawata S. and Fleits P. Recent progress of lithographic microfabrication by the TPA-induced photopolymerization. J. Photopolym. Sci. Technol.2004, 17, 385–392.
[17] Park S. H., Lim T. W., Yang D. Y., Yi S. W. and Kong H. J. Direct fabrication of micro-patterns and three-dimensional structures using nano replication printing (nRP) process. Sensor Mater.2005, 17, 65–75.

[18]Lee K. S., Kim R. H., Prabhakaran P., Yang D. Y., Lim T. W. and Park S. H. Two-photon stereolithography. J. Non. Opt. Phys. Mater.2007, 16, 59–73.
[19]Varadan V. K., Jiang X. and Varadan V. V. Microstereolithography and other fabrication techniques for 3D MEMS. Chichester: Wiley; 2001
[20]Lee K. S., Yang D. Y., Park S. H., and Kim R. H., Recent developments in two-photon polymerization for 2D and 3D microfabrications. Polym. Adv. Technol.2006, 17, 72–82.
[21]Göeppert-Mayer M. Elementary processes with two quantum transitions. Ann. Phys. 1931, 9, 273–294.
[22]Kaiser W. and Garret C. G. B. Two-photon excitation in CaF_2:Eu^{2+}. Phys. Rev. Lett.1961, 7, 229–231.
[23]Pao Y. H. and Rentzepis P. M. Laser-induced production of free radicals in organic compounds. Appl. Phys. Lett.1965, 6, 93–95.
[24]Farsari M., Vamvakaki M. and Chichkov B. N. Multiphoton polymerization of hybrid materials. J. Opt.2010, 12, 124001.
[25]Rumi M., Barlow S., Wang J., Joseph W., Seth P. and Marder R. Two-photon absorbing materials and two-photon-induced chemistry. Adv. Polym. Sci.2008, 213, 1–95.
[26]Belfield K., Schafer K., Liu Y., Liu J., Ren X. B. and Van Stryland E.W. Multiphoton-absorbing organic materials for microfabrication, emerging optical applications and non-destructive three-dimensional imaging J. Phys. Org. Chem.2000, 13, 837–849.
[27]Maruo S. and Fourkas J. Recent progress in multiphoton microfabrication. Laser Photon.Rev.2008, 2, 100–111.
[28]Maruo S. and Kawata S. Two-photon-absorbed near-infrared photopolymerization for three-dimensional microfabrication. J. Microelectromech. S.1998, 7, 411–415.
[29]Jia B. H., Li J. F., and Gu M. Two-photon polymerization for three-dimensional photonic devices in polymers and nanocomposites. Aust. J. Chem.2007, 60, 484–495.
[30]Strickler J. H. and Webb W. W. Three-dimensional optical data storage in refractive media by two-photon point excitation. Opt. Lett.1991, 16, 1780–1782.
[31]Sun H. B., Tanaka T., Takada K. and Kawata S. Two-photon photopolymerization and diagnosis of three-dimensional microstructures containing fluorescent dyes. Appl. Phys. Lett.2001, 79, 1411–1413.
[32]Wang J., Xia H., Xu B. B., Niu L. G., Wu D. and Chen Q. D. Remote manipulation of micro/Nano machines containing magnetic nanoparticles. Opt. Lett.2009, 34, 581–583.
[33]Xia H., Wang J., Tian Y., Chen Q. D., Du X. B., Zhang Y. L., He Y. and Sun H. B. Ferrofluids for fabrication of remotely controllable micro-nanomachines by two-photon polymerization. Adv. Mater.2010, 22, 3204–3207.
[34]Zhang Y. L., Chen Q. D., Xia H. and Sun H. B. Designable 3D nanofabrication by femtosecond laser direct writing. Nano Today 2010, 5, 435–448.
[35]Lee K. S., Kim R. H., Yang D. Y. and Park S. H. Advances in 3D nano/microfabrication using two-photon initiated polymerization. Prog.Polym.Sci.2008, 33, 631–681.
[36]He G. S., Tan L. S., Zheng Q.D. and Prasad P.N. Multiphoton absorbing materials: molecular designs, characterizations, and applications. Chem. Rev.2008, 108, 1245–1330.
[37]Jradi S., Croutxe-Barghorn C. and Carré C. "Expanding the spatial resolution of acrylic films for data storage applications", SPIE -Photonic Engineering, 2005, 5827, 410–417.
[38]Guttari F., Maire G., Contreras K., Arnaud C., Paulliat G., Roosen G., Jradi S. and Carré C. Balanced homodyne detection of bragg microholograms in photopolymer for data storage. Opt. Express 2007, 15, 2234–2243.
[39]Paulliat G., Maire G., Arnaud C., Paulliat F., Contreras K., Roosen G., Jradi S. and Carré C. Homodyne detections for Lippmann data storage", SPIE - Optical Data Storage, 6620, 66200F-1 to 7 (2007)

[40]Soppera O., Jradi S. and Lougnot D. J. Spatially controlled photopolymerization: Influence of physico-chemical parameters on the extent of polymerization at microscale. J. Polym. Sci. Pol. Chem.2008, 46, 3783–3794.
[41]Jradi S., Soppera O. and Lougnot D. J. Fabrication of polymer waveguides between two optical fibers using spatially controlled light induced polymerization. J. Appl. Opt. 2008, 47, 3987–3993.
[42]Zeng X., Plain J., Jradi S., Renaud-Goud P., Deturche R., Royer P. and Bachelot R. High speed sub-micrometric microscopy using optical polymer microlens. Chin. Opt. Lett. 2009, 17, 901–903.
[43]Zeng X., Plain J., Jradi S., Darraud C., Louradour F., Bachelot R. and Royer P. Integration of polymer microlens array at fiber bundle extremity by photopolymerization. Opt. Express 2011, 19, 4805–4814.
[44]Sedaght Z., Rumyantseva A., Bruyant A., Kostcheev S., Blaize S., Jradi S., Bachelot R. and Monmayrant A. Near-field optical imaging with a nanotip grown on fibered polymer microlens. Appl. Phys. Lett.2012, 100, 033107.
[45]Zheng S., Zeng X., Luo W., Jradi S., Plain J., Li M., Renaud-Goud P., Deturche R., Wang Z., Kou J., Bachelot R. and Royer P. Rapid fabrication of micro-nanometric tapered fiber lens and characterization by a novel scanning optical microscope with submicron resolution. Opt. Express 2013, 21, 30–38
[46]Moughames J., Jradi S., Chan T. M., Akil S., Battie Y., En Naciri A., Herro Z., Guenneau S., Enoch S., Joly L., Cousin J. and Bruyant A. Wavelength-scale light concentrator made by direct 3D laser writing of polymer metamaterials. Sci. Rep.2016, 6, 33627.
[47]Pitts J. D., Campagnola P. J., Epling G. A. and Goodman S. L. Submicron multiphoton free-form fabrication of proteins and polymers: studies of reaction efficiencies and applications in sustained release. Macromolecules 2000, 33, 1514–1523.
[48]Basu S., Wolgemuth C. W. and Campagnola P. J. Measurement of normal and anomalous diffusion of dyes within protein structures fabricated *via* multiphoton excited cross-linking. Biomacromolecules 2004, 5, 2347–2357.
[49]Watanabe T., Akiyama M., Totani K., Kuebler S. M., Stellacci F., Wenseleers W., Braun K., Marder S. R. and Perry J.W. Photoresponsive hydrogel microstructure fabricated by two-photon initiated polymerization. Adv. Funct. Mater.2002, 12, 611–614.
[50]Clauss E., Rehspringer J. L., Mager L., Fort A. and Fontaine J. "Laser micromachining of hybrid sol-gels: application to fabrication of micro-optical elements", Proc. SPIE 2016, 61901B
[51]Kim J. H., Jeong S. J., Lee H. J., Han S. W., Choi B. I. and Park S. H. Linear analysis of the viscoelastic response of polymer micro-pillars using the open-loop flat punch indentation test. Philos. Mag.2006, 86, 5679–5690.
[52]Galajda P. and Ormos P. Complex micromachines produced and driven by light. Appl. Phys. Lett.2001, 78, 249–251.
[53]Maruo S., Ikuta K. and Korogi H. Submicron manipulation tools driven by light in a liquid. Appl. Phys. Lett.2003, 82, 133–135.
[54]Chung T. T., Tseng C. L., Hung C. P., Lin C. L. and Baldeck P. L. Design and two-photon polymerization of complex functional micro-objects for lab-on-a-chip: rotating micro-valves. J. Neurosci. Neuroengin. 2013, 2, 48-52.
[55]Wang J., He Y., Xia H., Niu L. G., Zhang R., Chen Q. D., Zhang Y. L., Li Y. F., Zeng S. J., Qin J. H., Lin B. C. and Sun H. B. Embellishment of microfluidic devices *via* femtosecond laser micronanofabrication for chip functionalization. Lab Chip 2010, 10, 1993–1996.

[56]He Y., Huang B. L., Lu D. X., Zhao J., Xu B. B., Zhang R., Lin X. F., Chen Q. D., Wang J., Zhang Y. L. and Sun H. B. Overpass at the junction of a crossed microchannel: An enabler for 3D microfluidic chips. Lab Chip 2012, 12, 3866–3869.
[57]Amato L., Gu Y., Bellini N., Eaton S. M., Cerullo G. and Osellame R. Integrated three-dimensional filter separates nanoscale from microscale elements in a microfluidic chip. Lab Chip, 2012, 12, 1135–1142.
[58]Ovsianikov A., Viertl J., Chichkov B., Oubaha M., MacCraith B., Sakellari I., Giakoumaki A., Gray D., Vamvakaki M., Farsari M. and Fotakis C. Ultra-low shrinkage hybrid photosensitive material for two-photon polymerization microfabrication. ACS Nano, 2008, 2, 2257–2262.
[59]Ovsianikov A., Shizhou X., Farsari M., Vamvakaki M., Fotakis C. and Chichkov B. N. Shrinkage of microstructures produced by two photon polymerization of Zr-based hybrid photosensitive materials. Opt. Exp. 2009, 17, 2143–2148.
[60]Coenjarts C. A. and Ober C. K. Two-photon three dimensional microfabrication of poly(dimethylsiloxane) elastomers. Chem. Mater.2004, 16, 5556–5558.
[61]N. LaFratta C., Li L. J. and T. Fourkas J. Soft-lithographic replication of 3D microstructures with closed loops. PNAS 2006, 103, 8589–8594.
[62]Shukla S., Furlani P. E., Vidal X., Swihart M. T. and N. Prasad P. Two-photon lithography of sub-wavelength metallic structures in a polymer matrix. Adv. Mater.2010, 22, 3695–3699.
[63]Guo Q. C., Ghadiri R., Weigel T., Aumann A., L. Gurevich E., Esen C., Medenbach O., Cheng W., Chichkov B. and Ostendorf A. Comparison of in situ and ex situ methods for synthesis of two-photon polymerization polymer nanocomposites. Polymers 2014, 6, 2037–2050.
[64]Izquierdo-Lorenzo I., Jradi S. and Pierre-Michel A. Direct laser writing of random Au nanoparticle three-dimensional structures for highly reproducible micro-SERS measurements. RSC Adv. 2014, 4, 4128–4133.
[65]Zeng X., Jradi S., Proust J.,Bachelot R., Zhang X. P., Royer P., and Plain J. Direct functionalization of an optical fiber by a plasmonic nanosensor. Opt. Lett.2011, 36, 2919–2921.
[66]Jradi S., Balan L., Zeng X. H., Plain J., Lougnot D. J., Royer P., Bachelot R., Akil S., Soppera O. and Vidal L. Spatially controlled synthesis of silver nanoparticles and nanowires by photosensitized reduction. Nanotech. 2010, 21, 095605.
[67]Gansel J. K., Thiel M., Rill M. S., Decker M., Bade K., Saile V., Von Freymann G., Linden S. and Wegener M. Gold helix photonic metamaterial as broadband circular polarizer. Science 2009, 325, 1513–1515.
[68]Thiel M., Decker M., Deubel M., Wegener M., Linden S. and Von Freymann G. Polarization stop bands in chiral polymeric three-dimensional photonic crystals. Adv. Mater.2007, 19, 207–210.
[69]Thiel M., Fischer H., Von Freymann G. and Wegener M. Three-dimensional chiral photonic superlattices. Opt. Lett. 2010, 35, 166–168.
[70]Deubel M., Von Freymann G., Wegener M., Pereira S., Busch K. and Soukoulis C. M. Direct laser writing of three-dimensional photonic-crystal templates for telecommunications. Nat. Mater. 2004, 3, 444–447.
[71]Von Freymann G., Ledermann A., Thiel M., Staude I., Essig S., Busch K. and Wegene M. Three-dimensional nanostructures for photonics. Adv. Funct. Mater.2010, 20, 1038–1052.
[72]Duan X. M., Sun H. B., Kaneko K., and Kawata S. Two-photon polymerization of metal ions doped acrylate monomers and oligomers for three-dimensional structure fabrication. Thin Solid Films 2004, 453–454, 518–521

[73]Farsari M., Ovsianikov A., Vamvakaki M., Sakellari I., Gray D., Chichkov B. N. and Fortakis C. Fabrication of three-dimensional photonic crystals structures containing active nonlinear optical chromophore. Appl. Phys. A. Mater. Sci. Process.2008, 93, 11–15.
[74]Formanek F., Takeyasu N., Tanaka K., Chiyoda K., Ishihara T. and Kawata S. Selective electroless plating to fabricate complex three dimensional metallic micro/nanostructures. Appl. Phys. Lett.2006, 88, 083110.
[75]Formanek F., Takeyasu N., Tanaka T., Chiyoda K., Ishikawa A., and Kawata S. Three-dimensional fabrication of metallic nanostructures over large areas by two-photon polymerization. Opt. Exp.2006, 14, 800–809.
[76]Kuo W. S., Lien C. H., Cho K. C., Chang C. Y., Lin C. Y., Huang L. L. H., Campagnola P. J., Dong C. Y. and Chen S. J. Multiphoton fabrication of freeform polymer microstructures with gold nanorods. Opt. Exp.2010, 18, 27550–27559.
[77]Hoogh A. D., Hommersom B. and Koenderink A. F. Wavelength-selective addressing of visible and near-infrared plasmon resonances for SU8 nanolithography. Opt. Exp.2011, 19, 11405–11414.
[78]Masui K., Shoji S., Jin F., Duan X. M. and Kawata S. Plasmonic resonance enhancement of single gold nanorod in two-photon photopolymerization for fabrication of polymer/metal nanocomposites. Appl. Phys. A.2012, 106, 773–778.
[79]Drakakis T. S., Papadakis G., Sambani K., Filippidis G., Georgiou S., Gizeli E., Fotakis C. and Farsari M. Construction of three-dimensional biomolecule structures employing femtosecond lasers. Appl. Phys. Lett.2006, 89, 144108.
[80]Dinca V., Kasotakis E., Catherine J., Mourka A., Ranella A., Ovsianikov A., Chichkov B. N., Farsari M., Mitraki A. and Fotakis C. Directed three-dimensional patterning of self-assembled peptide fibrils. Nano Lett.2008, 8, 538–543.
[81]Basu S., Cunningham L. P, Pins G. D., Bush K. A., Taboada R., Howell A. R., Wang J., and Campagnola P. J. Multiphoton excited fabrication of collagen matrixes crosslinked by a modified benzophenone dimer: bioactivity and enzymatic degradation, Biomacromol.2005, 6, 1465–1474.
[82]Cunningham L. P., Veilleux M. P. and Campagnola P. J. Freeform multiphoton excited microfabrication for biological applications using a rapid prototyping CAD-based approach. Opt. Exp.2006, 14, 8613–8621.
[83]Otuka A. J. G., Corrêa D. S., Fontana C. R., Mendonça C. R. Direct laser writing by two-photon polymerization as a tool for developing microenvironments for evaluation of bacterial growth. Mater. Sci. Eng. C 2014, 35, 185–189.
[84]Terzaki K., Kalloudi E., Mossou E., P Mitchell E., TrevorForsyth V., Rosseeva E., Simon P., Vamvakaki M., Chatzinikolaidou M., Mitraki A. and Farsari M. Mineralized self-assembled peptides on 3D laser-made scaffolds: a new route toward scaffold on scaffold hard tissue engineering. Biofabrication 2013, 5, 045002.
[85]Serbin J., Egbert A., Ostendorf A., Chichkov B., Houbertz R., Domann G., Schulz J., Cronauer C., Frohlich L. and Popall M. Femtosecond laser-induced two-photon polymerization of inorganic-organic hybrid materials for applications in photonics. Opt. Lett.2003, 28: 301-303.
[86]Wu S. H., Serbin J. and Gu M. Two-photon polymerization for three-dimensional micro-fabrication. J. Photochem. Photobio. A: Chem.2006, 181, 1–11.
[87]Lee K. S., Yang D. Y., Park S. H. and Kim R. H. Recent developments in the use of two-photon polymerization in precise 2D and 3D microfabrications. Polym.Adv.Technol.2006, 17, 72–82.
[88]Xing J. F., Dong X. Z., Chen W. Q., Duan X. M., Takeyasu N., Tanaka T. and Kawata S. Improving spatial resolution of two-photon microfabrication by using photoinitiator with high initiating efficiency. Appl. Phys. Lett.2007, 90, 131106.

[89]Cao Y., Gan Z., Jia B., Evans R. and Gu M. High-photosensitive resin for super resolution direct-laser-writing based on photoinhibited polymerization. Opt. Exp.2011, 19, 19486–19494.
[90]Takada K., Sun H. B. and Kawata S. Improved spatial resolution and surface roughness in photopolymerization-based laser nanowriting. Appl. Phys. Lett.2005, 86, 071122.
[91]Lu W. E., Dong X. Z., Chen W. Q., Zhao Z. S. and Duan X. M. Novel photoinitiator with a radical quenching moiety for confining radical diffusion in two-photon induced photopolymerization. J. Mater. Chem.2011, 21, 5650–5659.
[92]Sakellari I., Kabouraki E., Gray D., Purlys V., Fotakis C., Pikulin A., Bityurin N., Vamvakaki M. and Farsari M. Diffusion-assisted high-resolution direct femtosecond laser writing. ACS Nano 2012, 6, 2302–2311.
[93]Sun Q., Juodkazis S., Murazawa N., Mizeikis V. and Misawa H. Freestanding and movable photonic microstructures fabricated by photopolymerization with femtosecond laser pulses. J. Micromech. Microeng.2010, 20, 035004.
[94]McLeod E. and Arnold C. B. Array-based optical nanolithography using optically trapped micro lenses. Opt. Exp.2009, 17, 3640–3650.
[95]Martínez-Corral M., Ibáñez-López C. and Saavedra G. Axial gain resolution in optical sectioning fluorescence microscopy by shaded-ring filters. Opt. Exp.2003, 11, 1740–1745.
[96]Malinauskas M., Rekštytė S., Jonavičius T., Gailevičius D., Mizeikis V., Gamaly E., and Juodkazis S. "Femtosecond pulsed light polarization induced effects in direct laser writing 3D nanolithography", Proc. SPIE 2016, 973608.
[97]Klar T. A., Jakobs S., Dyba M., Egner A., and Hell S.W. Fluorescence microscopy with diffraction resolution barrier broken by stimulated emission. Proc. Natl. Acad. Sci.2000, 97, 8206–8210.
[98]Rittweger E., Han K.Y., Irvine S. E., Eggeling C., and Hell S. W. STED microscopy reveals crystal color centres with nanometric resolution. Nat. Photonics 2009, 3, 144–147.
[99]Fischer J., Von Freymann G. and Wegener M. The materials challenge in diffraction unlimited direct-laser-writing optical lithography. Adv. Mater.2010, 22, 3578–3582.
[100] Cao Y., Gan Z., Jia B., Evans R. and Gu M. High-photosensitive resin for superresolution direct-laser-writing based on photoinhibited polymerization. Opt. Exp.2011, 19, 19486–19494.
[101] Mcleod R. R., Kowalski B. A. and Cole M. C. "Two-color photo-initiation/inhibition lithography", Proc. SPIE 2010,759102.
[102] Scott T. F., Kowalski B. A., Sullivan A. C.., Bowman C. N., and McLeod R. R. Two-color single-photon photoinitiation and photoinhibition for sub-diffraction photolithography. Sci.2009, 324, 913–917.
[103] Stocker M. P., Li L. J., Gattass R. R. and Fourkas J. T. Multiphoton photoresists giving nanoscale resolution that is inversely dependent on exposure time. Nat. Chem.2010, 3, 223.
[104] Li L. J., Gattass R. R, Gershgoren E., Hwang H. and Fourkas J. T. Achieving λ/20 resolution by one-color initiation and deactivation of polymerization. Sci.2009, 324, 910–913.
[105] Fischer J. and Wegener M. Three-dimensional optical laser lithography beyond the diffraction limit. Laser Photonics Rev.2013, 7, 22–44.
[106] Fischer J., Ergin T. and Wegener M. Three-dimensional polarization-independent visible-frequency carpet invisibility cloak Opt. Lett. 2011, 36, 2059–2061.
[107] Fischer J. and Wegener M. Ultrafast polymerization inhibition by stimulated emission depletion for three-dimensional nanolithography. Adv. Mater.2012, 24, OP65–OP69.

[108] Fischer J. and Wegener M. Three-dimensional direct laser writing inspired by stimulated-emission-depletion microscopy. Opt. Mater. Exp. 2011, 1, 614–624.
[109] Gu M. "Optical data storage with diffraction-unlimited resolution", presented at Conf. Lasers Electro-Optics Europe, Munich, 2013.
[110] Wiesbauer M., Wollhofen R., Vasic B., Schilcher K., Jacak J. and Klar T. A. Nano-anchors with single protein capacity produced with STED lithography. Nano Lett.2013, 13, 5672–5678.
[111] Emons M., Obata K., Binhammer T., Ovsianikov A., Chichkov B. and Morgner U. Two-photon polymerization technique with sub-50 nm resolution by sub-10 fs laser pulses. Opt. Mater. Exp. 2012, 2, 942-947.
[112] Prabhakaran P., Kim W. J., Lee K. S. and N. Prasad P. Quantum dots (QDs) for photonic applications. Opt. Mater. Exp.2012, 2, 578–593.
[113] Hezinger A. F. E., Teßmar J. and Göpferich A. Polymer coating of quantum dots– A powerful tool toward diagnostics and sensorics. Eur. J. Pharm. Biopharm.2008, 68, 138–152.
[114] Ledentsov N. N., Ustinov V. M., Shchukin V. A., Kop'ev P. S. and Alferov Zh. I. Quantum dot heterostructures: fabrication, properties, lasers. Semiconductors 1998, 32, 343–364.
[115] Fu H. K., Chen C. W., Wang C. H., Chen T. T. and Chen Y. F. Creating optical anisotropy of CdSe/ZnS quantum dots by coupling to surface plasmon polariton resonance of a metal grating. Opt. Exp.2008, 16, 6361–6367.
[116] Anikeeva P. O., Halpert J. E., Bawendi M. G. and Bulović V. Quantum dot light-emitting devices with electroluminescence tunable over the entire visible spectrum. Nano Lett. 2009, 9, 2532–2536.
[117] Chen C. Y., Cheng C. T., Lai C. W., Wu P. W., Wu K. C., Chou P. T., Chou Y. H. and Chiu H.T. Potassium ion recognition by 15-crown-5 functionalized CdSe/ZnS quantum dots in H_2O. Chem. Commun.2006, 3, 263–265.
[118] Pons T., Uyeda H. T., Medintz I. L. and Mattoussi H. Hydrodynamic dimensions, electrophoretic mobility, and stability of hydrophilic quantum dots. J. Phys. Chem. B 2006, 110, 20308–20316.
[119] Arya H., Kaul Z., Wadhwa R., Taira K., Hirano T., and Kaul S. C. Quantum dots in bio-imaging: Revolution by the small. Biochem. Biophys. Res. Commun.2005, 329, 1173–1177.
[120] Luther J. M., Jain P. K., Ewers T. and Alivisatos A.P. Localized surface plasmon resonances arising from free carriers in doped quantum dots. Nat. Mater.2011, 10, 361–366.
[121] Aoki K., Guimard D., Nishioka M., Nomura M., Iwamoto S. and Arakawa Y. Coupling of quantum-dot light emission with a three-dimensional photonic-crystal nanocavity. Nat. Photonics 2008, 2, 688–692.
[122] Martiradonna L., Qualtieri A., Stomeo T., Carbone L., Cingolani R. and De Vittorio M. Lithographic nanopatterning of colloidal nanocrystal emitters for the fabrication of waveguide photonic devices. Sens. Actuators B Chem.2007, 126, 116–119.
[123] Zhou X., Wenger J., N. Viscomi F., Le Cunff L., Béal J., Kochtcheev S., Yang X. Y., P. Wiederrecht G., Colas des Francs G., Bisht A.S., Jradi S., Caputo R., Volkan Demir H., Schaller R. D., Plain J., Vial A., Sun X. W. and Bachelot R. Two-color single hybrid plasmonic Nanoemitters with real time switchable dominant emission wavelength. Nano Lett.2015, 15, 7458–7466.
[124] Ganesh N., Zhang W., Mathias P. C., Chow E., Soares J. A. N. T., Malyarchuk V., Smith A. D. and Cunningham B. T. Enhanced fluorescence emission from quantum dots on a photonic crystal surface. Nat. Nanotechnol.2007, 2, 515–520.
[125] Achermann M. Exciton-plasmon interactions in metal-semiconductor nanostructures. J. Phys. Chem. Lett.2010, 1, 2837–2843.

[126] Gómez D. E., Vernon K. C., Mulvaney P. and Davis T. J. Surface plasmon mediated strong exciton-photon coupling in semiconductor nanocrystals. Nano Lett.2010, 10: 274–278.
[127] Gómez D. E., Vernon K. C., Mulvaney P. and Davis T. J. Coherent superposition of exciton states in quantum dots induced by surface plasmons. Appl. Phys. Lett.2010, 96, 073108.
[128] Zhao H., Wang D., Zhang T., Chaker M. and Ma D. Two-step synthesis of high-quality water-soluble near-infrared emitting quantum dots via amphiphilic polymers. Chem. Commun.2010, 46, 5301–5303.
[129] Cho S., Kwag J., Jeong S., Baek Y. and S. Kim. Highly fluorescent and stable quantum dot-polymer-layered double hydroxide composites. Chem. Mater.2013, 25, 1071−1077.
[130] Cao, Y.C. Preparation of thermally stable well-dispersed water-soluble CdTe quantum dots in montmorillonite clay host media. J. Colloid Interface Sci. 2012, 368, 139–143.
[131] Cho S., Jung S., Jeong S., Bang J., Park J., Park Y. and Kim S. Strategy for synthesizing quantum dot-layered double hydroxide nanocomposites and their enhanced photoluminescence and photostability. Langmuir 2013, 29, 441–447.
[132] Pellegrino T., Manna L., Kudera S., Liedl T., Koktysh D., Rogach A.L., Keller S., Radler J., Natile G. and Parak W.J. Hydrophobic nanocrystals coated with an amphiphilic polymer shell: a general route to water soluble nanocrystals. Nano Lett.2004, 4, 703–707.
[133] Ingrosso C., Fakhfouri V., Striccoli M., Agostiano A., Voigt A., Gruetzner G., Curri M. L. and Brugger J. An epoxy photoresist modified by luminescent nanocrystals for the fabrication of 3D high-aspect-ratio microstructures. Adv. Funct. Mater.2007, 17, 2009–2017.
[134] Jang K. K., Prabhakaran P., Chandran D., Park J. J. and Lee K. S. Solution processable and photopatternable blue, green and red quantum dots suitable for full color displays devices. Opt. Mater. Exp. 2012, 2, 519–525.
[135] Sun Z. B., Chen W. Q., Dong X. Z. and Duan X. M. A facile size-control method of CdS nanoparticles in-situ synthesized in polymer matrix by adjusting ratio of acidic acid with metallic complex in acrylate photoresist resin. Chem. Lett.2007, 36, 156–157.
[136] Sun Z. B., Dong X. Z., Chen W. Q., Shoji S., Duan X. M. and Kawata S. Two- and three-dimensional micro/nanostructure patterning of CdS–polymer nanocomposites with a laser interference technique and in situ synthesis. Nanotechnol. 2008, 19, 035611.
[137] Park J. J., Prabhakaran P., Jang K. K., Lee Y., Lee J., Lee K., Hur J., Kim J.M., Cho N., Son Y., Yang D.Y. and Lee K.S. Photopatternable quantum dots forming quasi-ordered arrays. Nano Lett. 2010, 10, 2310–2317.
[138] Zayatsa A. V., Smolyaninov I. I. and Maradudin A. A. Nano-optics of surface plasmon polaritons. Phys. Rep.2005, 408, 131–314.
[139] Ozbay E. Plasmonics: merging photonics and electronics at nanoscale dimensions. Sci.2006. 311, 189–193.
[140] Haes A. J., Chang L., Klein W. L. and Van Duyne R. P. Detection of a biomarker for alzheimer's disease from synthetic and clinical samples using a nanoscale optical biosensor. J. Am. Chem. Soc.2005, 127, 2264–2271.
[141] Zhao J., Zhang X. Y., Yonzon C. R., Haes A. J. and Van Duyne R. P. Localized surface plasmon resonance biosensors. Nanomedicine 2006, 1, 219–228.
[142] Zayats A. V. and Smolyaninov I. I. Near-field photonics: surface plasmon polaritons and localized surface plasmons. J. Opt. A: Pure Appl. Opt.2003, 5, S16–S50.
[143] Klimov V. I. Ed. Semiconductor and Metal Nanocrystals; Marcel Dekker: New York, 2004.
[144] Salter C. L., Stevenson R. M., Farrer I., Nicoll C. A., Ritchie D. A. and Shields A. J. An entangled-light-emitting diode. Nat.2010, 465, 594–597.

[145] Dousse A., Suffczyński J., Beveratos A., Krebs O., Lemaître A., Sagnes I., Bloch J., Voisin P., and Senellart P. Ultrabright source of entangled photon pairs. Nat.2010, 466, 217–220.
[146] O'Brien J. L., Furusawa A. and Vučković J. Photonic quantum technologies. Nat. Photonics 2009, 3, 687–695.
[147] Luxmoore I. J., Wasley N. A., Ramsay A. J., T. Thijssen A. C., Oulton R., Hugues M., Fox A. M. and Skolnick M. S. Optical control of the emission direction of a quantum dot. Appl. Phys. Lett.2013, 103, 241102.
[148] Reithmaier J. P. Strong exciton-photon coupling in semiconductor quantum dot systems. Semicond. Sci. Technol.2008, 21, 123001.
[149] Rastelli A., Ulhaq A., Kiravittaya S., Wang L., Zrenner A. and Schmidt O. G. In-situ laser microprocessing of single self-assembled quantum dots and optical microcavities. Appl. Phys. Lett.2007, 90, 073120.
[150] Benyoucef M., Kiravittaya S., Mei Y. F., Rastelli A. and Schmidt O. G. Strongly coupled semiconductor microcavities: a route to couple artificial atoms over micrometric distances. Phys. Rev. B2008, 77, 035108.
[151] Wang H., Wang H. Y., Toma A., Yano T., Chen Q. D., Xu H. L., Sun H. B. and Proietti Zaccaria R. Dynamics of strong coupling between CdSe Quantum Dots and surface plasmon polaritons in subwavelength hole array. J. Phys. Chem. Lett. 2016, 7, 4648–4454.
[152] Neogi A., Morkoç H., Kuroda T. and Tackeuchi A. Coupling of spontaneous emission from GaN-AlN quantum dots into silver surface plasmons. Opt. Lett.2005, 30, 93–95
[153] Gómez D. E., Lo S. S., Davis T. J. and Hartland G. V. Picosecond kinetics of strongly coupled excitons and surface plasmon polaritons. J. Phys. Chem. B 2013, 117, 4340.
[154] Arcari M., Söllner I., Javadi A., Lindskov Hansen S., Mahmoodian S., Liu J., Thyrrestrup H., Lee E. H., Song J. D., Stobbe S. and Lodahl P. Near-unity coupling efficiency of a quantum emitter to a photonic crystal waveguide. Phys. Rev. Lett.2014, 113, 093603.
[155] Zhang J. Y., Ye Y. H., Wang X. Y., Rochon P. and Xiao M. Coupling between semiconductor quantum dots and two-dimensional surface plasmons. Phys. Rev. B2005, 72, 201306.
[156] Akimov A. V., Mukherjee A., Yu C. L., Chang D. E., Zibrov A. S., Hemmer P. R., Park H. and Lukin M. D. Generation of single optical plasmons in metallic nanowires coupled to quantum dots. Nat.2007, 450, 402–407.
[157] Wei H., Ratchford D., Li X.Q., Xu H.X. and Shih C.K. Propagating surface plasmon induced photon emission from quantum dots. Nano Lett.2009, 9(12):4168-71.
[158] Gruber C., Trügler A., Hohenau A., Hohenester U. and R. Krenn J. Spectral modifications and polarization dependent coupling in tailored assemblies of quantum dots and plasmonic nanowires. Nano Lett.2013, 13: 4257-62.
[159] De Torres J., Ferrand P., Colas des Francs G., and Wenger J. Coupling emitters and silver nanowires to achieve long-range plasmon-mediated fluorescence energy transfer. ACS Nano.2016, 10 (4):3968-76.
[160] Bae W. K., Kwak J., Lim J., Lee D., Nam M. K., Char K., Lee C. and Lee S. Multicolored light-emitting diodes based on all-quantum-dot multilayer films using layer-by-layer assembly method. Nano Lett. 2010, 10, 2368–2373.
[161] Li, L. and Reiss, P. One-pot synthesis of highly luminescent InP/ ZnS nanocrystals without precursor injection. J. Am. Chem. Soc. 2008, 130, 11588.
[162] http://www.nanoscribe.de/en/products/photonic-professional-gt/
[163] Jradi S., Balan L., Zeng X. H., Plain J., Lougnot D. J., Royer P., Bachelot R., Akil S., Soppera O. and Vidal L. Spatially controlled synthesis of silver nanoparticles and nanowires by photosensitized reduction. Nanotech. 2010, 21, 095605.

[164] Laleveé J., Allonas X., Jradi S. and Fouassier J. P. Role of the medium on the reactivity of cleavable photoinitiators in photopolymerization reactions", Macromolecules 2006, 39, 1872–1879.
[165] Rufs A. M., Valdebenito A., Rezende M. C., Bertolotti S., Previtali C., Encinas M. V. Synthesis and photoinitiation activity of macroinitiators comprising benzophenone derivatives. Polymer 2008, 49, 3671–3676.
[166] Park S. H., Lim T. W., Yang D. Y., Kim R. H. and Lee K. S. Improvement of spatial resolution in nano-stereolithography using radical quencher. Macromol. Res.2006, 14, 559–564.
[167] Becker H. and Vogel H. The role of hydroquinone monomethyl ether in the stabilization of acrylic acid. Chem. Eng. Technol.2006, 29, 1227–1231.
[168] Colea M. A., Jankouskya K. C. and Bowmana C. N. Redox initiation of bulk thiol-ene polymerizations. Polym. Chem. 2013, 4, 1167–1175.
[169] Becker H. and Vogel H. Stabilization of acrylic esters. Chem. Eng.Technol.2004, 27, 1122–1126.
[170] Li R. J. and Schork F. J. Modeling of the inhibition mechanism of acrylic acid polymerization. Ind. Eng. Chem. Res.2006, 45, 3001–3008.
[171] Haske W., Chen V. W., Hales J. M.; Dong W.T., Barlow S.; Marder S. R. and Perry J. W. 65 nm feature sizes using visible wavelength 3D multiphoton lithography. Optics Express 2007, 15, 3426–3436.
[172] Tamborra M., Striccoli M., Curri M. L., Alducin J. A., Pomposo J. A., Kehagias N., Reboud V., Torres C. M. S. and Agositano A. Nanocrystal-based luminescent composites for nanoimprinting lithography. Small 2007, 3, 822–828.
[173] Andrzejewska E., Bogacki M. B., Andrzejewski M. and Janaszczyk M. Termination mechanism during the photo-induced radical cross-linking polymerization in the presence and absence of oxygen. Phys. Chem. Chem. Phys. 2003, 5, 2635–2642.
[174] Barichard A., Galstianc T. and Israeli Y. Physico-chemical role of CdSe/ZnS quantum dots in the photo-polymerization process of acrylate composite materials, Phys. Chem. Chem. Phys.2012, 14, 8208–8216.
[175] Chang D. E., Sørensen A. S., Hemmer P. R., and Lukin M. D. Strong coupling of single emitters to surface plasmons. Phys. Rev. Lett.2006, 97, 053002.
[176] Liao J. Q., Gong Z. R., Zhou L., Liu Y. X., Sun C. P. and Nori F. Controlling the transport of single photons by tuning the frequency of either one or two cavities in an array of coupled cavities. Phys. Rev. A 2010, 81, 042304.
[177] Tatebayashi J. Kako S., Ota Y., Iwamoto S. and Arakawa Y. Room-temperature lasing in a single nanowire with quantum dots. Nat. Photonics 2015, 9, 501–505.
[178] Kim N. C., Li J. B., Yang Z. J., Hao Z. H. and Wang Q. Q. Switching of a single propagating plasmon by two quantum dots system. Appl. Phys. Lett.2010, 97, 061110.
[179] Wang J., Gudiksen M. S., Duan X., Cui Y. and Lieber C. M. High polarized photoluminescence and photodetection from single indium phosphide nanowires. Sci.2001, 293(5534): 1455 –1457.
[180] Kremer P. E., Dada A. C., Kumar P., Ma Y., Kumar S., Clarke E. and Gerardot B. D. Strain-tunable quantum dot embedded in a nanowire antenna. Phys. Rev. B2014, 90, 201408.
[181] Kuo P. C., Chen G. Y. and Chen Y. N. Scattering of nanowire surface plasmons coupled to quantum dots with azimuthal angle difference. Srep.2016, 6, 37766.
[182] Kim W. S., Park K. M., Park J. J., Chang S. M., Kim I. H., Muramatsu H., Kim J. M. Polymer tips for application of atomic force microscopy. Current Appl. Phys.2007, 7, 528–531.
[183] Ducourtieux S., Grésillon S., Rivoal J. C., Vannier C., Bainier C., Courjon D. and Cory H. Imaging subwavelength holes in chromium films in scanning near-field optical

microscopy: Comparison between experiments and calculation. EPJ Appl. Phys. 2004, 26, 35–43.
[184] Fischer T., Stöttingr S., Hinze G., Bottin A., Hu N. and Basché T. Single semiconductor nanocrystals under compressive stress: reversible tuning of the emission energy. Nano Lett.2017, 17, 1559–1563.
[185] Van Hoorn C. H., Chavan D. C., Tiribilli B., Margheri G., Mank A. J. G., Ariese F. and Iannuzzi D. Opto-mechanical probe for combining atomic force microscopy and optical near-field surface analysis. Opt. Lett.2014, 39, 4800–4803.
[186] Ren H. L., Jiang C., Hu W. S., Gao M. Y., Wang J. Y., Wang H., He J. T. and Liang E. J. The preparation of optical fiber nanoprobe and its application in spectral detection. Opt. Laser Technol.2007, 39, 1025–1030.
[187] Lambelet P., Sayah A., Pfeffer M., Philipona C. and Marquis-Weible F. Chemically etched fiber tips for near-field optical microscopy: a process for smoother tips. Appl. Opt.1998, 37, 7289–7292.
[188] Cabrini S., Liberale C., Cojoc D., Carpentiero A., Prasciolu M., Mora S., Degiorgio V., De Angelis F. and Di Fabrizio E. Axicon lens on optical fiber forming optical tweezers, made by focused ion beam milling. Microelectron. Eng.2006, 83, 804–807.
[189] Cheong W. C., Ahluwalia S. B. P., Yuan X. C., Zhang L. S., Wang H., Niu H. B. and Peng X. Fabrication of efficient microaxicon by direct electron-beam lithography for long nondiffracting distance of Bessel beams for optical manipulation. Appl. Phys. Lett.2005, 87, 024104.
[190] Said A. A., Dugan M., De Man S. and Iannuzzi D. Carving fiber-top cantilevers with femtosecond laser micromachining. J. Micromech. Microeng.2008, 18, 035005.
[191] Jradi S., Soppera O., Lougnot D. J., Bachelot R. and Royer P. Tailoring the geometry of polymer tips on the end of optical fibers *via* control of physico-chemical parameters. Opt. Mater.2009, 31, 640–646.
[192] Le Feber B., Rotenberg N. and Kuipers L. Nanophotonic control of circular dipole emission. Nat.Commun.2015, 6, 7695.
[193] Ramos T., Pichler H., Daley A. J. and Zoller P. Quantum spin dimers from chiral dissipation in cold-atom chains. Phys. Rev. Lett.2014, 113, 237203.
[194] Mitsch R., Sayrin C., Albrecht B., Schneeweiss P. and Rauschenbeutel A. Quantum state-controlled directional spontaneous emission of photons into a nanophotonic waveguide. Nat. Commun.2014, 5, 6713.
[195] Zadeh I. E., Elshaari A. W., Jöns K. D., Fognini A., Dalacu D., Poole P. J., Reimer M. E. and Zwiller V. Deterministic integration of single photon sources in silicon based photonic circuits. Nano Lett. 2016, 16: 2289−2294.
[196] Reithmaier G., Senf J., Lichtmannecker S., Reichert T., Flassig F., Voss A., Gross R., Finley J. J. Optimisation of NbN thin films on GaAs substrates for in-situ single photon detection in structured photonic devices. J. Appl. Phys. 2013, 113: 143507.
[197] Petersen J., Volz J. and Rauschenbeutel A. Chiral nanophotonic waveguide interface based on spin–orbit interaction of light. Sci.2014, 346, 67–71.
[198] Feigel A., Veinger M., Sfez B., Arsh A., Klebanov M. and Lyubin V. Three-dimensional simple cubic woodpile photonic crystals made from chalcogenide glasses. Appl. Phys. Lett.2003, 83, 4480–4482.
[199] Bergman K., Carloni L. P., Biberman A., Chan J. and Hendry G. Photonic Network-on-Chip Design (Integrated Circuits and Systems), Springer: New York, 2014.
[200] Akselrod G. M., Argyropoulos, C., Hoang, T. B., Ciraci, C., Fang, C., Huang, J., Smith, D. R., Mikkelsen, M. H. Probing the mechanisms of large Purcell enhancement in plasmonic nanoantennas. Nat. Photonics 2014, 8, 835−840.

[201] Yang A. Y., Hoang A. B., Dridi M., Deeb. C., Maiken H., Mikkelsen M. H., Schatz J. C. and Odom T. W. Real-time tunable lasing from plasmonic nanocavity arrays. Nat. Commun.2015, 6, 6939.
[202] Zhang Q., Li G., Liu X., Qian F., Li Y., Sum T. C., Lieber C. M. and Xiong Q. A room temperature lowthreshold ultraviolet plasmonic nanolaser. Nat. Commun. 2014, 5, 4953.
[203] Deeb C., Bachelot R., Plain J., Baudrion A. L., Jradi S., Bouhelier A., Soppera O., Jain P. K., Huang L., Ecoffet C., Balan L. and Royer P. Quantitative analysis of localized surface plasmons based on molecular probing. ACS Nano 2010, 4, 4579–4586.
[204] Zhou X., Deeb C., Vincent R., Lerond T., Adam P.-M., Plain J., Wiederrecht G. P., Charra F., Fiorini C., Colas des Francs G., Soppera O., and Bachelot R. Polarization-dependent fluorescence from an anisotropic gold/polymer hybrid nanoemitter. Appl. Phys. Lett. 2014, 104, 023114.
[205] Jin S., DeMarco E., Pellin M. J., Farha O. K., Wiederrecht G. P. and Hupp J. T . Distance-engineered plasmon-enhanced light harvesting in CdSe quantum dots. J. Phys. Chem. Lett. 2013, 4, 3527–3533.
[206] Wu X., Gray S. K. and Pelton M. Quantum-dot-induced transparency in a nanoscale plasmonic resonator. Opt. Express 2010, 18, 23634–23645.

Ying PENG

Doctorat : Matériaux, Mécanique, Optique et Nanotechnologie

Année 2017

Matériaux photopolymérisables fonctionnels pour la lithographie 3D à haute résolution et la nano-optique

Les nanostructures photoluminescentes à forte efficacité d'émission présentent un intérêt majeur en nano-optique. En particulier, les boîtes quantiques (BQs) sont d'excellents candidats pour obtenir des sources de photons uniques, lorsqu'elles sont insérées dans des cavités photoniques appropriées. Ainsi, l'intégration de ces nano-émetteurs avec un contrôle spatial parfait constitue un réel défi. Dans cette thèse, nous avons développé un photopolymère greffé sur des BQs de différentes couleurs d'émission, pour la photolithographie 3D à très haute résolution spatiale. Nous avons ainsi fabriqué des nanostructures 1D, 2D et 3D par photopolymérisation à 2 photons (PDP). Une amélioration significative de la résolution a été obtenue grâce à un très fort confinement du volume réactionnel suite à l'ajout des inhibiteurs de radicaux. Le plus petit motif polymère est inférieur à 60 nm, obtenu au sein de structures organisées type « tas de bois » de 350 nm de période. Il s'agit d'un record dans la fabrication 3D par PDP utilisant un seul laser à 780 nm. Nous avons également montré que la présence des BQs améliore significativement la résolution. Des études photochimiques et cinétiques ont été réalisées pour comprendre l'influence des inhibiteurs et des BQs sur la structuration. Finalement, nous avons montré la possibilité d'intégrer nos BQs de manière contrôlée sur des nano-fils d'argent, des guides d'onde, des nano-cubes d'or et des fibres optiques microlentillées. Nos résultats devront stimuler d'autres travaux prometteurs dans le domaine de la nano-optique.

Mots clés : polymérisation - points quantiques - nanostructures - résines photosensibles - photoluminescence – photolithographie.

Functional Photopolymer Materials for High-resolution 3D Lithography and Nano-optics

Luminescent nanostructures with high emission efficiency and spatial resolution are of great interest for optics and photonics. Specifically in quantum optics, remarked as an attractive candidate for single photon sources, quantum dots (QDs) have shown promising quantum yield and stability. In this issue, the crucial point is to integrate QDs emitters with a spatially controlled manner into optical and plasmonic devices. In this thesis, photopolymer containing QDs with 3 different emission colors have been formulated and used for the fabrication of 1D, 2D and 3D nanostructures with sub-100 nm size by direct laser writing based on two-photon polymerization (TPP-DLW). The improvement of the spatial resolution of writing is realized through a strong confinement of the polymerization volume based on the use of free radical inhibitors. The results show that the smallest feature size of 3D polymer woodpiles could reach 60 nm with a period of 350 nm, which has never been reported in the fabrication via TPP-DLW using single laser emitting at 780 nm. Investigations showed that spatial resolution of writing is significantly improved in the presence of Qds. Photochemical and kinetics studies were performed to understand the effect of both inhibitors and Qds on the nanostructuring by TPP. Finally, the local integration of QDs into Ag nanowires, ion exchange-glass optical waveguides, Gold nanocubes and fiber tips was achieved. We believe that our results and approaches of nanofabrication will stimulated further promising works in nano-optics.

Keywords: polymerization - quantum dots – nanostructures - photoresists - photoluminescence - photolithography.

Thèse réalisée en partenariat entre :

Ecole Doctorale "Sciences et Technologies"